On the dynamics of C. reinhardtii subject to external periodic flows

A model system for synchronization in biology

Quaranta, Greta

Important note
To cite this publication, please use the final published version (if applicable).
Please check the document version above.

ON THE DYNAMICS OF *C. REINHARDTII* SUBJECT TO EXTERNAL PERIODIC FLOWS:

A model system for synchronization in biology

ON THE DYNAMICS OF *C. REINHARDTII*
SUBJECT TO EXTERNAL PERIODIC FLOWS:

A model system for synchronization in biology

DISSERTATION

for the purpose of obtaining the degree of doctor
at Delft University of Technology
by the authority of the Rector Magnificus prof. dr. ir. T.H.J.J. van der Hagen
Chair of the Board for Doctorates
to be defended publicly on
Friday 14 September 2018 at 12:30 o'clock

by

Greta QUARANTA
Master of Science in Biomedical Engineering
Polytechnic University of Turin, Italy
Born in Turin, Italy.

This dissertation has been approved by the promotors.

Composition of the doctoral committee:

Rector Magnificus,	chairperson
Prof. dr. ir. J. Westerweel	Delft University of Technology, promotor
Dr. D. S. W. Tam	Delft University of Technology, copromotor

Independent members:

Prof. dr. S. Hickel	Delft University of Technology
Prof. dr. ir. W. van de Water	Delft University of Technology
Prof. dr. ir. J. M. J. den Toonder	Eindhoven University of Technology
Prof. dr. ir. P. R. Onck	University of Groningen
Dr. M. Polin	University of Warwick, other member

To my family

CONTENTS

SUMMARY

Synchronization of oscillators is an ubiquitous phenomenon that involves mechanical systems, like pendulum clocks, but also biological systems, like peacemaker cells in the heart or neural activity in the brain. If we consider biological systems at the microscale, namely at the scale of cells, we find that processes like locomotion and fluid transport often exploit synchronization of mechanical oscillators called flagella or cilia. These oscillators at the microscale are whip-like structures extending from the cell body. They are present in a number of micro-organisms like sperm cells, *Paramecium* or the algae *C. reinhardtii*. In human, cilia are found in the lungs, the respiratory tract and the middle ear. Cilia are activated in a coordinated way to effectively carry out their function, such as draining mucus. The mechanism behind this cilia coordination is still debated. It is not clear how very simple organisms lacking any feedback system have developed complex oscillatory patterns involving coordination among a multitude of cilia or flagella. There is high interest in understanding the fundamental principles ruling ciliary dynamics, since they would impact medical and engineering applications. The purpose of this thesis is to investigate the mechanisms regulating the synchronization of cilia and flagella.

A long standing hypothesis is that synchronization of cilia and flagella is mediated by mechanical forces transmitted through the fluid, namely hydrodynamic forces. In the present study, we address this possibility experimentally. We design an experiment in which we dynamically interact with a micro-organism in real time. We focus our study on one particular micro-organism, the algae *C. reinhardtii*. We impose on *C. reinhardtii* hydrodynamic forces in the form of a periodic background flow, and we measured how these forces affect flagellar synchronization.

C. reinhardtii has two flagella that beat continuously together at a frequency of ≈ 53 Hz. Their synchronous beating allows the cells to feed and to propel forward in water. A peculiar characteristic of the two flagella is that, if isolated, they actually beat at two different frequencies. In particular, one flagellum named *cis-* flagellum beats at a frequency of ≈ 53 Hz, while the other flagellum, the *trans-* flagellum, beats at ≈ 70 Hz. However, when the cell is swimming, the two flagella are synchronized and beat at the frequency of the *cis*-flagellum. Understanding the mechanisms regulating such synchronous beating in *C. reinhardtii*, would broaden the understanding of ciliary dynamics in general. In fact, an important property of cilia and flagella is that their molecular structure is highly conserved among different eukaryotic organisms. Therefore the activation and behaviour of cilia is expected to be similar in different micro-organisms.

In our experiments on *C. reinhardtii*, we find that an external periodic hydrodynamic forcing is able to shift the intrinsic beating frequency of the cell, therefore establishing that flagellar behaviour can, in fact, be influenced by hydrodynamic interactions. However, we observe that, even if we impose an hydrodynamic forcing 10 times stronger than the hydrodynamic forces normally experienced by the cell, we are able to shift the intrinsic beating frequency of the cell by only few Hertz. Therefore, the

external hydrodynamic forcing has a relatively weak effect on flagellar beating frequency. Since the mismatch between the intrinsic frequencies of the two flagella is on the order of 20 Hz, it is unlikely that the synchrony between flagella would be a consequence of hydrodynamic interaction forces. These results are confirmed by numerical simulations in which the flow field around the cell in a typical experiment is computed.

Given that hydrodynamic interactions do not seem to be the main mechanism behind flagellar synchronization, we propose another synchronization mechanism based on intracellular mechanical coupling of flagella. In *C. reinhardtii*, the two flagella are mechanically connected inside the cell by a network of structural fibers. We perform experiments on a mutant (the *vfl3*), where this fiber structure is impaired. We neither observe synchronization between the two flagella of *vfl3*, nor observe synchronization with an external hydrodynamic forcing. These results suggest that synchronization between the two flagella is not possible if the intracellular mechanical connection in not present and, therefore, it seems likely that the mechanism responsible for flagellar synchronization is based on the intracellular coupling rather than on the hydrodynamic forces between the flagella.

In addition, our experiments demonstrate a very good analogy between *C. reinhardtii* and the prototypical model for an ideal self sustained oscillator. *C. reinhardtii* behaves like a self sustained oscillator with a well defined synchronization range, delimited by an Arnold tongue. Results on multiple cells are consistent and identify the same synchronization region. In addition, when the forcing is arrested, *C. reinhardtii* flagella return to beat at their original frequency within less than one beating cycle. No permanent alteration of the intrinsic frequency occurs after imposing an external forcing for up to 10 minutes.

We also perform experiments in which the periodic forcing is stronger on one flagellum than on the other one and we measure the coupling between the flagella and the external flow. We observe that a forcing acting more strongly on the *cis-* flagellum induces synchronization of the flagella with the forcing while a forcing of same strength acting more strongly on the *trans-* flagellum hardly triggers synchronization. This result confirms the dominant role of the *cis-* flagellum in controlling the beating pattern and the dominance in the coupling between flagella of intracellular coupling over hydrodynamic interaction.

Finally, we investigate the role of hydrodynamic interactions on the antiphase beating observed in a mutant of *C. reinhardtii*, the *ptx1* mutant. We compute the hydrodynamic viscous forces imposed by the flow on the flagella and the hydrodynamic interaction between the flagella. We find the first contribution to be over an order of magnitude larger than the second one. These results indicate that the antiphase beating mode is not sustained by hydrodynamic forces between the two flagella, similar to the normal in-phase beating mode.

SAMENVATTING

Synchronisatie van oscillatoren is een wijdverbreid fenomeen dat terug te vinden is in mechanische systemen, zoals slingerklokken, maar ook in biologische systemen, zoals pacemaker cellen in het hart of neurale activiteit in de hersenen. Als we biologische systemen op microschaal bekijken, op de schaal van cellen, vinden we dat processen als voortbeweging en stromingstransport vaak de synchronisatie van oscillatoren exploiteren. Om precies te zijn, deze oscillatoren op microschaal zijn zweepachtige structuren die zich uitstrekken uit het lichaam van de cel en flagella of cilia genoemd worden. Ze zijn terug te vinden in een aantal micro-organismen, zoals spermacellen, *Paramecium* en de algen *C. reinhardtii*. Bij mensen zijn cilia te vinden in de longen, luchtwegen en het middenoor. Cilia worden geactiveerd op een gecoördineerde manier om effectief hun functie uit te voeren, zoals bijvoorbeeld het draineren van slijm. De mechanismen achter de coördinatie van cilia zijn nog onderwerp van discussie. Het is niet duidelijk hoe zeer simpele organismen, zonder enig feedback systeem, complexe oscillatiepatronen kunnen ontwikkelen die coördinatie van een veelvoud van cilia of flagella omvatten. Er is grote interesse om de fundamentele principes die de dynamica van cilia bepalen te begrijpen, omdat dat belangrijke impact kan hebben voor medische en technische toepassingen.

Het doel van deze thesis is te onderzoeken welke mechanismen de synchronisatie van cilia en flagella reguleren.

Een hypothese is dat synchronisatie van cilia en flagella wordt gemedieerd door mechanische krachten die door de vloeistof worden overgedragen, namelijk hydrodynamische krachten. In deze studie bekijken we deze mogelijkheid experimenteel. We hebben een experiment ontworpen waarin we in realtime dynamisch reageren op een micro-organisme. We kozen als studie micro-organisme de algen *C. reinhardtii*. Op de *C. reinhardtii* leggen we hydrodynamische krachten op, in de vorm van een periodieke achtergrondstroom, en we meten hoe die krachten de flagellarische synchronisatie beïnvloeden. *C. reinhardtii* heeft twee flagella die continu samen kloppen met een frequentie van ongeveer 53 Hz. Door hun synchrone slagen kunnen de cellen voortstuwen in water en voer. Een bijzonder kenmerk van de twee flagella is dat ze op twee verschillende frequenties slaan wanneer ze worden geïsoleerd. In het bijzonder slaat één flagellum genaamd *cis-* flagellum op een frequentie van ongeveer 53 Hz, terwijl het andere flagellum, het *trans-* flagellum, op ongeveer 70 Hz slaat. Wanneer de cel echter zwemt, worden de twee flagella's gesynchroniseerd en kloppen ze op de frequentie van de *cis-*. Het begrijpen van het mechanisme dat zo'n synchrone slag in *C. reinhardtii* reguleert, zou het begrip van ciliaire dynamica in het algemeen vergroten. Een belangrijke eigenschap van cilia en flagellen is dat hun moleculaire structuur in hoge mate geconserveerd is onder verschillende eukaryote organismen en daarom wordt verwacht dat de activering en het gedrag van cilia in verschillende micro-organismen vergelijkbaar zijn.

In onze experimenten op *C. reinhardtii* vinden we dat een externe hydrodynamische versterking in staat is om de intrinsieke pulsfrequentie van de cel te verschuiven, wat

betekent dat flagellaire gedrag wordt beïnvloed door hydrodynamische interacties. We merken echter op dat zelfs door een hydrodynamische forcing op te leggen die 10 keer sterker is dan de hydrodynamische krachten die normaal door de cel worden ervaren, we slechts in staat zijn de intrinsieke pulsfrequentie van de cel enkele Hertz te verschuiven. Daarom heeft de externe hydrodynamische versterking een schaars effect op de flagellaire frequentie. Aangezien intrinsiek de frequentiemismatch tussen de twee flagella in de orde van 20 Hz ligt, is het onwaarschijnlijk dat de synchronie tussen flagella een gevolg is van hydrodynamische interactiekrachten. Deze resultaten worden bevestigd door numerieke simulaties waarin het stroomveld rond de cel in een typisch experiment is berekend.

Aangezien hydrodynamische interacties niet het belangrijkste mechanisme lijken te zijn achter flagellaire synchronisatie, stellen we een ander synchronisatiemechanisme voor dat gebaseerd is op intracellulaire mechanische koppeling van flagellen. In *C. reinhardtii* zijn de twee flagella mechanisch verbonden binnen de cel door een structuur van vezels. We voerden experimenten uit op een mutant (de *vfl3*), waar deze vezelstructuur in verminderd is. We hebben de synchronisatie tussen de twee flagella in *vfl3* nooit waargenomen, ook niet bij het opleggen van een externe hydrodynamische forcing. Deze resultaten suggereren dat synchronisatie tussen de twee flagella niet mogelijk is als de intracellulaire mechanische verbinding niet aanwezig is en het daarom waarschijnlijk lijkt dat het mechanisme dat verantwoordelijk is voor flagellarische synchronisatie gebaseerd is op de intracellulaire koppeling in plaats van de hydrodynamische krachten.

Bovendien toonden onze experimenten een zeer goede analogie tussen *C. reinhardtii* en een ideale zelfonderhoudende oscillator. *C. reinhardtii* gedraagt zich als een zelfonderhoudende oscillator met een goed gedefinieerd synchronisatiebereik dat wordt begrensd door een Arnold tong. Resultaten op meerdere cellen zijn consistent en identificeren hetzelfde synchronisatiegebied. Bovendien, wanneer het forceren is gestopt, keert de frequentie terug naar de oorspronkelijke frequentie binnen één slagcyclus. Er vindt geen permanente wijziging van de intrinsieke frequentie plaats na het tot 10 minuten lang opleggen van een externe forcering.

We hebben ook experimenten uitgevoerd waarbij de periodieke versterking sterker was op één flagellum dan op het andere flagellum, waarbij we de koppeling met de stroming maten. We hebben waargenomen dat de versterking die sterker op het *cis*-flagellum werkt, de synchronisatie van de flagellen met de forceren induceert, terwijl andersom nauwelijks synchronisatie wordt getriggert. Dit resultaat bevestigt de dominante rol van de *cis*- flagellum bij het beheersen van het slagpatroon en de dominantie van intracellulaire koppeling ten opzichte van hydrodynamische interactie in de koppeling tussen flagellen.

Ten slotte onderzochten we de rol van hydrodynamische interactie bij het antifase-kloppen dat wordt waargenomen in een mutant van *C. reinhardtii*, de *ptx1* mutant. We berekenen de hydrodynamische viskeuze krachten die worden veroorzaakt door de stroming en de hydrodynamische interactie tussen de flagellen. We vinden dat de eerste bijdrage een orde van grootte groter is dan de tweede. Deze resultaten geven aan dat het antifase-kloppen, evenals het normale infase-kloppen, niet wordt ondersteund door hydrodynamische krachten tussen de twee flagella.

NOMENCLATURE

LIST OF SYMBOLS

Latin Symbols

Symbol	Description	Units
a	cell radius	m
A_i	imposed amplitude of stage displacement	m
c	scaling factor	-
C	cost function	-
$\tilde{d}$	scaled pixel distance	-
D	surface of the cell and the pipette	m^2
$\mathcal{R}e$	Reynolds number	-
X	stage displacement signal	-
$\mathbf{f}$	distribution of hydrodynamic forces per unit length	N/m
f_0	intrinsic beating frequency	Hz
f_0^{post}	intrinsic frequency after forcing stops	Hz
f	average beating frequency	Hz
f_{F}	frequency of external forcing	Hz
f_{AP}	intrinsic frequency during antiphase beating	Hz
f_{IP}	intrinsic frequency during in-phase beating	Hz
f_{L}	beating frequency slow flagellum	Hz
f_{H}	beating frequency fast flagellum	Hz
$\mathcal{F}_0$	Stokes drag on a sphere	N
$\mathcal{F}$	magnitude of total force	N

$\mathbf{F}$	total force on a flagellum	N
$\mathbf{F}_{\text{motion}}$	force generated by flagellar motion	N
$\mathbf{F}_{\text{int}}$	flagella hydrodynamic interaction force	N
$\mathbf{F}_{\text{flow}}$	external background flow force	N
$\mathbf{G}_{ij}$	Stokeslet kernel	-
$\mathcal{H}$	Hilbert transform	-
$\mathbf{k}$	shape vector	-
I	pixel intensity	-
$I_{\text{cis}}(t)$	signal due to motion of *cis*-flagellum	-
$I_{\text{trans}}(t)$	signal due to motion of *trans*-flagellum	-
$\mathbf{I}$	identity matrix	-
l_{f}	flagellum length	m
L	characteristic length	m
m	Gaussian mean	-
$\mathbf{n}$	surface normal vector	-
p	pressure gradient	N/m^3
$\mathcal{P}$	rate of work of the hydrodynamic forces	W
$\mathcal{P}_{\text{e}}$	total elastic power	W
$\mathcal{P}_{\text{motion}}$	rate of work of the hydrodynamic forces due to flagellar motion	W
$\mathcal{P}_{\text{int}}$	rate of work of the hydrodynamic forces due to flagella interaction	W
$\mathcal{P}^{cis}$	total rate of work on *cis*-flagellum	W
$\mathcal{P}^{trans}$	total rate of work on *trans*-flagellum	W
P	probability density function	-
$\hat{P}$	time-independent solution	-
q_{max}	maximum of a periodic function	-
$\mathcal{Q}$	periodic function	-
r	radial position coordinate	m
$\mathbf{r}$	position vector along the centerline	m
$\mathbf{R}_{ij}$	rotlet kernel	-
s	arc-length along the flagellum	rad
$\mathbf{t}$	tangent vector	-
T	duration of the experiment	s
T_{Φ}	time duration for which the flagella are phase locked with the flow	s
T_{cis}	time duration for which the *cis*- flagellum is phase locked	s

T_{trans}	time duration for which the *trans*- flagellum is phase locked with the flow	s
$\mathbf{T}$	stresslet tensor	-
T_{eff}	intensity of Gaussian noise	-
$\mathbf{u}$	velocity field	m/s
$\mathbf{u}_S$	velocity field associated with a Stokeslet	m/s
U_0	cell free swimming velocity	m/s
U	swimming velocity	m/s
$\mathbf{U}$	velocity at the centerline	m/s
V	potential	-
w_1	weighting parameter of image intensity	-
w_2	weighting parameter of bending energy	-

Greek Symbols

Symbol	Description	Units
α	fitting constant	-
γ	flagella angle at the base	rad
Δ_0	steady state solution	-
Δ_{f}	phase difference between flagella	-
δ	Dirac-delta function	-
$\tilde{\Delta}$	transient solution	-
ϵ	coupling strength	Hz
θ_0	tangent angle	rad
κ	curvature	1/m
$\tilde{\kappa}_{\text{i}}$	non dimensional curvature	-
$\mathbf{\Lambda}$	linear operator	-
μ	fluid dynamic viscosity	Pa $\cdot$ s
ν	frequency detuning	Hz
$\boldsymbol{\nu}^T$	adjoint of the completion flow	-
ρ	fluid density	kg/m^3
σ	Gaussian standard deviation	-
τ	transient duration	s
$\tau*$	time to reach steady state	s
τ_R	relaxation time	s
$\phi^i_{\text{cis;trans}}$	instantaneous wrapped phase angle	rad
$\phi_{\text{cis;trans}}$	instantaneous unwrapped phase angle	rad

ϕ_F	forcing phase angle	rad
ϕ_{cis}	phase angle *cis-* flagellum	rad
ϕ_{trans}	phase angle *trans-* flagellum	rad
Ψ	double layer density	-
ζ	random noise in flagellar actuation	-

INTRODUCTION

1.1 SYNCHRONIZATION IN NATURE

The phenomenon that we now call synchronization was observed for the first time by the Dutch physicist Christiaan Huygens in 1665. In the winter of that year, while spending some time at home, he observed that two pendulum clocks hanging next to each other were swinging in perfect synchrony. He was surprised by this event given the imprecision of clocks at that time. Even if their motion was perturbed by some interference, the synchrony was restored shortly after. This accidental finding is recalled nowadays as the first documented investigation about the behaviour of 'coupled oscillators' [1]. But what happened to those pendulum clocks?

As Huygens explained in a letter to his father, since the two clocks were hanging from the same beam, a weak mechanical coupling was created between them through the beam. The transmission of imperceptible vibrations allowed the two pendulums to synchronize their swinging. Since Huygens observation, synchronization has been observed in physical, chemical and biological systems [2]. In nature, there are many examples of coupled oscillators. Regarding physiological processes, these include peacemaker cells in the heart that spontaneously synchronize with each other [3] and insulin secreting cells in the pancreas. In the brain, synchronized neural activity is associated both with normal physiological functions such as regulation of the circadian rhythm (the endogenous 24 hours oscillation in many biological processes), but also with diseases like schizophrenia, epilepsy or Parkinson's disease [4]. Fireflies blinking in synchrony at night or crickets chirping in unison are another spectacular example of synchronization involving a multitude of organisms [5, 6].

The aforementioned examples are synchronization processes at the macroscale. Synchronization is also observed in nature at the microscale and can involve one or a multitude of organisms, as discussed in the next paragraph. This thesis originates from the need to complete current knowledge on synchronization processes at the microscale.

SYNCHRONIZATION AT THE SMALL SCALE

Synchronization at the microscale is often observed to mediate processes like locomotion and fluid transport. Such processes are carried out by a number of micro-organisms including spermatozoa, bacteria and algae, which have developed the capability to propel in fluid environment in order to feed [7]. In these

micro-organisms, synchronization is found in the coordinated activation of whip-like structures extending from the cell body called flagella or cilia [8]. Synchronization of cilia and flagella's main purpose is to increase the efficiency in fluid transport. At the sub-micrometer scale characteristic of cilia and flagella, the viscous damping overcomes inertia by far. As a consequence, the physical principles ruling the swimming of a macroscopic organism like a fish or a human do not hold for a bacterium or a spermatozoon, making the propulsion at the microscale a very inefficient process. To illustrate this difficulty in motility, G.I. Taylor compares the motion of a sperm cell in its fluid environment with that of a human who is forced to swim in a pool filled with honey [9].

Since locomotion at the microscale cannot rely on inertia, micro-organisms developed particular propulsion strategies to overcome viscous dissipation and achieve an effective displacement in fluid medium. These strategies involve complex spatiotemporal organization in the activation and movement of cilia and flagella [10]. As a matter of fact, even if the environment is dominated by viscous dissipation, the coordinated beating of many cilia produces an effective fluid transport resulting in net propulsion. The ability of cilia and flagella to spontaneously beat and synchronize with one another has opened a rich discussion. It is still unclear which physical mechanisms allow a simple single cellular organism lacking any feedback system to develop complex oscillatory patterns involving coordination among a multitude of cilia [11] or among flagella in different cells [12]. A fundamental understanding of ciliary dynamics is still lacking, and would be of high interest for both medical and engineering applications [13, 14]. In the medical context, cilia are found in a variety of human organs and perform important physiological functions. Defects in ciliary activation are associated with a number of diseases, such as respiratory and cystic disorders of internal organs, alterations in vision, smell, hearings and infertility [15].

Engineering applications mimicking ciliary mixing properties have allowed the development of new biomimetic materials able to drive flows at the microscale [13]. Bio-inspired cilia closely resemble biological cilia and have the potential to be implemented in future biomedical applications [13, 16]. Ongoing investigations also include micro-robots for targeted drug delivery, minimally invasive medicine [17] and single cell manipulation [18]. Currently, artificial cilia are activated externally by magnetic fields but the future ambition is to control cilia internally by exploiting molecular motors as in the biological version [19].

As we discussed, cilia have an important role in human physiological processes and engineering applications, therefore have been largely investigated in the last decade to understand how the synchronous activation is achieved. Shedding light on this issue motivated the present work, as discussed in the next section.

1.2   AIM OF THE THESIS

In order to reproduce the beating patterns and organized activation of cilia, a thorough understanding of ciliary dynamics is needed. For example, cilia can form a metachronal wave to transport fluid. An open question is: which physical mechanisms regulate the transition from the disordered motion of thousand of cilia to the large

scale synchronous activation pattern? Mechanical interactions are a physical mechanism that has been suggested to mediate ciliary coordination.

In this thesis we investigate this hypothesis experimentally by mechanically interacting with flagellated micro-organisms in real time. The results obtained elucidate the role of mechanical forces in flagellar synchronization and challenge the actual models on flagellar motility.

1.3 OUTLINE OF THE THESIS

The following five chapters of this thesis are divided as follows. Chapter 2 is dedicated to the background on cilia and flagella synchronization and the relevance of this study within this research field. Given the current knowledge on cilia synchronization, it is not clear to which extent mechanical interaction among cilia through the fluid environment is involved in mediating their coordinated beating. We approach this problem experimentally and chapter 3 details the experimental setup and the experimental procedure. Chapter 4 presents the experiments, data analysis and results linking the behaviour of *Chlamydomonas reinhardtii* (*C. reinhardtii*) with that of an ideal oscillator. Details on the data analysis methodology are presented in this chapter since custom image processing algorithms are developed to extract the relevant information from experiments. Chapter 5 addresses in details the mechanism at the base of flagellar synchronization. Experimental data analysed in this chapter are combined with numerical flow reconstruction to provide quantitative description of the mechanical forces involved in flagellar motility. Finally, in chapter 6 we summarize the relevant findings in this study and provide an outlook for future perspectives on the investigation of flagellar motility.

BACKGROUND

The first visualization of spermatozoa and bacteria swimming dates back to 1677. The Dutch scientist Antoni van Leeuwenhoek developed the first microscope in Delft and discussed his observations on living creatures at the microscale in the 'Letter on Protozoa' [20]. His pioneering work raised numerous questions on fluid dynamics associated with the motility of microswimmers. From the second half of the 20th century, researchers started questioning the physical principles associated with micro-organism locomotion and proposed several theoretical models [9, 10].

In the last decade, improvements in experimental techniques allowed a more accurate visualization and characterization of the flow induced by swimming micro-organisms, resulting in more detailed modelling of the physical principles ruling this phenomenon. This chapter reviews the literature relevant to our study. After the details about the structure of cilia and flagella in 2.1, we discuss the state of art of theoretical models and experiments on microswimmers in 2.2, from G.I. Taylor's early work in 1951 until nowadays. In section 2.3, we describe the behaviour of *C. reinhardtii* and the reasons why it is now considered a model organism for cilia motility. In section 2.4, we highlight the most recent findings and open questions on the role of mechanical forces in flagellar synchronization. In section 2.5, we briefly discuss how our study challenges the current state of art.

2.1 STRUCTURE AND FUNCTION OF CILIA AND FLAGELLA

Living organisms can be classified as Prokaryotes and Eukaryotes. The former are simple and primitive organisms like bacteria, while the latter have a more complex internal structure and include animals, plants and fungi [21]. Flagella are present in both Eukaryotic and Prokaryotic organisms and are exploited for cell motility. These flagella present very different biomolecular structure between Eukaryotic and Prokaryotic cells, resulting in different propulsion mechanisms. Prokaryotic flagella are semi-rigid helical structures rotated at their base by a rotary motor [22]. Instead, Eukaryotic flagella are active structures displaying multiple bending modes (see figure 2.1).

Eukaryotic cilia and flagella share the same internal structure called '9 + 2 axoneme'. This structure is composed by nine outer microtubule doublets surrounding a central pair of singlet microtubules [23, 24]. Independently from the organism size or cell type, the axoneme diameter is widely conserved and measures about 0.25 μm (see inset in figure 2.2), while it varies significantly in length, from a few microns in cilia to more

than 2 mm in flagella [25]. As shown in figure 2.2, a doublet is composed by a complete A tubule with 13 protofilaments and an incomplete B tubule with 10 protofilaments. An inner and an outer row of dynein arms is attached to the A tubule of each doublet, connected to the B tubule of the neighbouring doublet. The axoneme deforms because of sliding between microtubule doublets relative to one another. The active sliding develops all along the axoneme, resulting in bend propagation. The generation of this movement relies on attachment and release of dynein arms at different times [26]. The molecular activation of the axoneme leads to different deformation and stroke patterns between flagella and cilia. A bending pattern is observed in uniflagellated organisms such as sperm cells (see figure 2.1 (a)) and consists of wave-like flagellar motion. This pattern is modelled as a sequence of travelling waves propagating from the flagellar base with increasing amplitude [27]. On the other hand, multi-ciliated organisms and the biflagellated organism *C. reinhardtii* display the beating pattern shown in figure 2.1 (b-d), that is modeled as a two components stroke. These components are a power stroke, in which effective force is imposed on the surrounding fluid and propulsion is generated, and a recovery stoke, in which the flagella return to their initial configuration, as shown in figure 2.1 (d). Given the simplicity of the organism, a fundamental question arises regarding the mechanisms leading to the coherent activation of dynein arms and the generation of precise self-organized beats [28]. This work does not address the details of the molecular structure of flagella but focuses on the generation of organized motion of multiple flagella in a fluid. The physical principles ruling flagella and fluid interaction are presented in the following section.

2.2 MICROSWIMMERS HYDRODYNAMICS

We now consider how flagella deformations interact with the fluid environment to generate motility.

2.2.1 THE STOKES EQUATIONS

At the macroscopic length scale, an organism, like a fish or a man, swims by pushing large volumes of water in one direction in order to effectively move in the opposite one. This propulsion mechanism exploits inertia. Due to the size of the organism, the stresses imposed on the fluid due to inertia are orders of magnitude larger than the stresses due to viscous interaction between the swimmer and the fluid. This ratio of forces is described by the Reynolds number:

$$\mathcal{Re} = \frac{\rho L U}{\mu}, \tag{2.1}$$

where L is the characteristic length of the body, U is the swimming velocity, ρ is the fluid density and μ is the fluid dynamic viscosity. In the case of a swimming fish, the Reynolds number is $\mathcal{Re} \sim 10^3$ [10]. However, the swimming of a *C. reinhardtii* cell at the microscopic length scale is governed by completely different physical principles. Due to the small size of the cell (approximately 10 μm), the magnitude of viscous forces
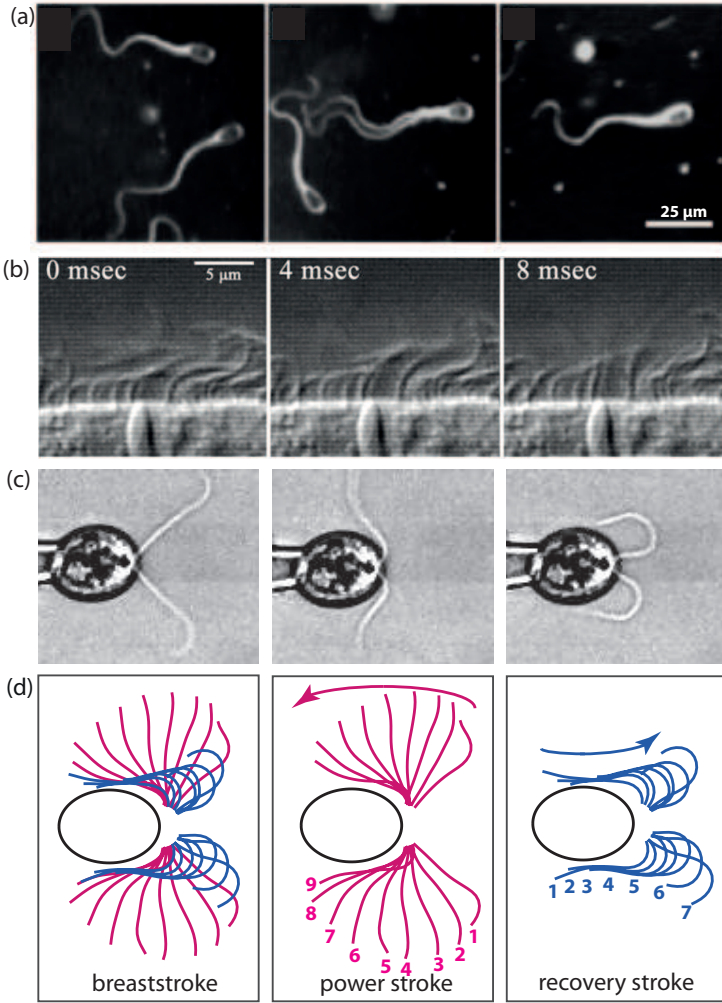
Figure 2.1: (a) Sequence displaying synchronization between two cells of bull spermatozoa. Adapted from [29]. **(b)** Snapshots of cilia in epithelium of planarian *Schmidtea mediterranea* synchronized in a metachronal wave. Adapted from [30]. **(c)** Frames displaying the breaststroke synchronization between flagella of the same cell in *C. reinhardtii*. **(d)** Flagellar strokes in *C. reinhardtii* during one beat cycle. The beating cycle is composed by a power stroke (*purple*) and a recovery stroke (*blue*).

generated in the fluid is typically three orders of magnitude larger than inertial forces, such that $\mathcal{Re} \sim 10^{-3}$.

The dynamics of the fluid can be described by the Navier-Stokes equations:

$$\rho\left(\frac{\partial \mathbf{u}}{\partial t} + \mathbf{u} \cdot \nabla \mathbf{u}\right) = -\nabla p + \mu \nabla^2 \mathbf{u}, \tag{2.2}$$

$$\nabla \cdot \mathbf{u} = 0, \tag{2.3}$$

Figure 2.2: *Left* The eyespot is a light sensor. The flagellum close to the eyespot is named *cis*, the one on the opposite side of the cell body is named *trans*. *Top inset* Transmission Electron Micrography of *C. reinhardtii* flagella showing one flagellum. Image provided by Da Wei. *Bottom inset* Internal structure of the Eukaryotic flagellum [31].
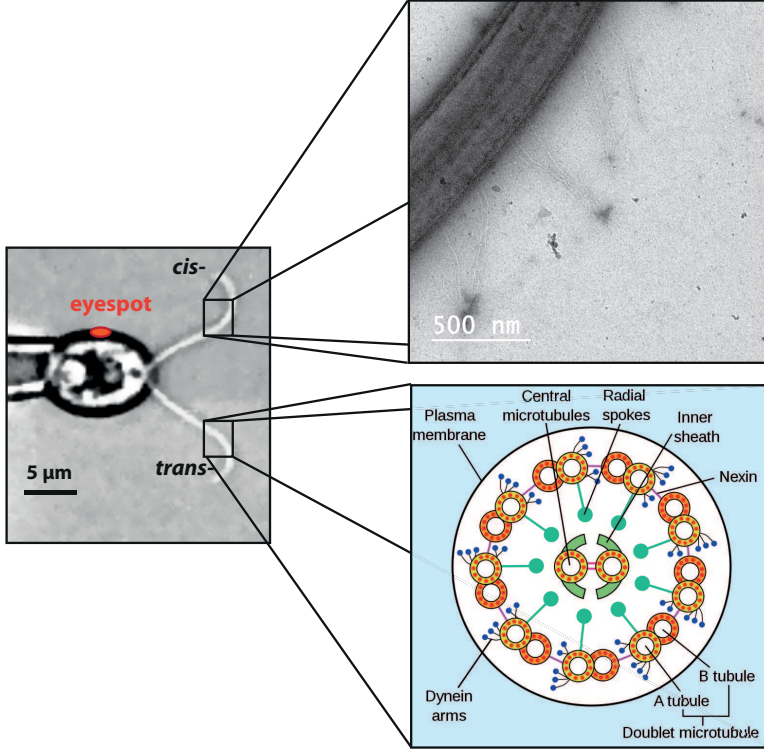
where p is the pressure and $\mathbf{u}$ is the velocity field. Given the swimmer length scale L and the characteristic velocity U, equations 2.2 and 2.3 can be rewritten in non-dimensional form:

$$\mathcal{R}e\left(\frac{\partial \mathbf{u}^*}{\partial t^*} + \mathbf{u}^* \cdot \nabla^* \mathbf{u}^*\right) = -\nabla^* p^* + \nabla^{*2} \mathbf{u}^*, \qquad (2.4)$$

$$\nabla^* \cdot \mathbf{u}^* = 0, \qquad (2.5)$$

where $\nabla^* = L\nabla$, $\mathbf{u}^* = \mathbf{u}/U$, $p^* = p/(\mu U/L)$ and $t^* = t/(L/U)$. At the length scale typical of *C. reinhardtii*, the left term in equation 2.4 (representing inertial forces) can be neglected and locomotion is governed by the Stokes equations:

$$0 = -\nabla p + \mu \nabla^2 \mathbf{u}, \qquad (2.6)$$

$$\nabla \cdot \mathbf{u} = 0. \qquad (2.7)$$

The absence of all inertia terms on the left hand side of Eq. 2.6 results in linearity and time independence and leads to kinematic reversibility [32].

The linearity of Stokes equations allows solutions to be found by superposition of fundamental solutions. This analytical property is exploited by numerical methods, such as the Boundary Element Method (BEM), which is used in this thesis to compute flow velocity fields and hydrodynamic forces relevant to flagellated microswimmers (details in 5.1). A fundamental singular solution in low Reynolds flows is called the *Stokeslet* [33]. It represents the flow field generated by a point force perturbation of strength **f**. This solution is obtained by solving the Stokes equations for a point force $\delta(\mathbf{x})\mathbf{f}$, where $\delta(\mathbf{x})$ is the three-dimensional Dirac-delta function centred at $\mathbf{x} = \mathbf{0}$. Eq. 2.6 then becomes:

$$0 = -\nabla p + \mu \nabla^2 \mathbf{u} + \delta(\mathbf{x})\mathbf{f}. \tag{2.8}$$

The solution to Eq. 2.7-2.8 yields the Stokeslet, Green's function for the Stokes equations. The solution for velocity can be written as:

$$\mathbf{u}_S(r) = \frac{1}{8\pi\mu}\left(\frac{\mathbf{I}}{|\mathbf{r}|} + \frac{\mathbf{rr}}{|\mathbf{r}|^3}\right)\mathbf{f}, \tag{2.9}$$

where **I** is the identity matrix and **r** is the position vector from the origin, assuming that the point force **f** is applied at the origin. The flow due to such a point force is long ranged and decays as $1/r$ (see Eq. 2.9). The far field approximation of the flow generated by a sphere translating under the influence of an external force is an application of the Stokeslet. However, when modelling free swimming micro-organisms, the far field flow cannot be represented by the Stokeslet, since the swimmer does not impose a net force on the surrounding fluid. Higher order fundamental solutions can be derived from the Stokeslet, one derivative of the Stokeslet is the Stokes dipole which decays as $1/r^2$ [34]. It can be separated in a symmetric part, the *stresslet* [35], and an anti-symmetric part, the *rotlet*. Physically, the stresslet represents stretching of the fluid along the stresslet principal axes. The rotlet corresponds to the flow due to a point torque. Several far-fields around microswimmers can be described by superposition of singularities. As an example, the sperm cell generates a positive force dipole and is therefore called *pusher* while the algae *C. reinhardtii* creates a negative dipole, hence is modelled as a *puller* [34] (see section 2.3).

2.2.2 THEORETICAL MODELS FOR MICROSWIMMERS

In our study of flagellar synchronization, we also discuss the agreement between experimental observations and theoretical model. Several models regarding cilia motility and synchronization are available in the literature. The studies most relevant to our work are presented in this section and grouped into early pioneering work on flagella motility, models of propulsion at low Reynolds number, studies on cilia swimming efficiency and models of cilia synchronization based on hydrodynamic forces. The dynamics of ciliary synchronization is very complex and involves the coordination of structures at multiple length scales, from the molecular level to the continuum of the flow field. Therefore, models need to simplify certain aspects, based on the specific question addressed [36].

EARLY WORKS ON FLAGELLA MOTILITY

Early studies of collective swimming date back to the middle of the 20th century. Since, at low Reynolds numbers viscous forces are larger than inertial forces, how can a small organism propel itself? This question, first addressed by Sir Geoffrey Taylor in 1951, initiated the study of the hydrodynamics of microswimmers [9]. To gain insights into the motion of the sperm flagellum, G.I. Taylor investigated the swimming of thin sheets immersed in viscous fluid [34]. A few years before, James Gray observed that two sperm cells in close contact tend to synchronize their flagella [37] (see figure 2.1 (a)). Taylor investigated the consequence of such synchronization in terms of swimming efficiency. He observed two adjacent waving sheets and found that, when the waves are in phase, the viscous dissipation is minimized, resulting in more efficient propulsion.

PROPULSION AT LOW REYNOLDS NUMBER

The problem of characterizing swimming efficiency and the hydrodynamic forces at the microscale initiated several studies on propulsion at low Reynolds number, based on the observation of flagellated cells (mostly sperm cells). These models suggested that an organism swimming at low Reynolds number can propel only by generating an anisotropic movement. This property is indeed observed in the algae *C. reinhardtii* that is the object of this investigation. This phenomenon was named 'the Scallop theorem' by Purcell [10] (see figure 2.3). If a swimmer at low Reynolds number deforms with a scallop-like time-reversible sequence of shapes, it will not experience a net displacement. Consequently, the flagella in a microswimmer should undergo anisotropic non-reciprocal deformations to generate propulsion [34].

From these early intuitions on cilia hydrodynamics, deciphering the physics behind the activation of those tiny appendages has encouraged the development of many theoretical models. Overall, two main approaches have emerged on modelling the ciliary beating dynamics.

THE STROKE EFFICIENCY IN CILIA

The first approach focuses on the energetics of the ciliary stroke. Ciliary beating is a two phase mechanism, composed by an effective stroke, in which the cilium moves as a rod and pushes the fluid, and a recovery stroke, where the cilium folds and returns to the initial position with low drag motion [38]. This mechanism has been studied theoretically to show the different rate of work involved in the power and in the recovery stroke and also to explain how the coordination of many cilia to form a metachronal wave (shown in figure 2.1(b)), increases the drag efficiency [39, 40]. The mechanism inducing this metachronal coordination is however largely debated; some models supporting the necessity to have a strong hydrodynamic coupling between cilia [41], others suggesting that synchronization can occur independently from the strength of hydrodynamic coupling [42].

SYNCHRONIZATION THROUGH HYDRODYNAMIC FORCES

The second approach focuses on the role of hydrodynamic forces in mediating synchrony among many cilia. In this group of models, cilia are coarse grained and represented by spheres. Since in the far field the filament is visualized as a point, the flow field generated is also considered analogous to the one generated by a moving sphere [43]. The model by Lenz shows that synchronization can be achieved in arrays of cilia via hydrodynamic interactions for any beating pattern. This model has been improved by Niedermayer, Eckhardt and Lenz by treating each cilium as a separate oscillator generating a certain flow field. The total velocity field is given by the superposition of the separate flow fields generated by each cilium. As a result, adjacent cilia interact hydrodynamically and adjust their radius of oscillation to phase-lock [44]. This model has been extended to a variety of trajectory shapes, showing that several beating patterns are efficient in inducing synchronization [45–47]. This variety of beating patterns includes also the breaststroke in *C. reinhardtii*, in which flagella can be approximated by two spherical beads rotating in antiphase along circular trajectories [48]. Regarding the ciliary beat representation, the first approach based on power and recovery strokes is more accurate, however the second approach provides useful insight into the role of hydrodynamic in cilia synchronization [8].
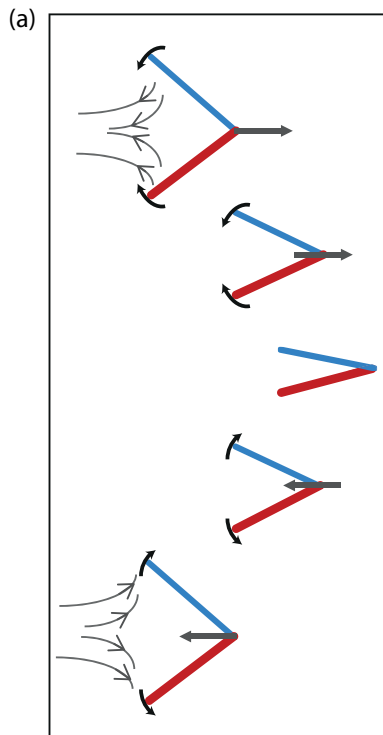

Figure 2.3: In absence of inertia the scallop is a non swimmer model.

2.2.3 EXPERIMENTS ON MICROSWIMMERS

The first observation of micro-organisms swimming dates back to 1677, when Antoni van Leeuwenhoek developed the first microscope. However, quantitative studies on biological organisms and in particular on flagellated cells are more recent [20]. Here we discuss relevant experimental studies on biological and artificial swimmers that present flagellar and ciliary properties of interest in the context of this thesis.

BIOLOGICAL SWIMMERS

Among biological flagellated cells, the sperm cell has largely been investigated. In 1949, Rothschild measured the swimming velocity of bull sperm [49]. More recently, studies on the collective behaviour of dense sperm cell suspensions have highlighted that sperm cells are likely to aggregate in vortices. These vortices are arranged in hexagonal patterns. Transition from random distribution of spermatozoa to hexagonal clusters is based on the density of the suspension, indicating the primary role played by hydrodynamic forces in clusters formation [50].

The algae *C. reinhardtii* is another biological organism widely investigated in the last decades and it is the organism studied in this thesis. The large body of literature available for *C. reinhardtii* is further discussed in section 2.3.

ARTIFICIAL SWIMMERS

Research on micro-motility and synchronization has also focused on artificial microswimmers. These swimmers represent a good reproduction of the behaviour of biological ones. Studies on artificial swimmers allow to focus on specific aspects of flagellar motility, such as flagellar actuation [51] and fluid transport [52]. Apart from contributing to a better understanding of the behaviour of real flagella and cilia, artificial swimmers hold promises in bio-robotic applications [53]. In 2005, Dreyfus *et al.* created artificial flagella for the first time [54]. Moreover, artificial cilia have been investigated for microfluidics applications. Examples include cilia embedded with paramagnetic particles controlled via an external magnetic field [13] or light-actuated cilia obtained by inkjet printing that bend when exposed to certain light wavelengths [55]. Also computational studies were performed to characterize the hydrodynamics of artificial cilia [56]. A recent application of artificial cilia is in the assembly of micropumps and mixers [52].

The understanding of cilia synchronization mechanisms is another application of artificial systems of swimmers. Optical tweezers were used to study colloids interaction. The periodic motion of two beads can be synchronized through hydrodynamic interactions if they are sufficiently close [57]. Similarly, two chiral microrotors, actuated by optical tweezers, can be synchronized by hydrodynamic interactions alone [58]. Carpets of actuated magnetic slender rods were used to study collective behaviour showing that, while isolated cilia follow circular trajectories at constant angular speed, the cilia in the carpet do synchronize at constant angular speed, but with elliptic trajectories [59].

All these experimental studies on the synchronization of many oscillators address questions about the collective behaviour of active elements and highlight the synchronization properties of large ciliary systems. Recently, studies of flagella synchronization have focused mainly on a system with few biological flagella: the algae *C. reinhardtii*. This unicellular organism constitutes an excellent model organism for synchronization studies, as discussed in 2.3 [8, 36].

2.3 C. REINHARDTII

One organism that has been of particular interest for motility studies and flagellar hydrodynamics is the the unicellular algae *C. reinhardtii*, which is also object of the present study. The structure of cilia and flagella is highly conserved within eukaryotes [60]. Their properties and functioning are common to a variety of organisms. *C. reinhardtii* is widely used in studies of flagellar dynamics as it is simple to grow and visualize. Furthermore, a wide variety of mutants is available, allowing to investigate cell properties related to motility, phototaxis, and photosynthesis.

STRUCTURE AND FUNCTION OF C. REINHARDTII

C. reinhardtii is a unicellular species in the family of the volvocine green algae, as shown in figure 2.4. The cell body has an oval shape with a major axis of approximately 10 μm. At the anterior edge of the body grow two flagella, 12 μm long and capable of beating in synchrony for long periods of time [61]. The two flagella, named *cis*-flagellum and *trans*-flagellum, are distinguished according to their proximity to the eyespot, a light sensor located on the cell body (see figure 2.2 (a)). During cell division, flagella are retracted in the cell body. Each mother cell is divided in two daughter cells and the basal bodies, tubular structures that anchor the flagella to the cell body, duplicate. The *trans*-flagellum is grown from the mother basal body (the basal body that was already present before cell division), while the *cis*-flagellum originates from the daughter basal body, which is assembled during the division [62–64]. The two basal bodies are mechanically connected by the distal striated fiber, a contractile fiber $\approx$ 200 nm long, shown in figure 2.5 [65, 66]. *C. reinhardtii* performs phototaxis, and this process requires light. Therefore the cell usually swims in a helical path so that the eyespot can sense light in all directions [67].

2.3.1 EARLY STUDIES

Early works on *C. reinhardtii* motility have highlighted several important aspects and properties of *C. reinhardtii*, such as the beating patterns, the response to light changes, or the intrinsic frequency differences between *cis*- and *trans*-flagellum. Furthermore, these early studies are at the origin of recent modelling based on non-linear oscillator theory. The synchronous beating of flagella is called *breaststroke*, as it is reminiscent of the breaststroke swimming in a human, shown in figure 2.1(c). This movement was first observed in 1967 by Ringo along with the undulatory beating in which flagella move with a pattern very similar to the sperm cell waveform, shown in figure 2.6(b) [69].
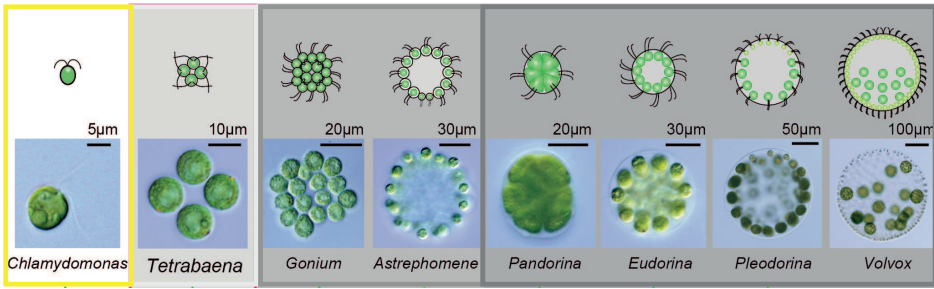
CHAPTER 2

Figure 2.4: Family of the volvocine green algae to which *Chlamydomonas reinhardtii* belongs. Adapted from [68].
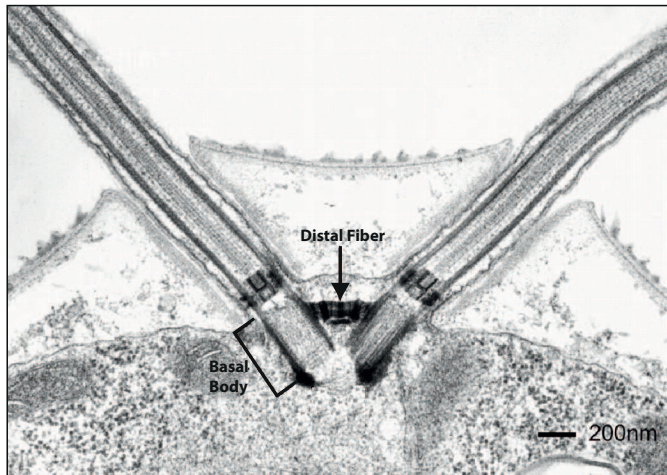

Figure 2.5: Longitudinal section of *C. reinhardtii* by electron micrography. Adapted from [66].

Rüffer and Nultsch performed the first high speed visualization on *C. reinhardtii*. They recorded freely swimming cells at up to 500 fps and tracked the flagellar waveforms of consecutive beats and the motion of the cell. They observed that flagella beat together at a frequency of $f_0 = 40 - 64$ Hz, and the swimming velocity U_0 varies between 100 and 200 μm.s^{-1}. Furthermore, the cell swims along a helical path and, every $30 - 36$ beats, a complete rotation is achieved, suggesting that the flagellar beating and position is not planar but 3-dimensional, causing this rotation [61]. Kamiya and Hasegawa found that, intrinsically, the *trans*-flagellum beats at frequency 30% higher than the *cis*-flagellum, although in normal conditions the two flagella beat together at the frequency of the *cis*-. Furthermore, they suggested that the dominance of *cis*- or *trans*-flagellum depends on calcium concentration [70, 71].

The flagellar photoresponse has been investigated by performing cinematography on a cell held with a micro-pipette and applying light changes. When subjected to a sudden increase in light, 40% of cells have a transient decrease in beating frequency for 10-20 beats, while the other cells display a slight increase in frequency that is sustained for a longer time than the decrease. This frequency change is accompanied

by a change in beating pattern [72, 73] that is later defined as *slip* [74], shown in figure 2.6 (a). Investigation on phototactic behaviours have reported the existence of other beat patterns such as the shock response, shown in figure 2.6(b). This phenomenon is triggered by a sudden exposure to high light intensities. It consists of a switch to an undulatory beating followed by a change in swimming direction and often also a tumble or circle. After the shock response, the beating frequency slows down. It also happens that one flagellum or both become temporarily inactivated.

MOTILITY PATTERNS

To summarize, three beating patterns have been observed in the wild-type (wt) strain of *C. reinhardtii*: synchronous beating, asynchronous beating, and undulatory beating [75]. The breaststroke is composed of a power stroke, where flagella impose a higher force on the fluid and the cell propels in direction opposite to flagella displacement, and of a recovery stroke in which flagella are folded along the cell body to minimize drag (see figure 2.1(d)) [34]. During breaststroke, both flagella beat at the same frequency in the range f_0=45-60 Hz [61]. The asynchronous beating is made of slips (shown in figure 2.6(a)). A slip is a sudden interruption of frequency locking between the flagella, where the *trans*-flagellum beats at a frequency that is 30% higher than the *cis*-flagellum [71]. It causes a rotation of the cell body[76] and has been suggested to be at the origin of sudden changes in swimming direction [61, 74]. At the origin of a *slip*, there is possibly a differential response of the two flagella to modifications in calcium levels inside the cell [60]. The *cis*-flagellum seems dominant at low calcium concentration (less than 10^{-8} M), while the *trans*-flagellum seems to prevail at higher calcium levels ($10^{-7} - 10^{-6}$ M) [70, 77]. The third type of beating pattern observed in *C. reinhardtii* is the undulatory beating, shown in figure 2.6(b) [78]. This pattern resembles the sperm cell's waveform and results in the cell swimming in the direction opposite to that of the breaststroke. This behaviour is also called shock response and can be triggered by a sudden light flash [79]. It is suggested to happen as consequence of a sudden influx of calcium ions in the flagella. After the shock response is initiated, calcium in excess is gradually expelled by the flagella. While the switch to undulatory beating is simultaneous in both flagella, the recovery of the breaststroke takes a different time for each of them and is usually faster in the *cis*-flagellum [79].

MUTANTS

The study of mutants yields important insights into the properties of an organism [80]. A rich variety of *C. reinhardtii* mutants is available and many of them have mutations that affect motility. We only discuss two types of mutants that are relevant to our study. The mutant *vfl3* has defects in the distal striated fiber. The role of the striated fibers in regulating motility remains unclear. However, these fibers are present in most ciliated cells, including the cilia in sensory organs [21]. Possible functions of these fibers include coordination of flagellar movement, strong anchoring and proper positioning of the basal body [81, 82]. The beating pattern in *vfl3* is different than in wild-type (*wt*).
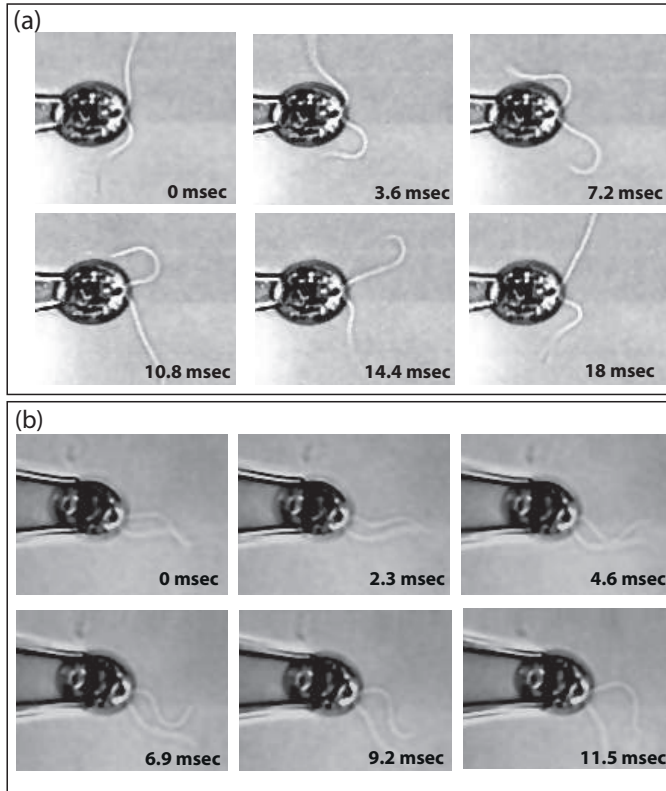
Figure 2.6: (a) Snapshots showing a *slip* in wild-type (wt). **(b)** Sequence showing the undulatory beating in wild-type.

Flagella do not perform breaststroke and do not synchronize with each other (see figure 2.7(a)).

Another mutant investigated is *ptx1*. It does not have known structural defects as for *vfl3*, but shows anomalous phototaxis [61, 77, 83], and performs a peculiar beating pattern, later referred to as antiphase (AP) [83]. *Ptx1* seems to lack the differential response of the two flagella to calcium that mediates phototaxis. Therefore, the two flagella are suggested to respond to calcium variations in analogous way and not oppositely as in wt, with consequences on the beating pattern. In this mutant, two synchronization modes are observed: an in-phase (IP) mode identical to the synchronous breaststroke in wt and an antiphase (AP) synchronization mode in which the two flagella beat at higher frequency, and one flagellum performs the power stroke, while the other one performs the recovery stroke (see figure 2.7 (b)).

2.3.2   RECENT DEVELOPMENTS ON MOTILITY

Thanks to a recent development in visualization tools, in particular high speed digital recording and image processing, quantitative insight on flagellar behaviour became apparent [84]. New biophysical studies on flagellar synchronization have focused on
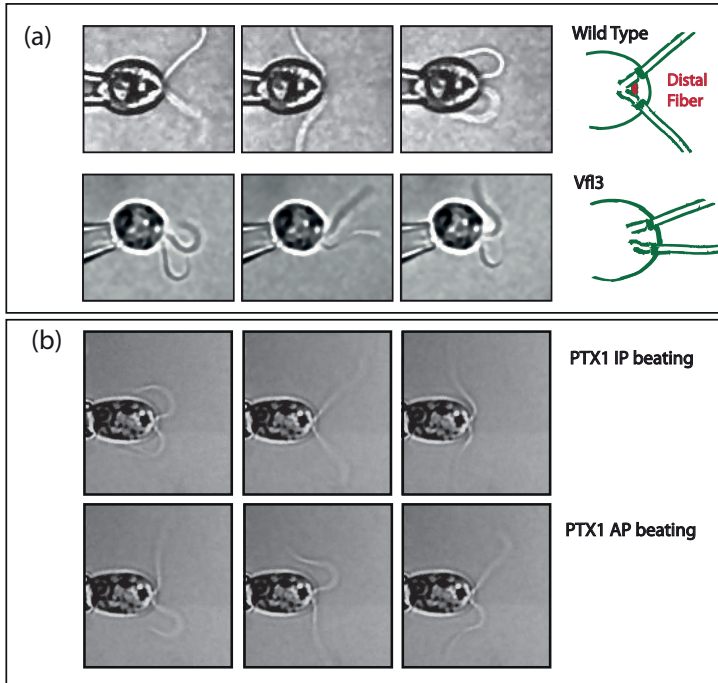
Figure 2.7: (a) Comparison between beating pattern in wild-type (wt)(*top*) and *vfl3* mutant (*bottom*). **(b)** *Ptx1* mutant during in-phase (IP) beating (*top*) and during anti-phase (AP) beating (*bottom*).

the green algae *C. reinhardtii*. These studies have provided insight into the flow field generated by the algae swimming and the synchronization between flagella.

In our study, we focus on interflagellar synchronization and we also characterize the flow field in experiments with *C. reinhardtii* held fixed at the tip of a micropipette. Therefore, we discuss in this section the state of the art on velocity field computation in *C. reinhardtii*. The findings on synchronization between flagella are discussed in 2.4.

The velocity field around a swimming flagellated organism has been characterized experimentally for organisms like the sperm cell [85], the algae *C. reinhardtii* [86, 87], and the algae *Volvox carteri* [86]. *Volvox carteri* is a multicellular species in the volvocine algae (see figure 2.4), having a radius of about ≈ 200 μm, which propels thanks to about 10^3 *Chlamydomonas*-like cells located on its surface [88]. The flow field around *C. reinhardtii* freely swimming in solution has been measured [86, 87]. We are interested in the flow field generated by a single *C. reinhardtii* cell. This flow field is quantified numerically from our experimental data in section 5.2.

For *C. reinhardtii*, the puller-stresslet representation holds only in the far-field, at a distance $\gtrsim 7R$ (with R the cell radius of about 5 μm) where the flow velocity is $\lesssim 1$ μm.s^{-1} [86]. In proximity of the cell, the flow is well described by a three-Stokeslet model, with one source corresponding to the cell body, and two located at the average position of the flagella [86]. The full velocity field around a swimming *C. reinhardtii* cell has also been characterized and the mechanical power dissipated by *C. reinhardtii*

computed [87]. The flagellar motion, and hence flow field generated by flagella, is mainly planar with small three dimensional components. The velocity field measured in [87] is more than 4 times larger than predictive models of the mean velocity field.

2.4 DO HYDRODYNAMIC FORCES MEDIATE FLAGELLAR SYNCHRONIZATION?

In recent years, many studies have looked into the role of hydrodynamic forces in flagellar synchronization. Several theoretical studies have suggested that groups of cilia can be entrained by hydrodynamic interactions [44, 45, 89, 90] (see section 2.2.2). In 2009, Polin *et al.* [74] characterized the synchronization and incidence of slips in a single cell held at the tip of a micropipette. Flagella were modelled as two self-sustained oscillators with different intrinsic frequencies. During breaststroke, these oscillators are coupled together in phase at the frequency of the *cis*-flagellum [74, 91]. Estimation of the coupling strength (ϵ) between the flagella was found to be in good agreement with the idealized flagellar model from Niedermayer [44], hinting at the fact that hydrodynamic coupling is a major contribution to flagella synchronization [74]. Additional work by Goldstein *et al.* [91] addressed the dependence of flagellar coupling on their length, as predicted in Niedermayer's model [44].

Synchronization was investigated during flagella regrowth following deflagellation induced by a mechanical damage [60, 91]. This study brought new insights on the mechanism leading to synchronization. The coupling strength ϵ between the flagella was found to scale with the flagellar length, and the scaling is consistent with Niedermayer's model [92]. The aforementioned studies reported in the literature suggest that flagellar synchronization is mediated by hydrodynamic forces. Our study is motivated by the need to quantify those forces and their role in flagellar synchronization. In very recent years, Brumley *et al.* [12] investigated whether flagella could synchronize through hydrodynamic interactions only. Two *Volvox* somatic cells, each with one flagellum, were captured with two micropipettes. When flagella are close enough, phase locking occurs, and the coupling strength ϵ scales inversely with the distance between the two cells. These results are in agreement with Niedermayer's model. Namely, when the power strokes are parallel, flagella synchronize in phase, as it happens in cilia, while when the power strokes are in opposite direction, flagella synchronize in antiphase, as in *C. reinhardtii*. This study provides experimental evidence that hydrodynamic interactions alone can induce phase locking of otherwise uncoupled flagella. It must be noted that the intrinsic frequency mismatch between *Volvox carteri* somatic cells is about 10%, hence much smaller than in *C. reinhardtii*.

The work discussed so far highlights the putative role played by hydrodynamic interactions in the mediation of flagellar synchronization. However, it has been long discussed that hydrodynamic interaction between the flagella is not necessary to achieve synchronization. Early work from Ringo [69] combined observation of motile cells with microscope imaging of the flagellar apparatus, and hypothesised that the distal fibers could play a role in flagellar coupling. Further observations that isolated cell apparatus of *C. reinhardtii* can perform breaststroke like normal cells, suggest that flagellar coordination is mediated internally to the flagellar apparatus and not due to

hydrodynamic interactions [93]. More recently, Leptos *et al.* [83] studied the mutant *ptx1* by high speed visualization. Observations of the AP beating mode in *ptx1* required a re-visitation of the elastohydrodynamic model, and suggested that AP beating is the expected coupling mechanism predicted by Niedermayer's model. According to the model, the AP coupling observed in cilia is sustained by hydrodynamic interactions. As a consequence, Leptos *et al.* [83] suggested that the AP synchronization in *C. reinhardtii* is sustained by hydrodynamic interaction forces, while *C. reinhardtii* breaststroke is not.

Other studies by Friedrich *et al.* [48] and Geyer *et al.* [76] have challenged the view that flagellar synchronization is mediated by hydrodynamic interactions. In this model for *C. reinhardtii* swimming, flagellar synchronization is obtained through hydrodynamic friction forces instead of hydrodynamic interactions [48, 76, 94]. According to this model, yawing of the cell body during swimming is due to flagella beating. If flagella beat in phase, the cell swims straight, but when flagella lose synchrony the imbalance in the torque imposed by left and right flagella is compensated by the rotation of the cell [48, 76]. The model shows that hydrodynamic interaction forces between the two flagella are negligible with respect to the forces due to the cell yawing. The main conclusion of this work is that synchronization observed in *C. reinhardtii* is a direct consequence of the cell's rocking motion rather than of the hydrodynamic interactions between flagella. A limitation of this work is that it does not account for the synchronization observed in cells held at the tip of a micropipette, in which yawing is not possible.

Despite the fact that the extent to which hydrodynamic interactions influence flagellar synchronization remains unclear, there is a consensus that hydrodynamic forces do affect synchronization. Our study quantifies the extent of the role of hydrodynamic forces in *C. reinhardtii* motility.

2.5 SCIENTIFIC APPROACH

This thesis work is originally motivated by the need to shed light on the dominant synchronization mechanism in cilia motility. As discussed above, several studies support the hypothesis that hydrodynamic interactions are at the origin of synchronization. Does this result imply that hydrodynamic interactions are the mechanism behind cilia synchronization or should other contributions be considered? As a model organism for our investigation we chose the algae *C. reinhardtii*. Then, we addressed the following questions. In *C. reinhardtii*, do flagella synchronize via hydrodynamic interactions [91], or via yawing motion of the organism [76], or via mechanical stresses directly transmitted between the flagella through the basal bodies [83]? Is it possible to actively control flagellar beating with an external periodic oscillator? Early work on starfish sperm cells showed that it was possible to entrain the flagellar beating frequency by vibrating a microneedle close to the flagellar base. This is the first example of coupling between flagella and an external periodic oscillator [95]. A sperm cell held at the tip of a micropipette was rhythmically vibrated, and the cell frequency synchronized with the pipette vibration [96, 97]. Recently, mode-locking of the hair cells has been investigated by attaching an elastic glass fiber to a stereociliary bundle. A periodic sinusoidal displacement was imposed to the fiber to

reproduce the mechanical stimulation imposed on the hair cells by sound *in vivo*. In absence of any stimulation, the ciliary bundle displays spontaneous anharmonic noisy oscillations. When the elastic fiber is attached and kept still, the oscillation becomes more regular. Subsequently, a weak stimulus at increasing frequency is imposed on the fiber and complete mode locking is observed for several periods in proximity of the characteristic frequency of the hair cell($\approx$ 20 Hz) [98]. All these studies highlight that flagella and cilia show some properties of ideal oscillators and respond to external mechanical forcing. Despite the extensive research available on *C. reinhardtii*, no evidence is available on the influence of external oscillatory perturbations on the motility of this organism.

We developed an experimental method that allows to dynamically interact with micro-organisms in real time. This is performed by imposing controlled mechanical forces on the organism at the relevant length and time scales and within the relevant force range. We investigate synchronization of flagella in *C. reinhardtii* with an external periodic forcing in the form of a periodic background uniform flow. The flow mimics the hydrodynamic forces experienced by a cell during swimming (details are discussed in 4.1). Our results challenge the present understanding of flagellar motility and set the ground for more accurate theoretical modelling of the collective dynamics in active biological systems.

EXPERIMENTAL METHODOLOGY AND DATA ANALYSIS

We want to address to what extent hydrodynamic forces are involved in flagellar synchronization in *C. reinhardtii*. For this purpose, we developed a custom made experimental setup that allows us to impose a periodic hydrodynamic forcing on a single cell. This forcing of controlled frequency and amplitude mimics the background flow generated by a freely swimming cell. The possibility of the cell to couple with this external flow yields insights into the role of hydrodynamic forces in mediating flagellar synchronization. In this chapter, we discuss in details the experimental setup along with the experimental methodology. In section 3.1 we provide an accurate description of the cell growth and monitoring procedure. In section 3.2 we describe all the setup components, including the necessary calibration tests. In section 3.3 we explain the experimental procedure and image acquisition.

3.1 CELL CULTURE

Our study focuses on the behaviour of *C. reinhardtii*, a model organism for studies on synchronization and motility [99]. Established growth protocols have been followed for cell culture. Quiescent cells are kept in solid agar slants (see figure 3.1) under constant light with low intensity equivalent to $\approx 30 \ \mu E^1.m^{-2}.s^{-1}$. Cells are re-streaked monthly on fresh agar to prevent ageing of the slants [101]. Cell cultures are initiated in liquid medium by dispersing a sample of quiescent cells from the agar into a flask containing cell growth medium. The flask is a 250 ml Erlenmeyer containing 100 ml of medium. In this study, we have two different growth media: Tris-minimal medium [60] for wt (strain CC125) and *ptx1* (strain CC2894), and TAP medium for *vfl3* (strain CC1686) [60].

We use two growth conditions in our study: phototrophic and photoheterotrophic. Under phototrophic conditions, cell metabolism depends entirely on light. Cells reduce carbon dioxide into nutrients (glucose) through photosynthesis. In photoheterotrophic conditions, cells can grow and divide also in absence of light, thanks to an organic carbon source present in the medium.

In Tris-minimal medium, the cells grow fully phototrophically. Under these conditions, CO_2 bubbling in the flask is needed to facilitate photosynthesis. In TAP medium, on the other hand, the growth is photoheterotrophic. Under photoheterotrophic conditions, acetic acid is present in solution as carbon source, and CO_2 bubbling is not necessary. In both growth media, we added air bubbling with a

---

1 An Einstein is defined as a mole of photons in studies of photosynthesis [100].
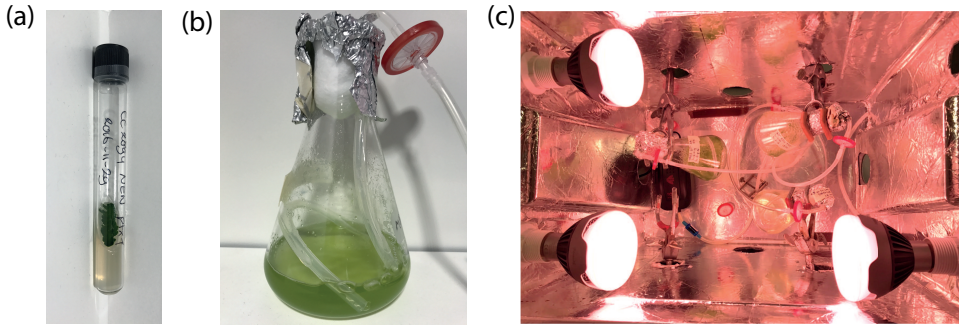
Figure 3.1: (a) Tube containing agar slant on which are conserved quiescent cells. **(b)** 250 ml Erlenmeyer flask containing a cell culture. A silicone tube allows air bubbling into the solution. Air is filtered with sterile syringe filter (Whatman Puradisc, pore size 0.2 μm). The inlet is closed to prevent contamination by a cotton foam covered by aluminium foil. **(c)** Custom-made growth chamber with three light bulbs (Philips Green Power LED flowering dr/w).

commercial aquarium pump to facilitate mixing in the suspension. Given the small volume of medium in the flask, bubbling air provides an amount of CO_2 (5%) that is sufficient for the phototrophic growth. The advantage of growing cells in phototrophic conditions is that they tend to synchronize their division, and there is less variance in cells size within one culture [60]. Therefore, phototrophic growth conditions using Tris-minimal medium are favoured in studies of photosynthesis [102] and motility, as flagellar beating is overall more consistent with less variance in the intrinsic beating frequency of the cells [60]. For *vfl3*, the growth in Tris-minimal medium is almost three times slower than for wt. For this reason, *vfl3* are grown in TAP medium.

All cells transfers and handling are done in a sterile laminar flow hood to avoid bacterial contamination. Before starting a new culture, empty flasks were autoclaved with a silicon tube inside and a cotton foam with aluminium foil placed on top of the flask inlet. After sterilization, the medium is introduced in the Erlenmeyer flask under the hood, and a sterile syringe air filter (Whatman Puradisc, pore size 0.2 μm) is placed at the end of the tube, connected to the air pump, as shown in figure 3.1(b). The temperature in the growth chamber is monitored and regulated at 25 °C. The light is provided by three light bulbs (Philips Green Power LED flowering dr/w). For both growth conditions, the cells are subject to light:dark (14 : 10 hours) cycles with light intensity of 230 μE.m^{-2}.s^{-1}.

The growth of wt cells in Tris-minimal medium has been monitored as shown in figure 3.2. Cells were counted with a hemocytometer (Neubauer Chamber, Marienfeld). Given that cells of *C. reinhardtii* are swimming, in order to count them, 100 μl of iodine solution was mixed with 900 μl of cell suspension, and a few μl were injected by the capillarity effect in the hemocytometer with a coverslip on top. For each single experiment, cells were harvested when the culture reached a cell density of 10^6 cells.ml^{-1}, corresponding to the midlog phase in the growth curve [91]. This concentration is achieved the fourth day after the cells are suspended from solid agar into fresh medium.
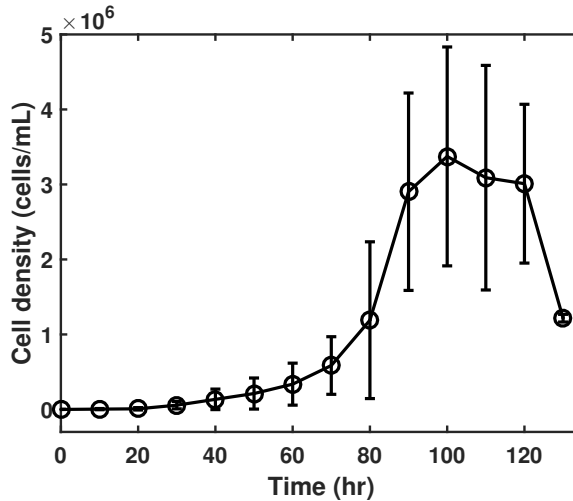
Figure 3.2: Growth curve for two cultures of wt *C. reinhardtii* cells in Tris-minimal medium. After four days (96 hours), cells reach the midlog phase, and they are harvested for the experiment.

3.2 THE EXPERIMENTAL SETUP

The goal in our experiments is to impose a controlled oscillatory flow of known velocity and frequency on a single *C. reinhardtii* cell, corresponding to a periodic forcing. During each experiment, the cell behaviour is recorded at high frame rate. To this purpose, we implemented an experimental setup (see figure 3.3), composed as follows:

  (a) Custom-made flow chamber.

  (b) Inverted microscope (Nikon Eclipse Ti-U) with a $60\times$ water-immersion objective.

  (c) Piezoelectric stage and controller (Nano-Drive, Mad City Labs).

  (d) Micropipette (Inner diameter 2 μm, Thin-Wall, without filament, World Precision Instruments).

  (e) Micromanipulator (SYS-HS6, World Precision Instruments).

  (f) sCMOS camera (PCO.edge 5.5).

  (g) LED light.

3.2.1 FLOW CHAMBER FABRICATION AND CHARACTERIZATION

The flow chamber is custom-made by cutting a semi-circular shape of 15 mm diameter out of a 1.5 mm thick plexiglass microscope slide, as shown in fig 3.5(a). The top and bottom free surfaces were sealed with glass coverslips, leaving a 15mm × 1.5mm rectangular opening on one side. Through this opening, the chamber is filled completely with cell suspension. During a typical experiment, a micropipette is inserted in the chamber, and one cell is suctioned, as explained in details in 3.3.

CHAPTER 3
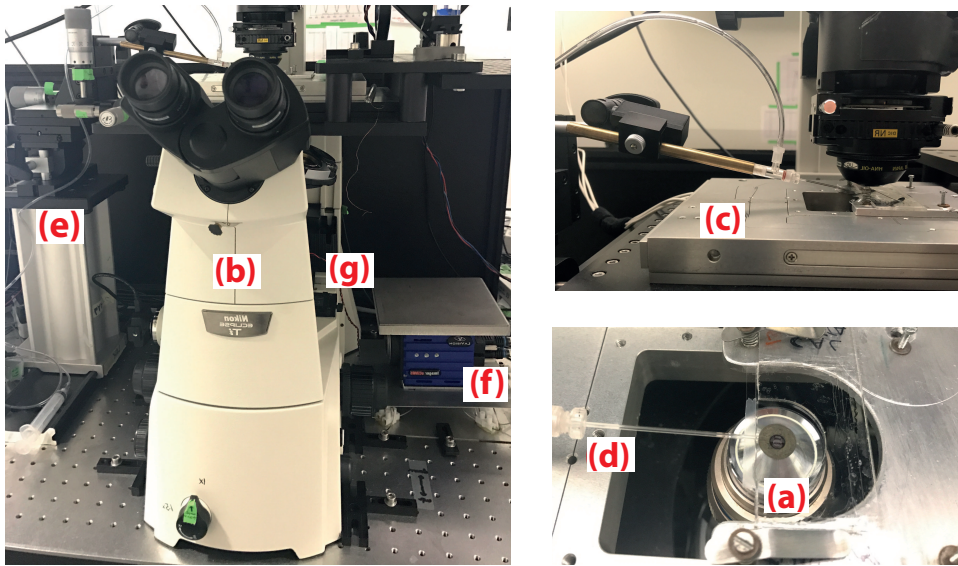
Figure 3.3: Photographs of the experimental setup highlight the different components: flow chamber (a), microscope (b), piezoelectric stage(c), micropipette (d), micromanipulator (e), camera (f) and LED light (g).

Figure 3.4: (a) Sketch of the experimental setup. **(b)** Sketch representing directions of the periodic background flow. Axial flow is oriented parallel to the pipette axis ($\theta = 0$), cross flow is perpendicular to the pipette axis ($\theta = \pi/2$).

3.2.2   STAGE AND FLOW CALIBRATION

The oscillatory flow around the cell is generated by imposing a displacement to the flow chamber that in turn creates a bulk motion of the 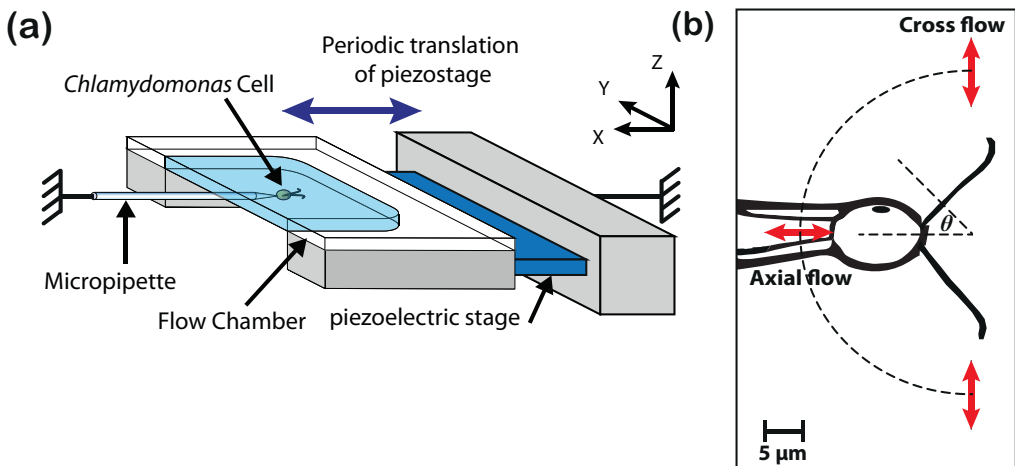cell suspension. This results in a uniform relative motion between the stationary pipette holding a cell and the surrounding fluid. The movement of the chamber is achieved by placing the chamber on a piezoelectric stage and by imposing to the stage a periodic motion of amplitude A_F and frequency f_F. Details on the stage displacement can be found in Appendix A.

The stage motion generates a periodic background flow in the chamber of velocity $U_F(t) = \pm 2 A_F f_F$. To characterize the flow in the chamber, we measured the flow velocity at different heights z inside the chamber, by imposing a flow parallel to the pipette axis (named axial flow) with frequency $f_F = 53$ Hz and amplitude $A_F = 10$ μm, which corresponds to a flow velocity $U_F(t) = 1060$ μm.s^{-1}. We monitored the displacement of a glass bead of 2 μm diameter, as shown in figure 3.5(d). The flow chamber is visualized by fixing the piezoelectric stage on top of an inverted microscope with a $60\times$ water-immersion objective. A high speed camera is connected to the microscope to record each experiment. Figure 3.5(e) represents the average amplitude A_R of the bead motion measured in the laboratory reference frame as a function of z *(red dots)*. At the bottom of the chamber, the bead is stuck to the surface, and the amplitude of the motion directly corresponds to the amplitude of the piezo motion A_0. When moving upward inside the chamber, we find that A_R decreases. This is due to deformation of the free air/water interface that is accelerated by the stage motion. Pinning the free interface, to inhibit surface deformation, suppresses any flow inside the chamber. We pinned the surface by placing a layer of tape on the bottom coverslip, as shown in figure 3.5(b). We found that this modification is sufficient to obtain a bulk flow. As shown in figure 3.5(e)(*black dots*), for a pinned contact line, the displacement of a bead in the bulk follows the displacements of the piezo and $A_R = A_0$.

However, when imposing a flow perpendicular to the pipette axis (named cross flow), deformation of the free air/water interface is still present (*red dots* in figure 3.5(f)). This happens because the flow direction is parallel to the open side of the chamber and the high shear stresses imposed on the free surface of the flow deform the air/water interface. This issue was overcome by designing a flow chamber with a smaller opening, shown in figure 3.5(c). In this chamber, the free surface of the flow is only 5 mm $\times$ 1.5 mm large; hence, surface deformation is very small, as highlighted by the average bead displacement (see *black dots* in figure 3.5(f)).

The range of motion of the piezoelectric stage is 0 to 100 μm in 3 directions, and the frequency of motion is $0 - 100$ Hz. In our experiments we impose planar stage motion (x and y directions), since, considering the analogy between the oscillatory flow and the flow generated by flagellar beating, the latter is mainly planar with small three dimensional components [87]. We are interested in flow frequencies of 40 Hz to 80 Hz, since the two flagella beat at 53 Hz and 70 Hz, while we impose velocities in the range of 100 μm to 1600 μm, having in mind that the free swimming velocity of a cell is ≈ 100 μm.s^{-1} [60]. At such high speed and frequency of motion, the behaviour of the stage is highly non-linear, and the piezoelectric stage movement can no longer follow

accurately the movement imposed by LabView. Therefore, we need to perform separate experiments to directly calibrate the response of the stage, discussed in Appendix A.
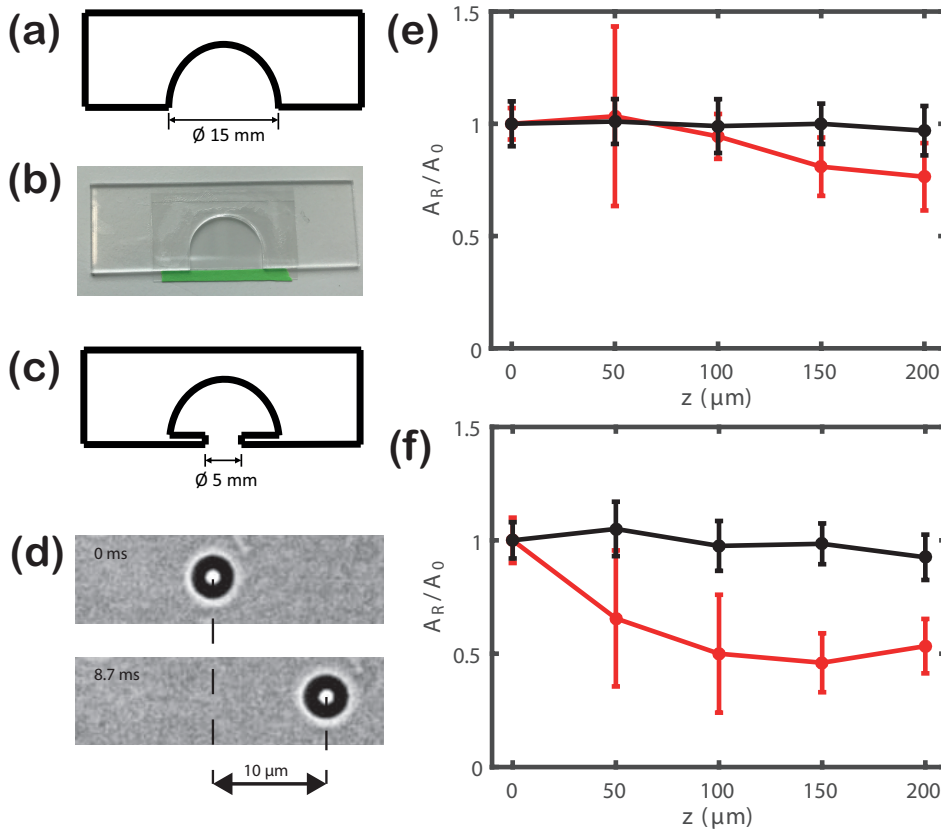

Figure 3.5: (a) Sketch of the flow chamber with large opening. **(b)** Picture showing the air-water interface pinned by a layer of tape (green). **(c)** Sketch of the flow chamber with narrow opening. **(d)** Two frames taken during piezostage calibration show the displacement of a glass bead sticking to the bottom of the flow chamber. **(e)** Calibration tests of the amplitude of displacement A_R at different heights in the chamber z. The amplitude of displacement at the bottom of the flow chamber is A_0. The imposed background flow is axial flow with frequency $f_F = 53$ Hz and amplitude $A_F = 10$ μm. The *red* dots represent the flow chamber with large opening and unpinned air-water interface. The *black* dots represent the same flow chamber, but with pinned air-water interface. Error bars represent variation in the measurement. **(f)** Displacement of a bead during cross flow with frequency $f_F = 53$ Hz and amplitude $A_F = 10$ μm. This shows that, for this flow direction, pinning the air-water interface is not sufficient to avoid diffusion effects (*red* dots). This necessitates a flow chamber with narrower air-water interface (*black* dots).

In our setup, the camera is controlled by the software Camware, which allows real-time visualization and image acquisition, while the piezoelectric stage is controlled with LabView. The time resolution of Labview stage controller is limited by the USB connection with the computer that has a fluctuating latency of few milliseconds. This uncertainty in the measurement does not allow an accurate assessment of the flagellar

beating frequency, as one beating cycle in *C. reinhardtii* lasts approximately 20 ms. To accurately determine the time at which the motion of the flow starts and stops, we directly extract the stage position from the stage controller output signal. In this way, we avoid the latency due to the USB connection. This output position signal needs to be combined during post-processing with the information on the flagellar frequency, in order to relate the flagellar beating cycle to the flow velocity and direction. Therefore, the stage position signal from the controller is connected (via the Arduino interface) to a LED light that is detected by the camera and is visible in the video. When the stage is activated, the LED emits a light flash lasting 5 ms, and it emits a second flash when the stage is stopped. These flashes are clearly visible in the video recording and, during post-processing, information about the flash activation $P(t)$ is combined with the stage motion signal $X(t)$ (as shown in figure 3.6). The LED activation has been calibrated by recording the motion of a bead attached to the chamber.
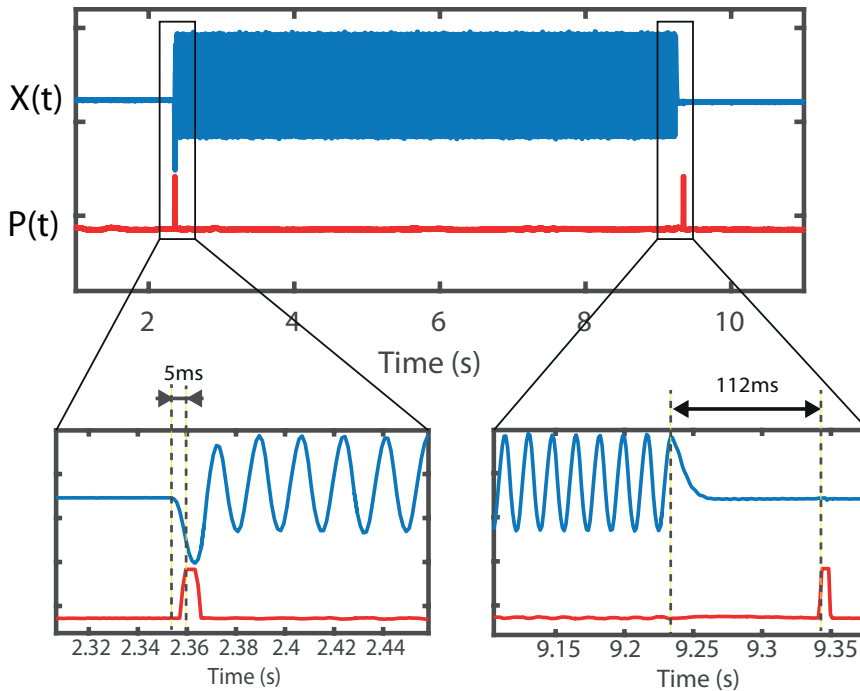

Figure 3.6: Signal of the stage displacement in time $X(t)$ (*blue* line) and signal of the LED activation $P(t)$ (*red* line), obtained after processing the video recording. Left inset shows the section in time when the stage is activated, the delay between stage start movement and light pulse is 5 ± 1 ms. Right inset shows a section of the signals when the stage is arrested. After 112 ± 1 ms from the last peak in the stage displacement, the second light pulse occurs.

Figure 3.6 shows the signal of the bead displacement (*blue*) and the LED signal (*red*). There is a constant 5 ± 1 ms delay between the activation of the stage and the start of the light flash. This time is necessary to the algorithm in Arduino to detect the initial displacement. The algorithm considers the piezoelectric stage to stop when its position remains constant for 80 ms, and a second flash is emitted by the LED. The time

between the last peak in $X(t)$ and the second LED pulse is 112 ± 1 ms. The accuracy in the LED stage detection is 1.1 ms, corresponding to 5% of the cell beating cycle. This custom made detection procedure increases our accuracy in the flagellar frequency measurement, as it bypasses the fluctuating latency in stage motion detection caused by the USB connection. The LED must be clearly visible in the video, but cannot directly illuminate the flow chamber. Therefore it is placed underneath the stage. As a matter of fact, cells must receive a controlled amount of light during the experiment, otherwise their motility and functioning are affected (the shock response was discussed in Chapter 2). For this reason, we record the motion of flagella under bright field illumination of light intensity $160 \ \mu\text{E.m}^{-2}.\text{s}^{-1}$ so the cells are exposed to a lower light intensity than in the growth chamber. We use a sCMOS camera that is characterized by a high signal to noise ratio and high dynamic range, allowing to record at 800 frames per second (fps) with moderate light exposure.
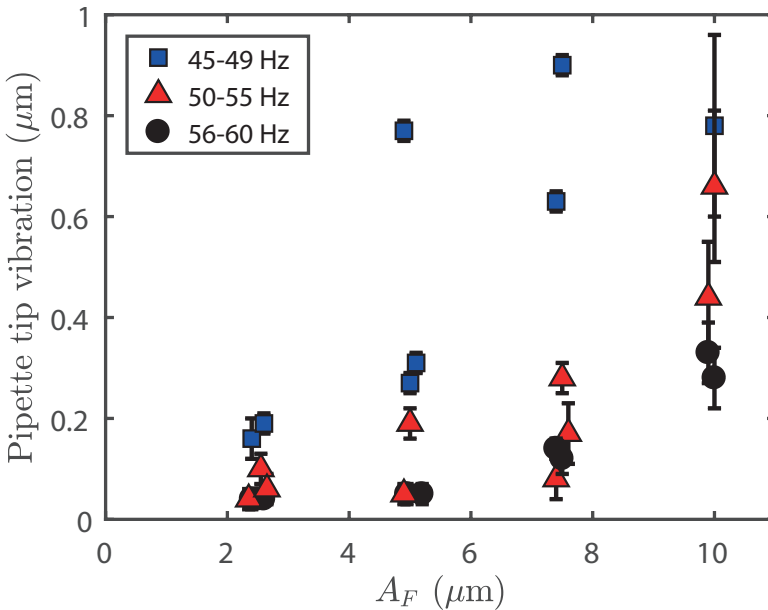
Figure 3.7: Pipette tip vibration as function of the forcing amplitude A_F. For $A_F \gtrsim 5 \ \mu\text{m}$, pipette tip vibration for $f_F = 45 - 49$ Hz becomes significant ($\approx 1 \ \mu\text{m}$).

3.3   EXPERIMENT AND PRELIMINARY IMAGE PROCESSING

To prepare the setup for a typical experiment, a diluted cell suspension is inserted in the flow chamber. Subsequently, the chamber is mounted on top of the stage, and a glass micropipette is inserted in the chamber opening with the aid of the micromanipulator. Once the pipette is properly positioned inside the chamber, one cell is suctioned at the tip of the micropipette and oriented to leave the flagella outside of the pipette and the flagellar beating plane corresponding to the microscope focal plane (see figure 3.4(b)).

Figure 3.8: (a) Snapshots recorded during an experiment without background flow. **(b)** Snapshots after preprocessing.
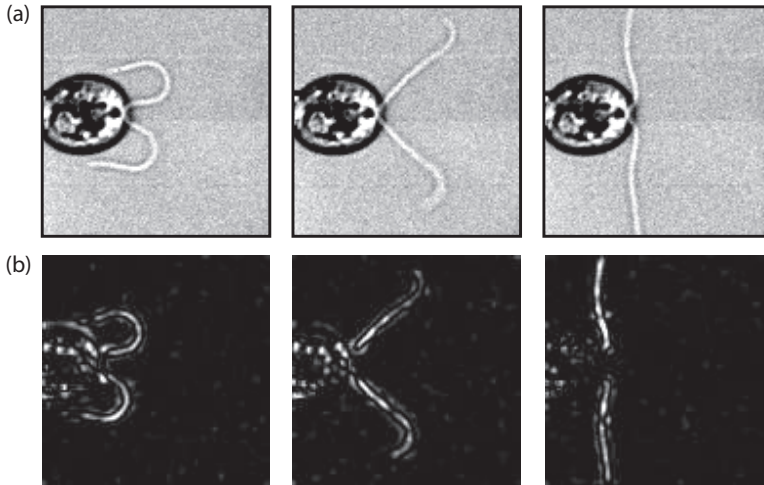
It is crucial not to have direct contact between the micropipette and the chamber walls, as we want to create a periodic background flow around the cell by varying the stage position $X(t)$, while keeping the cell fixed in the laboratory frame of reference. In all our experiments, the cell's intrinsic beating frequency is in the range 52.0 ± 1.6 Hz. Once the cell is properly placed and its intrinsic beating frequency has been characterized, we observe the cell's response to periodic background flows. Between two consecutive experiments where the cell is subjected to different flow conditions, there is a time interval of at least one minute with no flow imposed. During this interval, the cell beating frequency is restored, as discussed in 4.3. The recording of the experiment needs some preliminary processing before performing image analysis and data extraction.

The first step is the correction for pipette motion. This effect is a consequence of the oscillatory flow, and it adds unwanted noise to the detection of flagellar position. As shown in figure 3.7, for flows with amplitudes $A_F \geq 5$ μm, the pipette motion caused by the external flow is 0.4 ± 0.4 μm, with higher vibration for $f_F = 45 - 49$ Hz (see figure 3.7). We applied a correction algorithm, for flows with amplitude $A_F \geq 5$ μm, that recenters all the frames in a recording in order to have the pipette aligned with respect to the first frame. Subsequent steps in preprocessing are then performed: application of a median filter, to reduce noise and enhance edges, and finally subtraction of the background. During the video acquisition slight image intensity variations occur; a running average of 10 images is subtracted from each frame to correct for this. Figure 3.8 shows a raw image and an image after preprocessing. Details of the experimental observations and image processing are discussed in chapter 4.

C. REINHARDTII AS A MODEL SELF-SUSTAINED OSCILLATOR

As discussed in section 2.3, the unicellular organism *C. reinhardtii* has two flagella capable of beating in synchrony for long periods of time, allowing the cell to propel in fluid. The continuous synchronous beating of the two flagella at $\approx$ 53 Hz resembles the behaviour of a self sustained oscillator. The dynamics of self-sustained oscillators have been investigated theoretically, and the mathematical formalism describing model oscillators is well established [104, 105]. These theoretical models are able to predict the behaviour of periodic oscillators under the influence of external forces. A general approach to study the periodic dynamics of an oscillator is to perturb it with an external forcing [96–98]. We applied this general approach to study the beating of eukaryotic flagella. On a single cell we imposed periodic hydrodynamic forcing of controlled frequency and amplitude that reproduces the background flow generated by a freely swimming cell. The possibility for the cell to couple with this external flow yields insights into the role of hydrodynamic forces in mediating flagellar synchronization. Forcing directions both parallel and perpendicular to the pipette axis have been tested. Moreover, the response time of the organisms to external frequency perturbations has been investigated. It is conceivable that long and/or strong mechanical perturbations provoke alterations in the physiology of the cell, which could persist even after the perturbation ceases. This phenomenon is named adaptation. We address the possibility of permanent alterations in the physiology and behaviour of the cell by investigating the influence of long and strong flows on the intrinsic beating frequency.

Adaptation in *C. reinhardtii* has never been investigated previously. Therefore after forcing the intrinsic frequency externally, we also quantify whether the intrinsic frequency is permanently or temporarily affected by the forcing. Our results are compared with established models for periodic oscillators, and we characterize how closely the dynamics of beating flagella agrees with the one of an ideal self-sustained oscillator. We begin our discussion in section 4.1 by describing the experiments performed and how we extract the phase dynamics from our experimental data. In section 4.2, we summarize the main theoretical results for the dynamics of self sustained oscillators. In section 4.3, we present the obtained results that are relevant to characterize the behaviour of *C. reinhardtii* as a self sustained oscillator perturbed by hydrodynamic forcing. Finally, in section 4.4 we comment on the results and give an

interpretation of the role of hydrodynamic forces in *C. reinhardtii* interflagellar synchronization.

4.1 EXPERIMENTS AND DATA PROCESSING

A possible approach to study the dynamics of a self sustained oscillator is the observation of its behaviour when perturbed by an external periodic forcing. Experiments on the effect of a non-biological forcing on the beating of flagella and cilia have been attempted previously [96–98], and results have been discussed in 2.5. In the present study, we impose a hydrodynamic forcing on *C. reinhardtii* and measure the cell response.

4.1.1 THE EXPERIMENTS

Here we describe the experiments performed to characterize the dynamics of the eukaryotic flagella, by using the model organism *C. reinhardtii* as case study. We use the experimental setup described in section 3.2. The forcing that we impose is a periodic oscillatory flow. We tested two flow directions on wt: a flow aligned with the pipette axis (axial flow), and a flow perpendicular to the pipette axis (cross flow); see figure 3.4(b) in section 3.2. In both flow directions, we varied forcing velocity U_F in the range $100 - 1200$ μm.s^{-1} and frequency $f_F = 43 - 77$ Hz. Regarding the range of velocities, we started by imposing 100 μm.s^{-1} flows to reproduce the forces experienced by the cell during free swimming (free swimming velocity discussed in subsection 2.3.1) and then we increased the forcing velocity. The frequency range was chosen to include the *cis-* and *trans-* intrinsic beating frequency (for details the reader is referred to section 2.3).

All the experiments performed can be grouped into two types:

- **Experiment type 1** We investigate the oscillatory steady state. We start the video acquisition $\approx$ 5s after starting the forcing, and we stop the video acquisition $\approx$ 5s before stopping the forcing. In the post processing, we extract from the video information about the flagellar beating phase.

- **Experiment type 2** We address the transient and in particular how the beating frequency transitions from the intrinsic frequency f_0 towards the forcing frequency f_F and vice-versa. Therefore, we start the video before starting the forcing and stop the acquisition a few seconds after stopping the forcing. In the post processing, we extract not only the flagellar dynamics, but also the piezoelectric stage position in each frame, since in this experiment it is crucial to know the phase of both the flagella and the piezoelectric stage in each single video frame.

In the following subsection, we discuss how to extract the phase of flagella, and compare it with the phase of the external forcing.

4.1.2 EXTRACTION OF THE PHASE DYNAMICS

After the preprocessing steps discussed in 3.3, we obtain images like the ones shown in figure 4.1(a). From these images, we extract the phase dynamics of flagella, following the method in [74]. The flagellar beating cycle is well described by a single scalar phase angle $\phi(t)$, which is a function of time. At a given time t the phase angle $\phi(t)$ parametrizes the location of the flagella in time along its limit cycle. $\phi(t)$ increases by an angle 2π during each single beat period. We call $\phi_{\text{cis}}(t)$ and $\phi_{\text{trans}}(t)$ the phase angles determined separately for the *cis-* and *trans-* flagella. The phase angle $\phi(t)$ is extracted from the videos following an approach similar to the one developed by Polin *et al.* [74]. Two regions in the image, named 'interrogation windows' in [12, 74], are selected in proximity of the cell body such that the flagellum swipes through the interrogation window once per beating period; see figure 3.8(a). The average pixel intensity $I(t)$ in each interrogation window is computed for each frame, and leads to a pseudo periodic signal, owing to the periodicity of the flagellar motion. Separate signals are recorded for the *cis*-flagellum ($I_{\text{cis}}(t)$) and for the *trans*-flagellum ($I_{\text{trans}}(t)$). Larger values in the average pixel intensity $I_{\text{cis;trans}}(t)$ indicate the passage of the flagellum through the interrogation window, while the value of $I_{\text{cis;trans}}(t)$ is lower when the flagellum is not in the interrogation window. Figure 3.8 (b) represents a typical signal obtained for $I_{\text{cis;trans}}(t)$ in our experiments. Each pseudo period delimits one beating period of the flagella. The beating frequency of flagella can be inferred by computing the discrete Fourier transform of $I_{\text{cis;trans}}(t)$ using the Fast Fourier Transform (FFT) algorithm [106]. Figure 4.1 (c) shows the Fourier spectrum, a visual representation of the FFT.

Frequency fluctuations in flagellar beating are visualized by computing the Short-Time Fourier Transform (STFT) of $I_{\text{cis;trans}}(t)$ over short time intervals [107]. A visual representation of the STFT is the spectrogram, shown in figure 3.8 (d). It represents the frequency spectrum of $I_{\text{cis;trans}}(t)$ as a function of time. Since the intrinsic beating frequency of *C. reinhardtii* displays frequency fluctuations, computing the STFT allows to visualize these changes.

The phase of each flagellum in time $\phi_{\text{cis;trans}}(t)$ can be deduced from the intensity signal $I(t)$ by computing the Hilbert transform, similarly to [108]. The Hilbert transform is a linear operation that shifts by $\pi/2$ the phase of the negative frequency components of a signal, while it shifts by $-\pi/2$ the phase of the positive frequency components in the same signal [109].

The Hilbert transform of $I_{\text{cis;trans}}(t)$ is computed as:

$$\mathcal{H} = \hat{I}_{\text{cis;trans}}(t) = \frac{1}{\pi} PV \int_{-\infty}^{\infty} \frac{I_{\text{cis;trans}}(\tau)}{t-\tau} d\tau, \tag{4.1}$$

The real time signal $I_{\text{cis;trans}}(t)$ can be also expressed in the analytical form $\zeta_{\text{cis;trans}}(t) = I_{\text{cis;trans}}(t) + i\hat{I}_{\text{cis;trans}}(t)$, where the imaginary part is the Hilbert transform. The instantaneous phase angle $\phi^i_{\text{cis;trans}}(t)$ for each flagellum is then computed as:

$$\phi^i_{\text{cis;trans}}(t) = tan^{-1}\frac{\hat{I}_{\text{cis;trans}}(t)}{I_{\text{cis;trans}}(t)}, \tag{4.2}$$
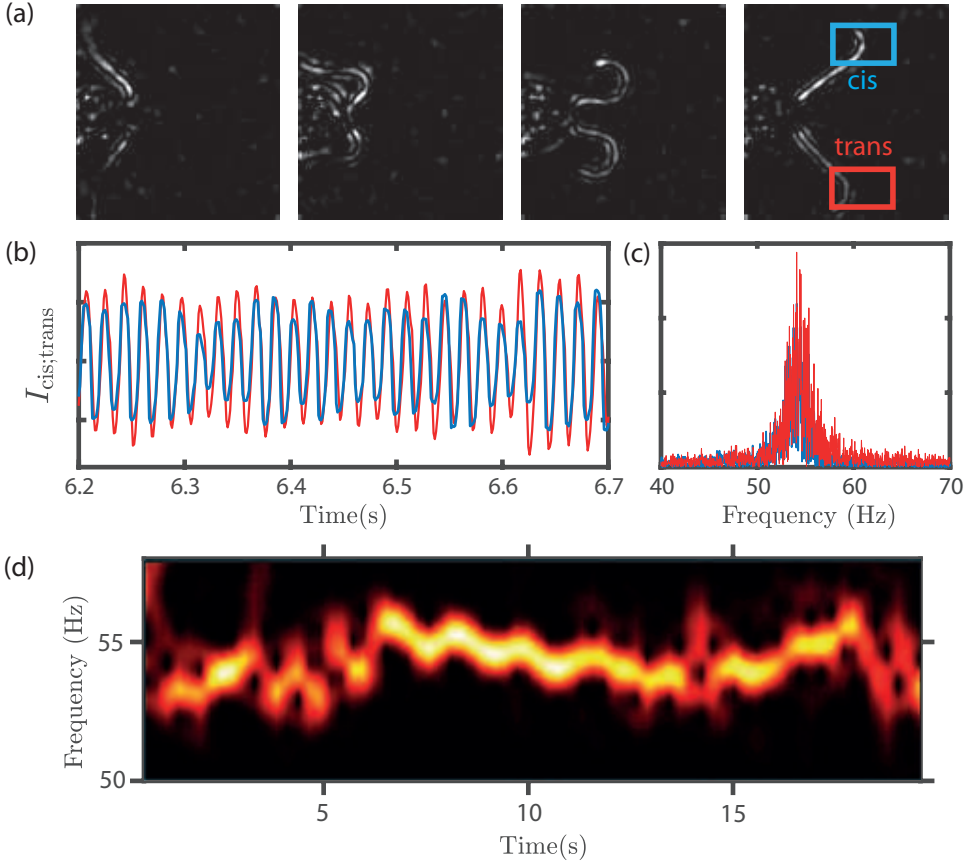
Figure 4.1: Experiment without background flow to monitor f_0. **(a)** Snapshots after preprocessing steps. In the right snapshot are sketched the interrogation windows used to extract the flagellar beating cycle. **(b)** The flagellar signal $I_{\text{cis;trans}}$ represents the average pixel intensity inside the two interrogation windows. Peaks in the signal indicate the passage of flagella through the window. **(c)** Fast Fourier Transform (FFT) of $I_{\text{cis;trans}}$. **(d)** Spectrogram of I_{cis} displays intrinsic beating frequency fluctuations in time.

Unwrapping the instantaneous phase angle yields the phase of each flagellum as a monotonically increasing function of time ($\phi_{\text{cis;trans}}(t)$). Figure 4.2(a) represents the instantaneous wrapped phase angle $\phi_{\text{cis;trans}}^i(t)$, computed from the experiment without forcing and using equation (4.2). Figure 4.2(b) represents the unwrapped flagellar phase $\phi_{\text{cis;trans}}(t)$ for the same experiment discussed in figure 4.1. We normalize the phase angle by 2π such that the phase $\phi_{\text{cis;trans}}/2\pi$ increases by 1 over each flagellum beating period. Since we are interested in comparing the flagellar phase dynamics with respect to the external periodic forcing, we consider $\phi(t)$ to represent the phase of both beating flagella. This assumption is made possible by the fact that in our experiments, the phase dynamics of the two flagella are nearly identical ($\phi_{\text{cis}}(t) \approx \phi_{\text{trans}}(t)$), with few

interflagellar slips recorded. See Appendix B for a more detailed discussion. We deduce the time-dependent phase difference $\Delta(t)$ between the flagella and the forcing:

$$\Delta(t) = \phi(t)/2\pi - \phi_F(t)/2\pi, \tag{4.3}$$

where $\phi_F(t)$ denotes the phase of the periodic forcing. In Experiment type 1, the external periodic forcing has a constant frequency f_F. Therefore, the unwrapped phase of the forcing is $\phi_F(t) = 2\pi f_F t$. The phase of forcing $\phi_F(t)/2\pi$ increases linearly by 1 every $1/f_F$ seconds, since we imposed a flow having a constant frequency. In Experiment type 2, the forcing is zero at the beginning and at the end of the experiment, and therefore, we deduce the phase angle $\phi_F(t)$ from the experimental signal of the stage motion (details in subsection 3.2.2) by computing the Hilbert transform analogously to the flagella signal.
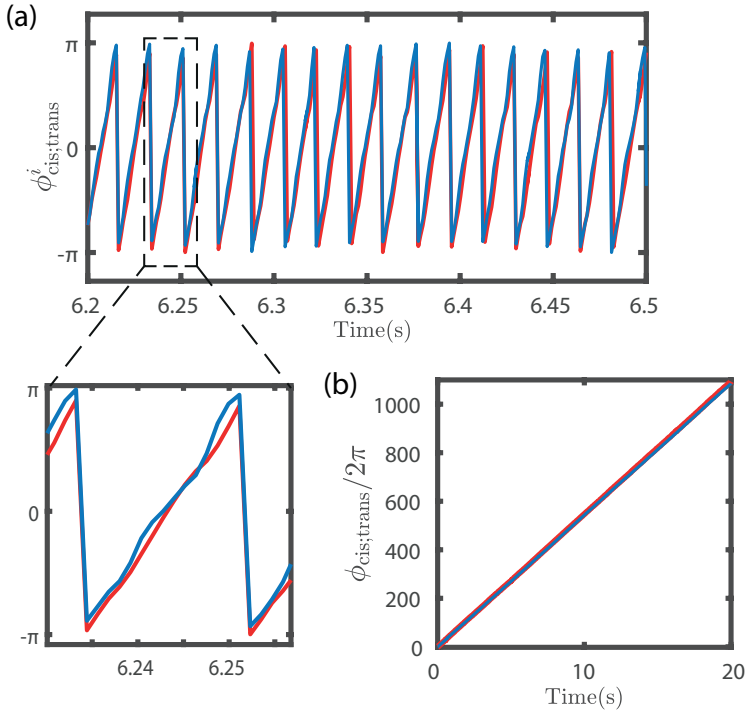
Figure 4.2: (a) Instantaneous phase angle $\phi^i_{cis;trans}(t)$ of the two flagella obtained by computing the Hilbert transform of $I_{cis;trans}(t)$. Inset shows the fluctuations in flagella phase angle, due to the fluctuations in flagellar beating frequency. **(b)** Flagella phase obtained by unwrapping $\phi^i_{cis;trans}(t)$.

4.2 THEORETICAL MODEL

We presented details about the performed experiments in section 4.1 and the information extracted regarding the flagellar phase. Information about the phase dynamics allows a comparison between flagella behaviour in *C. reinhardtii* and a self sustained oscillator. Mechanical oscillators can be entrained by external forcing [104,

105], and we explore experimentally this possibility of entraining flagella by a hydrodynamic forcing. The concepts of non-linear dynamics theory that we adopted to model the behaviour of *C. reinhardtii* are summarized in this section. Theoretical models of *C. reinhardtii* as a self sustained oscillator have been proposed in several studies discussing the role of hydrodynamics in inter-flagellar synchronization [48, 74, 75, 83, 91] and are based on the Adler equation [105] presented in 4.2.1. In this thesis, our focus is not to compare the phase dynamics of the two flagella and model the synchronization between them as in Polin *et al.* [74] or Friedrich *et al.* [48]. Instead, we are interested in a comparison between the flagella phase dynamics and the one of the external periodic forcing. In this section, we present the theoretical model applied to our data to describe the behaviour of a self sustained oscillator synchronized with an external periodic forcing. We first describe the formulation for the ideal situation in which there is no external noise perturbing synchrony (subsection 4.2.1). In the next subsection 4.2.2, we discuss the synchronization of a noisy oscillator, as it better approximates the actual behaviour of *C. reinhardtii* captured in our experiments [104].

4.2.1 THE SYNCHRONIZATION REGION OF AN OSCILLATOR

We consider an oscillator that in the absence of external forcing has an intrinsic frequency f_0. We impose an external forcing that is periodic and has a frequency of f_F. The difference between the intrinsic frequency and the frequency of forcing is the frequency detuning $\nu = f_F - f_0$. The phase dynamics of the system can be modeled with a first-order Ordinary Differential Equation (ODE) [74, 104, 105] for the phase difference $\Delta(t)$ (introduced in equation 4.3) as:

$$\frac{d\Delta(t)}{dt} = -\nu + \epsilon \mathcal{Q}(\Delta(t)), \tag{4.4}$$

with $\mathcal{Q}$ a periodic function, and ϵ the amplitude of the external forcing. $\mathcal{Q}(\Delta(t))$ has in each period a maximum q_{max} and a minimum q_{min}. For $\mathcal{Q}(\Delta(t))$ equal to $-\sin(2\pi\Delta(t))$, equation (4.4) is called the Adler equation [105]. The solution to equation 4.4 depends on the values of ν and ϵ. We can distinguish 3 cases:

  (i) $\nu < \epsilon q_{min}$ or $\nu > \epsilon q_{max}$. The ODE (equation 4.4) has no fixed points, see figure 4.3(a,b).

  (ii) $\nu = \epsilon q_{max;min}$. For this value of the detuning parameters, fixed points are created through a saddle-node bifurcation (see figure 4.3(c)) which corresponds to the transition to synchronization.

  (iii) $\epsilon q_{min} < \nu < \epsilon q_{max}$. There is at least a pair of fixed points to equation 4.4. One is a stable fixed point, while the other one is unstable; see figure 4.3(d-f). The stable fixed point corresponds to the constant solution to equation 4.4. We call Δ_0 the steady state value of the phase difference $\Delta(t)$. In figure 4.3(d), ν is negative and Δ_0 is positive. In figure 4.3(f), the opposite situation occurs, since ν is positive and Δ_0 is negative. In figure 4.3(e), ν is 0 and the frequency of the external forcing f_F coincides with frequency of the self sustained oscillator f_0.
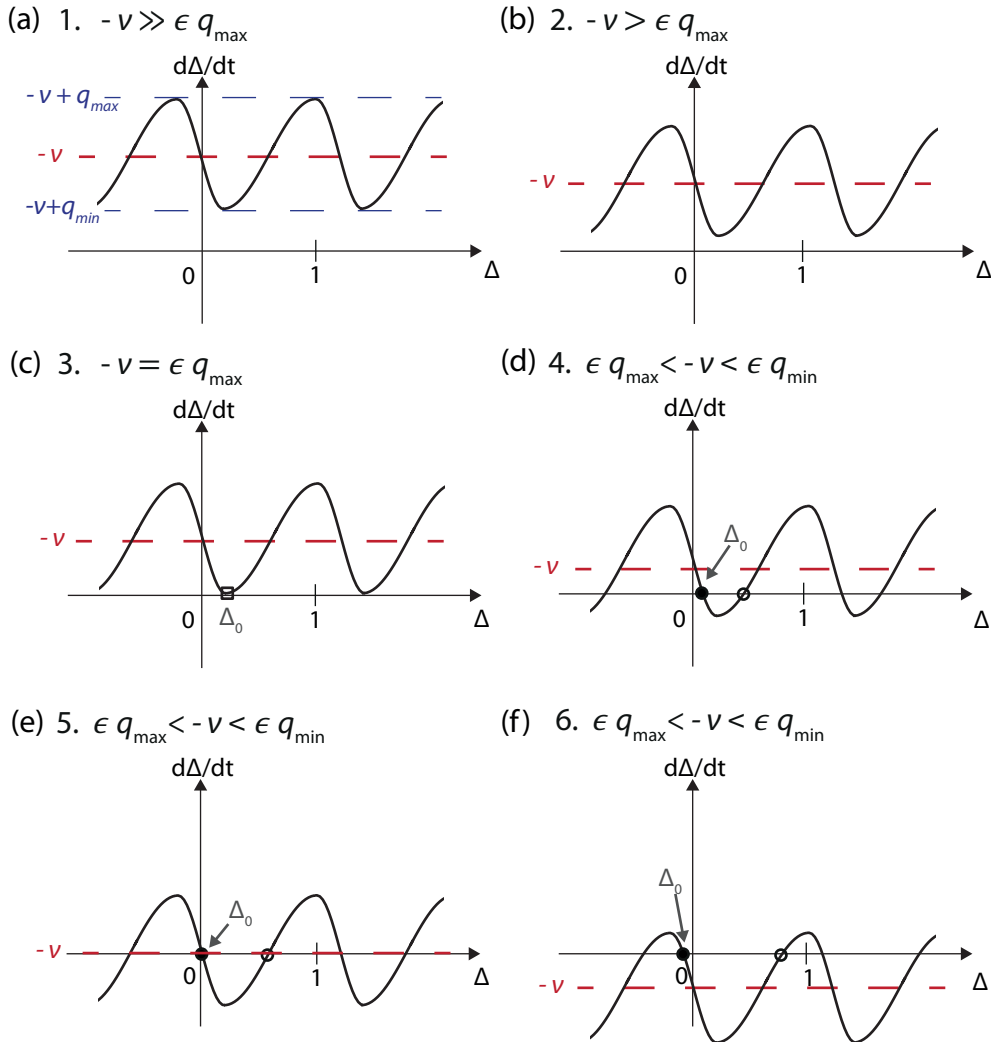
Figure 4.3: Graphic solutions for equation 4.4. Figures **(a)** to **(f)** represent the function $-\nu + \epsilon \mathcal{Q}(\Delta)$ as a function of Δ for increasing values of ν. **(a,b)** When f_F is outside the synchronization region ($-\nu > \epsilon q_{max}$), there are no solutions. **(c)** If f_F is at the border of the tongue ($-\nu = \epsilon q_{max}$), a saddle-node bifurcation is formed. Equation 4.4 has one solution Δ_0. **(d-f)** When f_F is inside the Arnold tongue ($-\nu < \epsilon q_{max}$), at least a pair of stationary solutions exists. Δ_0 ranges from positive in **(d)** to negative in **(f)** depending on the frequency detuning $-\nu$.

SYNCHRONIZATION REGION

In figure 4.4(a) we represent the synchronization phase diagram as a function of the forcing amplitude ϵ and frequency of oscillation f. There is a range of forcing frequencies f_F, symmetric with respect to f_0, in which frequency locking between the self sustained oscillator and the external forcing occurs. This region has a triangular shape as shown in figure 4.4(a). Frequencies of oscillation inside this region are within

the frequency locking range (see figure 4.4(a) points 4, 5, 6). The size of this range depends on the forcing amplitude ϵ: the larger the amplitude, the larger the range of frequency detuning where synchronization occurs. This region in the (f, ϵ) domain is called Arnold tongue. The synchronization region of a given oscillator is characterized by an Arnold tongue.

PHASE DYNAMICS

(i) When $-\nu > \epsilon q_{max}$ (or $-\nu < \epsilon q_{min}$) we can observe the situation shown in figure 4.3(a,b) and figure 4.4(a,b) points 1, 2. In this case, $d\Delta(t)/dt > 0$ (respectively $d\Delta(t)/dt < 0$), and the phase difference between the self sustained oscillator and the external forcing $\Delta(t)$ increases monotonically (see figure 4.3(a,b), point 1, curve 1). Therefore, there can be no phase locking, and synchronization cannot be established. In point 2, $-\nu$ is smaller as the external forcing frequency is closer to the intrinsic frequency of the oscillator, and $d\Delta(t)/dt$ can get closer to zero (see figure 4.3(a,b) point 2, curve 2). Thought still monotonic, the growth of $\Delta(t)$ is not as uniform as in point 1 and $\Delta(t)$ is nearly constant for longer periods of time.

(ii) When $-\nu \approx \epsilon q_{max;min}$, the oscillator is on the edge of the synchronization region (see figure 4.3(a,b) point 3, curve 3 and figure 4.4(c)). As shown in figure 4.3(b) curve 3, the phase $\Delta(t)$ alternates between long periods where the phase $\Delta(t)$ is nearly constant and short jumps in phase corresponding to synchrony loss. During these events, called phase slips, the phase of the oscillator gains or loses one unit with respect to the forcing.

(iii) When $\epsilon q_{min} < -\nu < \epsilon q_{max}$, for all initial conditions, the solutions to equation 4.4 are attracted to the stable fixed point. After a transient, the phase difference reaches a constant steady state (see figure 4.3(a,b) points 4-6, curves 4-6 and figure4.4(d-f)). In this range of ν, the phases of the oscillator and the forcing are locked. This corresponds to synchronization. $\Delta(t)$ in the steady state is always constant, as shown by curves 4,5,6 in figure 4.3(b).

The constant steady state phase Δ_0 corresponds to the stable fixed point of equation 4.4 and is therefore defined by:

$$0 = -\nu - \epsilon \mathcal{Q}(\Delta_0), \tag{4.5}$$

The steady state phase difference Δ_0 depends on ν. When $f_F < f_0$, Δ_0 is positive, as shown in figure 4.3(d), meaning that the self sustained oscillator is phase-locked with the flow with a certain lag since it is forced to oscillate at a frequency lower than f_0. Instead, if $f_F > f_0$, the opposite situation occurs, namely Δ_0 is negative because the flow is forcing the flagella to beat at a higher frequency, as sketched in figure 4.3(f) [104, 110].

The transient and its duration strongly depend on the initial phase difference at the time the external forcing is first activated. One can get insights into the transient behaviour close to the fixed point by linearizing equation 4.4 around the fixed point:

$$\Delta(t) = \Delta_0 + \tilde{\Delta}(t), \tag{4.6}$$

here $\tilde{\Delta}(t)$ is the transient solution and is assumed to be small. Equation 4.4 simplifies into a first order linear ODE for $\tilde{\Delta}$:

$$\frac{d\tilde{\Delta}(t)}{dt} = -\epsilon \frac{d\mathcal{Q}}{d\Delta}\Big|_{\Delta_0} \cdot \tilde{\Delta}(t), \tag{4.7}$$

The solution to this First-Order ODE is:

$$\tilde{\Delta}(t) = \Delta_0 e^{+\epsilon \frac{d\mathcal{Q}}{d\Delta}|_{\Delta_0} t}, \tag{4.8}$$

From equation 4.8, the timescale associated with the transient phase difference between the oscillator and the forcing is:

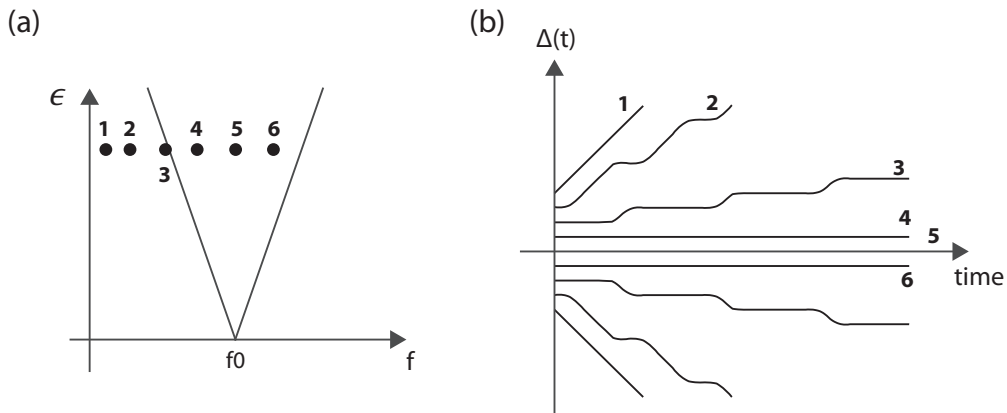$$\tau = \frac{1}{\epsilon d\mathcal{Q}/d\Delta|_{\Delta_0}}. \tag{4.9}$$

Figure 4.4: Synchronization range and phase dynamics for a self-sustained oscillator with intrinsic frequency f_0. **(a)** The synchronization region of a given oscillator has the shape of an Arnold tongue. **(b)** Phase difference between the oscillator and the external forcing $\Delta(t)$ as a function of time. If the forcing frequency f_F is outside the synchronization region (curves 1 and 2), the phase difference tends to grow uniformly. Right at the border of the Arnold tongue (curve 3), the phase difference is characterized by periods of synchrony as well as periods of linear growth. Inside the synchronization region (points 4,5 and 6), the phase difference is always constant. Symmetric phase behaviour occurs at the right side of the Arnold tongue.

We consider how the frequency of the oscillator is affected by the external forcing as a function of ν and ϵ. For a given ϵ, it follows the trend shown in figure 4.5. Within the synchronization range $f_F = f$, as there is frequency locking. Outside of this range, the frequency mismatch is too large, and synchronization does not occur. Hence, the oscillator frequency f is different from f_0, although it leans asymptotically towards $f = f_0$. Close to the synchronization transition, for $f_F - f_0 \approx \epsilon q_{max}$, the behaviour of f is approximated as:

$$f_F - f \approx \sqrt{(f_F - f_0 - \epsilon q_{max})}, \tag{4.10}$$

The trend of $f_F - f$ is typical of a saddle node bifurcation. If we consider $f_F - f_0 \geq \epsilon q_{max}$ there are two clear trends (see figure 4.5). For ν in a small surrounding of ϵq_{max}, $f_F - f$ increases drastically. For larger values of ν, $f_F - f$ tends asymptotically to linear [104, 105].
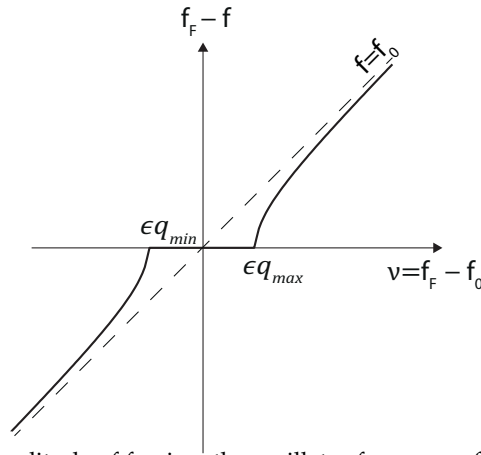

Figure 4.5: For a given amplitude of forcing, the oscillator frequency f depends on the frequency detuning ν.

4.2.2   SYNCHRONIZATION OF A NOISY OSCILLATOR

In 4.2.1 we discussed a model for the synchronization dynamics of an ideal oscillator. Periodic oscillators in biology, however, display stochastic fluctuations in their phase dynamics [5, 111]. An example of this fluctuations for *C. reinhardtii* is shown in figure 4.1(d). These fluctuations, or biological noise, are to be taken into account to model the phase dynamics. Stochastic fluctuations of the phase difference $\Delta(t)$ can be modelled by assuming a Langevin dynamics for the phase difference $\Delta(t)$. With this assumption equation (4.4) can be rewritten as:

$$\frac{d\Delta(t)}{dt} = -\nu + \epsilon \mathcal{Q}(\Delta(t)) + \xi(t), \tag{4.11}$$

where $\xi(t)$ represents a random noise in the flagellar actuation. We can define a potential $V(\Delta)$ associated with the deterministic force driving $\Delta(t)$, such that $-dV(\Delta)/d\Delta = -\nu - \epsilon\mathcal{Q}(\Delta(t))$. Equation (4.11) can then be rewritten as:

$$\frac{d\Delta(t)}{dt} = -\frac{dV(\Delta)}{d\Delta} + \xi(t). \tag{4.12}$$

We assume $\xi(t)$ to be a δ-correlated Gaussian noise of intensity T_{eff}, such that $\langle \xi(\tau)\xi(\tau + t)\rangle = 2T_{\text{eff}}\delta(t)$. The probability density function $P(\Delta, t)$ satisfies the Fokker-Plank equation:

$$\frac{\partial P}{\partial t} = \frac{\partial V(\Delta)}{\partial \Delta} + T_{\text{eff}}\frac{\partial^2 P}{\partial \Delta^2}. \tag{4.13}$$

The Fokker-Planck equation (4.13) has a time-independent solution

$$\hat{P}(\Delta) = \frac{1}{C}\int_{\Delta}^{\Delta+1} \exp\left(\frac{V(\Delta') - V(\Delta)}{T_{\text{eff}}}\right) d\Delta', \tag{4.14}$$

where C is a normalization constant [104]. The solution (4.14) only depends on three parameters (ν, ϵ and T_{eff}) and can be computed numerically using Gauss-Laguerre quadrature. The steady state probability distribution can be inferred from the model external coupling, $\mathcal{Q}(\Delta) = -\sin(2\pi\Delta)$. For large $|\nu|$, $\hat{P}(\Delta)$ is uniform. When $|\nu|$ is decreased, the probability $\hat{P}(\Delta = 0)$ of in-phase beating increases, while the probability $\hat{P}(\Delta = \pm 0.5)$ of anti-phase beating decreases. For small $|\nu|$, the phase is locked. $\hat{P}(\Delta)$ is Gaussian-like, with a zero probability to beat in anti-phase.

4.3 RESULTS

In this section we present the experimental results relative to the characterization of *C. reinhardtii* as a self sustained oscillator. In subsection 4.3.1, we discuss the response of the cell to an axial flow. In subsection 4.3.2, we discuss the analogy between the experimental results and the theoretical model of a self sustained oscillator. In subsection 4.3.3 we impose on *C. reinhardtii* a cross flow, and we define a synchronization region similarly to the experiments with axial flow. In subsection 4.3.4 we focus on forcing frequencies inside the synchronization region for axial flow, and we discuss the time evolution of the phase difference $\Delta(t)$. Finally, in subsection 4.3.5, we analyse the presence of adaptation in the intrinsic frequency. As mentioned in the introduction of this chapter, biological oscillators can adapt to the external environment, and we address this possibility for *C. reinhardtii*.

4.3.1 THE CELL RESPONSE TO AN EXTERNAL FORCING

In order to characterize the range of synchronization in *C. reinhardtii*, we imposed axial flow with U_{F} in the range $100 - 1200$ μm.s^{-1} on a single cell, and we characterized separately the response of the cell to a forcing with constant amplitude and varying frequency, as well as to a forcing with constant frequency and different amplitudes. We measured the phase difference between the cell and the external forcing $\Delta(t)$ following the definition in section 4.2.

FORCING WITH CONSTANT AMPLITUDE, VARYING FREQUENCY

We first describe the flagellar response to an external periodic flow of constant amplitude $A_F = 5$ μm. Since the intrinsic frequency of C. *reinhardtii* is ≈ 53 Hz (see section 2.3), we chose a range of flow frequencies from $f_F = 49.9$ to $f_F = 60.3$ Hz. Therefore, the imposed flow velocities are in the range $U_F = 499 - 603$ μm.s^{-1}. We investigated these flow conditions on a single cell with intrinsic frequency $f_0 = 53.6 \pm 0.7$ Hz. Figure 4.6(a), represents $\Delta(t)$ for this set of experiments.

The phase dynamics

When we compare the experimental results in figure 4.6(a) with the theoretical model discussed in 4.2 and sketched in figure 4.4, we can identify several analogies for the phase dynamics. For $f_F = 49.9$ Hz, i.e. lower than the intrinsic frequency f_0, the phase difference $\Delta(t)$ increases uniformly with time, and the flagella do not synchronize with the background flow. This behaviour in figure 4.6(a) is analogous to curves 1 and 2 in figure 4.4(b). When the forcing frequency increases to $f_F = 51.2$ Hz, periods of phase locking appear alternating with few occasional phase slips, in which the cell performs one additional beat and Δ rapidly increases by one unit. $f_F = 51.2$ Hz is at the edge of the Arnold tongue, in analogy with curve 3 in figure 4.4(b). By further increasing the frequency, we observe that for $f_F = 53.4 - 55$Hz, the phases remain constant for the entire 30s of each recording. This constant phase is characteristic of phase locking, and our experimental results show that, for $A_F = 5$ μm, the two flagella beat in synchrony with the external periodic flow. The range of forcing $f_F = 53.4 - 55$Hz is inside the Arnold tongue, and the trend of $\Delta(t)$ resembles curves 4, 5 and 6 in figure 4.4(b). When f_F increases again, the opposite transition to asynchronous behaviour takes place. In detail, at $f_F = 55.8$Hz, $\Delta(t)$ is archetypical of a synchronization transition [104]. The phase difference $\Delta(t)$ decreases monotonically, and hence it is not locked with the external forcing. However, the presence of the external forcing can be clearly seen in the stepwise decrease of $\Delta(t)$. For a long time (up to 4s), the phase decreases very slowly and remains nearly constant, nearly following the phase of the forcing. Then, rapidly, $\Delta(t)$ decreases as $\phi(t)$ progressively slips compared to $\phi_F(t)$. Finally, for $f_F = 57.5 - 60.3$Hz, i.e. higher than the intrinsic frequency, the phase difference $\Delta(t)$ decreases uniformly with time, and flagella do not synchronize with the background flow.

The frequency dynamics

In figure 4.6(b) are shown the spectrograms for 3 different forcing frequencies f_F that represent well the frequency dynamics of the cell. The three experiments are:

1. Forcing frequency $f_F = 60.3$Hz (see figure 4.6(b) *top*). In this experiment, the beating frequency f remains close to f_0 with variations that are within the long range frequency fluctuations existing in wt [75]. This forcing frequency is outside the synchronization region as in points 1 and 2 in figure 4.4(a).

2. Forcing frequency $f_F = 55.8$ Hz (figure 4.6(b) *center*). The spectrogram for $f_F = 55.8$Hz indicates a synchronization transition. The cell is forced to beat at the border of its synchronization region and the intrinsic beating frequency switches
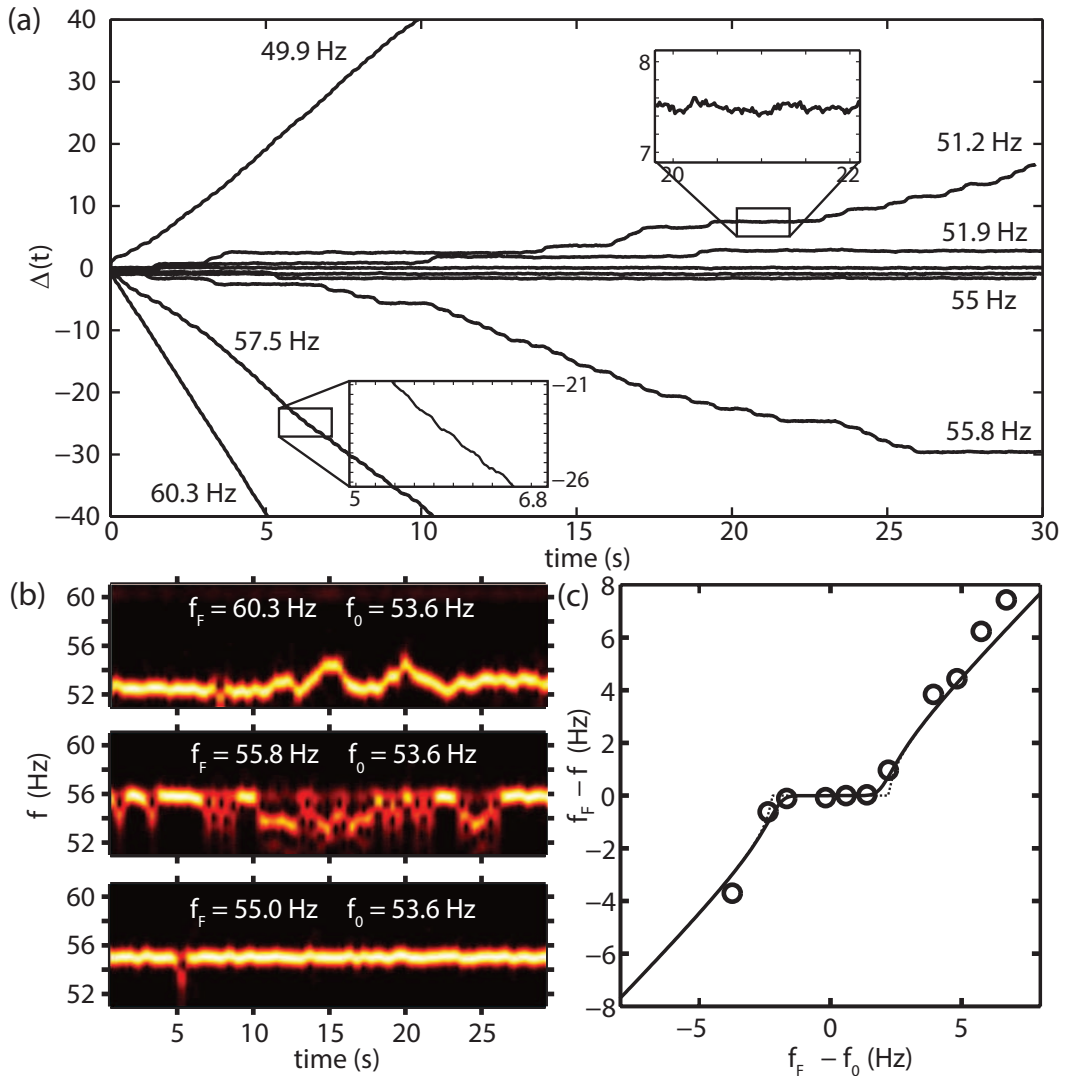
Figure 4.6: Experimental data for one dataset. The same cell is subject to an external flow $A_F = 5$ μm and $f_F = 49.9 - 60.3$ Hz. **(a)** Time variations of the phase difference between the flagella and the external flow for separate recordings. Inset for $f_F = 57.5$ Hz shows a stepwise decay of $\Delta(t)$. Inset for $f_F = 51.2$ Hz shows fluctuations during phase-locking. **(b)** Spectrograms of flagellar motion for different f_F. Black/white correspond to low/high amplitude in the frequency spectrum. From top: no synchrony ($f_F = 60.3$ Hz), partial frequency locking ($f_F = 55.8$ Hz) and complete frequency locking ($f_F = 55.0$ Hz). **(c)** $f_F - f$ as a function of $f_F - f_0$: (Symbols) experimental data, (solid line) f is computed from equation (4.15) with the fitted values for f_0, ϵ_0 and T_{eff}, (dotted line) f is computed from equation (4.15) in the limit of zero noise.

in time between f_0 and f_F. In this experiment, the forcing frequency is at the edge of the synchronization region, similar to point 3 in figure 4.4(a).

3. Forcing frequency $f_F = 55$ Hz (see figure 4.6(b) *bottom*). In this experiment, the frequency is equal to the forcing frequency ($f = f_F$). The spectrogram shows that the frequency remains locked, since $f = f_0$ for the entire 30s of recording. This is possible when the oscillator frequency is close to the forcing frequency, and during synchronization the two frequency become equal [104], similarly to points 4, 5, 6 in the theoretical model in figure 4.4(a).

Also, the dependence of the cell frequency f from the frequency detuning ν is in very good agreement with the model. In figure 4.6(c), are shown the experimental data for $A_F = 5$ μm (symbols) and the theoretical model obtained by fitting equation 4.14 on $\hat{P}(\Delta)$, solid and dashed line. Details about the fitting parameters are discussed in subsection 4.3.2.

SYNCHRONIZATION OF FLAGELLA WITH EXTERNAL PERIODIC BACKGROUND FLOW

We also varied the amplitude of the axial flow. For each frequency within the same range of frequencies $f_F = 49.9 - 60.3$, the flow amplitude was increased from $A_F = 2.5$ μm to $A_F = 7.5$ μm. Figure 4.7 (a) describes the experimental results for $\Delta(t)$. In each frame of figure 4.7(a) the evolution of $\Delta(t)$ for varying A_F is represented at the same f_F.

We first consider an external forcing with frequency $f_F = 49.9$ Hz, lower than the intrinsic beating frequency of the cell. For flows of low amplitude ($A_F = 2.5$ μm and $A_F = 5$ μm), $\Delta(t)$ increases uniformly with time and flagella do not synchronize with the background flow (red and blue curves in 4.7(a)). These trends are analogous to curves 1 and 2 in figure 4.4(b). For a larger amplitude of $A_F = 7.5$ μm, the influence of the external forcing can be seen from the increase of $\Delta(t)$ in a stepwise fashion. This trend indicates the proximity of a synchronization transition (black curve in 4.7(a)), similar to curve 3 from figure 4.4(b).

For $f_F = 51.2$ Hz, the experimental results are similar to our previous results for $f_F = 49.9$ Hz, but the transition to synchronization occurs already at lower flow amplitude. While $A_F = 2.5$ μm is outside the synchronization region, $A_F = 5$ μm and $A_F = 7$ μm are already inside the synchronization region. At the forcing frequency $f_F = 54.2$ Hz, phase locking occurs for long periods of time for all flow amplitudes $A_F = 2.5 - 7.5$ μm. Experiments for higher frequencies, $f_F = 55.8$Hz and $f_F = 57.8$ Hz, are similar to experiments for $f_F = 49.9$ Hz and provide evidence for the reverse transition to asynchronous behaviour.

To summarize, for $A_F = 7.5$ μm, the synchronization transition starts at $f_F = 49.9$Hz and ends at $f_F = 57.5$ Hz, while for $A_F = 2.5$ μm, the transition starts at $f_F = 54.2$Hz and ends at $f_F = 55.8$. These results indicate a linear correlation between amplitude of the external forcing and frequency range at which phase locking occurs. In the next section, we fully characterize the synchronization region.
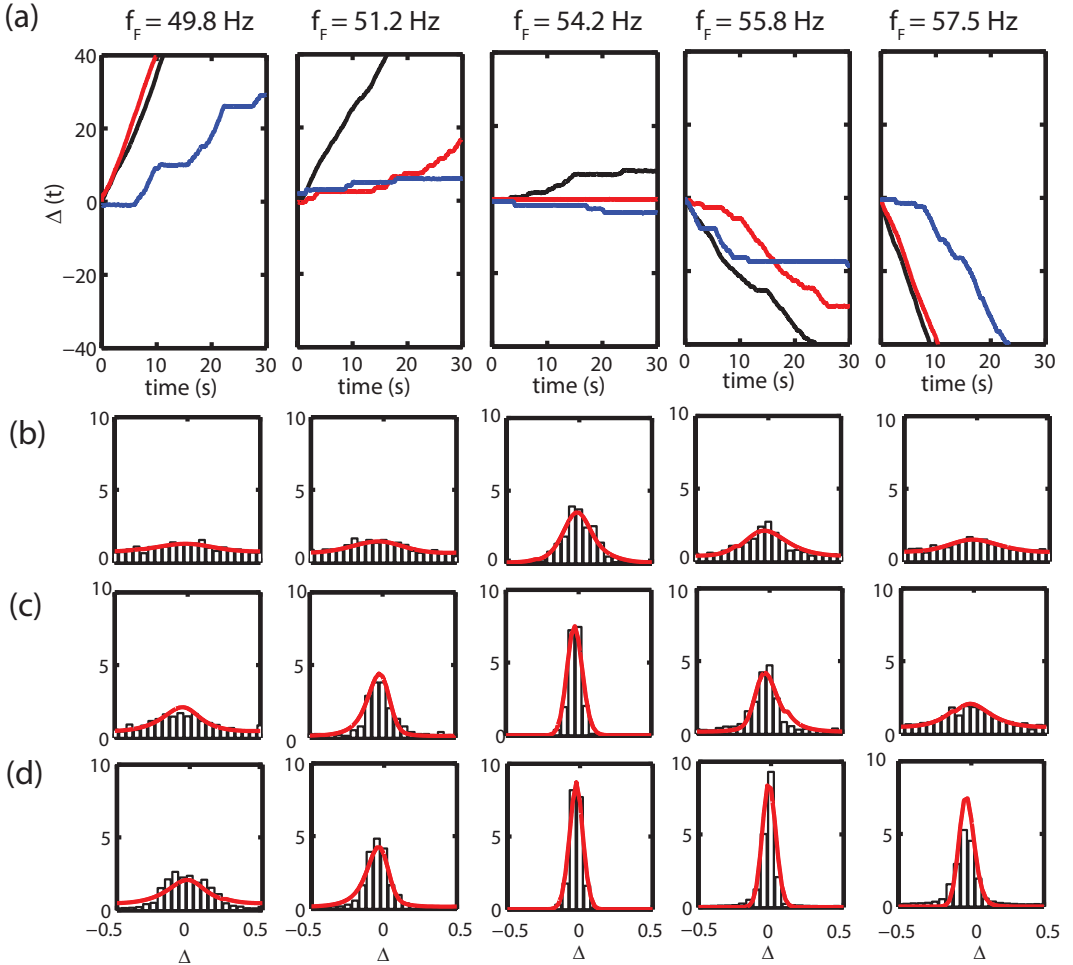
Figure 4.7: Experimental data for the same cell experiencing an external flow $A_F = 2.5 \ \mu m$ (black line), $A_F = 5 \ \mu m$ (red line), $A_F = 7.5 \ \mu m$ (blue line). **(a)** Time variations of the phase difference between the flagella and the external flow during separate recordings. Each panel represents the evolution of $\Delta(t)$ at a certain f_F, where f_F is in the range $49.9 - 60.3$ Hz. **(b-d)** Histograms representing the distributions of phase difference $\Delta(t)$ at specific f_F. **(b)** $A_F = 2.5 \ \mu m$. **(c)** $A_F = 5 \ \mu m$. **(d)** $A_F = 7.5 \ \mu m$. The red line indicates $\hat{P}(\Delta)$ obtained by fitting the parameters $f_0 = 53.6$Hz, $T_{eff}/f_0 = 0.0006$, $\epsilon_0/f_0 = 0.021$ **(b)**, $\epsilon_0/f_0 = 0.042$ **(c)**, $\epsilon_0/f_0 = 0.075$ **(d)**.

4.3.2 SYNCHRONIZATION PHASE DIAGRAM

The same experiments as described in subsection 4.3.1 were repeated for a multitude of cells; overall the range considered is $A_F = 1 - 10 \ \mu m$ and $f_F = 43 - 68$ Hz, equivalent to $U_F = 0 - 1360 \ \mu m.s^{-1}$. Experiments performed on several cells are combined to fully characterize the synchronization region from each cell. By combining the synchronization region where the flagella of *C. reinhardtii* synchronize with the external flow. Furthermore, we compare our experimental results with the

theoretical model discussed in 4.2.2. From this analysis we learn how well our biological oscillator *C. reinhardtii* resembles a model self sustained oscillator.

THE EXPERIMENTAL ARNOLD TONGUE

Figure 4.8(a,b) represents the experimental results for 41 data sets and 373 separate recordings of experiments for the entire range of amplitude and frequency. Each dot represents a separate experiment in the (ν, U_F)-phase domain. In figure 4.8(a), the x-axis indicates the frequency detuning $\nu = f_F - f_0$ to take into account cells with different intrinsic frequency f_0. The y-axis represents the velocity of the forcing flow U_F, non-dimensionalized with the cell free swimming velocity $U_0 = 110 \ \mu m.s^{-1}$.

The colormap indicates the time fraction when flagellar beating is phase-locked with the external forcing. When phase locking is observed for the entire recording time, the time fraction is 1 (black). When phase locking never occurs, the time fraction is 0 (white). Figure 4.8 (a) gives a clear representation of the synchronization region in the (ν, U_F)-phase domain, which is in agreement with the tongue-shaped synchronization region (see figure 4.4(a)) predicted by the model system.

We also investigated frequency locking at f_F, i.e. close to what has been reported to be the intrinsic beating frequency of *trans*-flagellum. We imposed an axial flow with $U_F = 100 - 1500 \ \mu m.s^{-1}$ and $f_F = 64.7 - 76.6$ Hz. Experiments on 5 cells show no events of synchrony with the external forcing; the cells keep beating normally at f_0, slip events are within statistics discussed in appendix B. This evidence suggests that in *C. reinhardtii* wt, the *trans*-flagellum is strongly locked to the *cis*-flagellum and, hence, even a strong external hydrodynamic forcing at ≈ 70 Hz is neither able to perturb the intrinsic beating frequency of the cell, nor to increase slip occurrences.

FITTING OF THE EXPERIMENTAL ARNOLD TONGUE

Since we are interested in modelling the behaviour of *C. reinhardtii* as a self-sustained oscillator under the influence of an external forcing, we want to fit equation 4.14, presented in section 4.2.2, to our experimental data. From equation 4.11, the phase dynamics is determined for each experiment by three constant parameters: $\nu = f_F - f_0$, T_{eff}, and ϵ. For each experiment we infer the values of ν, ϵ, and T_{eff} by fitting the solution for the steady probability distribution of the phase difference $\hat{P}(\Delta)$ to the probability distribution (equation 4.14) measured in the experiment. The value for $\nu = f_F - f_0$ is known for each experiment, and we assume the noise level T_{eff} to be a cell-dependent constant, due to stochasticity in the flagellar actuation. Hydrodynamic forces depend linearly on the flow velocity in the inertialess regime. The coupling strength with the external forcing ϵ is assumed to scale directly with the hydrodynamic force on the flagella, hence scaling linearly with the flow velocity ($\epsilon \sim U_F$). Within a dataset, A_F is constant while f_F is varied and we express ϵ as $\epsilon_0 f_F / f_0$ accordingly. Therefore $\hat{P}(\Delta)$ depends on f_0, ϵ_0, and T_{eff}, whose values are obtained for each A_F by least-square fitting equation 4.14 to all experimental probability distributions within the dataset. For each dataset Figure 4.7(b-d) represents $\hat{P}(\Delta)$ with $A_F = 2.5 \ \mu m$ (Figure 4.7(b)), $A_F = 5 \ \mu m$ (Figure 4.7(c)) and
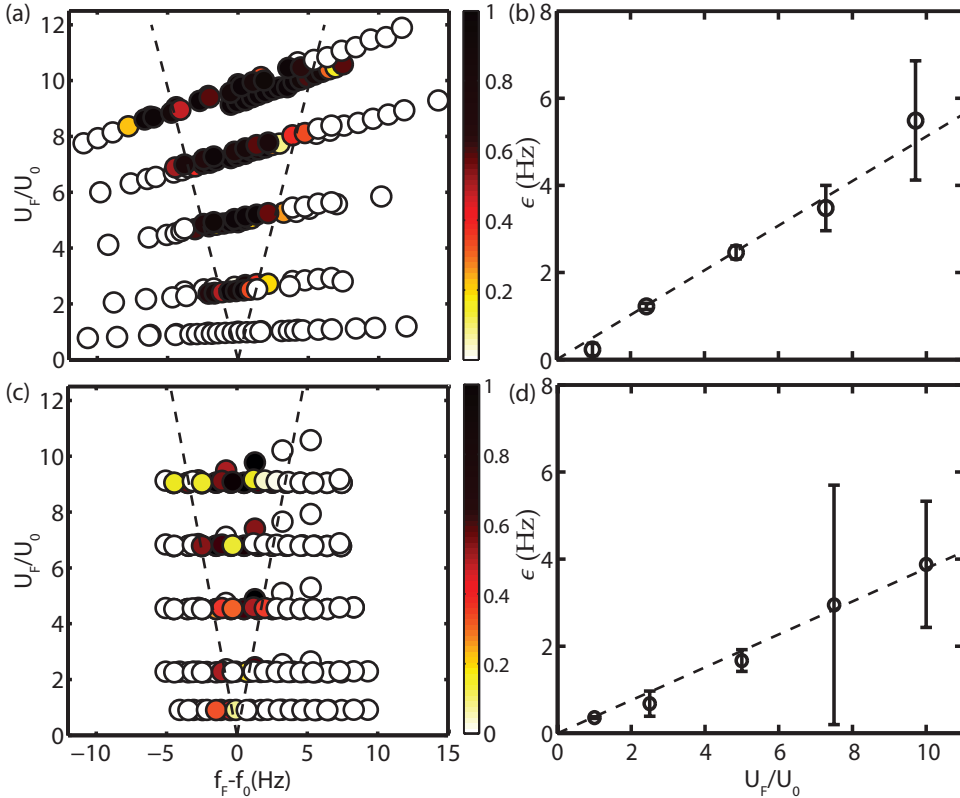
Figure 4.8: (a,c). Synchronization region in (f_F, U_F)-domain in presence of axial flow **(a)** and cross flow **(c)**. Each marker represents a separate recording. U_F ranges from 86 μm.s^{-1} to 1300 μm.s^{-1} and is normalized with $U_0 = 110 \pm 12$ μm.s^{-1}, i.e. the free swimming velocity of the cells. The colormap represents the time fraction when flagellar beating is phase-locked with external flow. It is equal to 1 (black) when phase-locking is observed for the entire time of recording, while it is 0 (white) when phase-locking is never observed. **(b,d)**. Coupling strength ϵ as a function of external flow U_F/U_0, when the cell is experiencing axial flow **(b)** and cross flow **(d)**.

$A_F = 7.5$ μm (Figure 4.7(d)). We also estimated the average beating frequency predicted by equation (4.12) as:

$$f = \int_0^1 -\frac{dV}{d\Delta}\hat{P}(\Delta)d\Delta. \tag{4.15}$$

Figure 4.6(c) shows the agreement between measurements of f from experimental data and the value predicted by the model of equation (4.15). The stochastic phase dynamics is therefore well modelled with the three fitted parameters f_0, T_{eff}, and ϵ_0. For experiments with axial flow, these values are $f_0 = 52.6 \pm 1.1$ Hz and $T_{\text{eff}}/f_0 = 0.0008 \pm 0.0003$. We find a value for T_{eff}, in agreement with previously reported values [91, 112]. Figure 4.8(b) shows the values fitted for the coupling strengths ϵ as a function of the nondimensional flow velocity U_F/U_0. We find ϵ to increase linearly with the flow velocity U_F, and we thus estimate ϵ directly as a function of the hydrodynamic forces $\epsilon = \alpha U_F/U_0$ with $\alpha = 0.51$ s^{-1} for axial flow.

Overall, the experimental results in Figure 4.8(a,b) define a synchronization region having the characteristic signature of the Arnold tongue presented in 4.2.1, suggesting that the analogy between *C. reinhardtii* and a self sustained oscillator is robust. Moreover, from figure 4.8(a), we observe that the synchronization ranges of different cells are consistent with each other. The synchronization region is well defined by fitting parameters f_0, T_{eff} and ϵ_0.

4.3.3 SYNCHRONIZATION REGION WITH CROSS FLOW

Additional experiments with cross flow, in the direction transverse to the cell axis, have been performed on several cells (see figure 3.4(b)). The flow velocities imposed are similar to the experiments with axial flow, namely $A_F = 1 - 10$ μm and $f_F = 47 - 60$ Hz, equivalent to $U_F = 0 - 1150$ $\mu m.s^{-1}$. For cross flow, the theoretical model has been fitted on the experimental phase distributions following the same approach as for axial flow (section 4.3.2). Figure 4.8(c,d) shows the synchronization region and coupling strength ϵ in this flow configuration. Overall, cross flow triggered phase locking only in a small range of f_F. When $U_F \approx 100$ $\mu m.s^{-1}$, three experiments have revealed a synchronization transition (see figure 4.8(c)). For stronger flows, $U_F = 250 - 1150$ $\mu m.s^{-1}$, synchronization is observed systematically only in a very narrow range of f_F around f_0, with the synchronization region increasing slightly with forcing amplitude (see Figure 4.8 (d)). There is however large variation among different cells, and phase locking with cross flow is less consistent than with axial flow. This result confirms the importance of the direction along which an hydrodynamic forcing is acting. For cross flow, we fitted the experimental phase distributions with the solution 4.14 of equation 4.13, similarly as for the axial flow. For this set of cells, we find $f_0 = 51.5 \pm 1.1$ Hz and $T_{\text{eff}}/f_0 = 0.0011 \pm 0.0004$. The coupling strength ϵ with cross flow increases linearly with U_F, and we find $\alpha = 0.38s^{-1}$ where $\epsilon = \alpha U_F/U_0$. For comparison, the Arnold tongue for cross flows with $\alpha = 0.38s^{-1}$ is much narrower than $\alpha = 0.51s^{-1}$ in presence of axial flow (see Figure 4.8(c)).

4.3.4 PHASE DIFFERENCE INSIDE THE ARNOLD TONGUE

In this section, we discuss the time evolution of the phase difference $\Delta(t)$ when the forcing frequency f_F is within the synchronization range. Inside the synchronization region, for $\nu \neq 0$, the solution of equation 4.4 is the sum of a steady state solution Δ_0 and a transient term $\tilde{\Delta}(t)$ (see equation 4.6 and subsection 4.2.1). The transient solution of the oscillator, in this case *C. reinhardtii*, is expected to be strongly dependent on the initial phase angle of the flagella at the moment when the forcing is activated [113], as we discuss below. Both the transient and steady state solutions of the phase dynamics provide insights into the coupling between flow and flagella, characterized by the function $\mathcal{Q}(\Delta)$ in equation 4.11. In particular, the transient solution defines the characteristic time response of *C. reinhardtii*, which has never been investigated before.

To study the transient and steady state solution, we executed the Experiment type 2 described in section 4.1. We imposed axial flow on 3 cells at velocities $U_F = 680, 901, 1109, 1307$ $\mu m.s^{-1}$. At each velocity, we tested frequencies in the range

$f_F = 50 - 60$Hz. As mentioned in subsection 4.2.1, phase locking is required to study the transient and steady state solutions, and we therefore limit the discussion to experiments where phase locking occurred. We extract the forcing phase angle $\phi_F(t)$ and the flagella phase angle $\phi(t)$ in each experiment (details on the method are in subsection 4.1.2). In each recording, the phase angle of the piezoelectric stage depends on the starting position of the bead in the flow chamber, and the phase angle of flagella depends on the position of the interrogation window. These two contributions determine the steady state solution Δ_0. We are interested in comparing Δ_0 in different experiments. Therefore we define a reference phase angle for both the piezoelectric stage and the flagella. We define the phase reference for flagella $\phi = 0$ when flagella are at the start of the power stroke, as in the second snapshot in figure 4.10. Instead, the phase reference for the piezo stage is the maximum in the stage displacement signal $X(t)$ (details on stage calibration in subsection 3.2.2). Then the phase difference is zero, $\Delta = 0$ when flagella are initiating the power stroke precisely at the same time that the stage displacement signal $X(t)$ is maximal. This configuration is shown in the video frames in figure 4.10 (a). The stage position in each frame has been reconstructed during post processing, and it is shown by the red dot (details on the method in 4.1.2 and in 3.2).

Once this reference configuration is defined, the transient and the steady state solutions of $\Delta(t)$ in different experiments can be compared, as discussed in the following two subsections.

THE TRANSIENT TO SYNCHRONIZATION

In this subsection, we discuss the transient response of *C. reinhardtii* when axial flow is activated. Figure 4.9 shows an experiment with forcing velocity $U_F = 1071$ μm.s^{-1} and forcing frequency $f_F = 55.6$ Hz, resulting in $\nu = 2.3$ Hz. Figure 4.9 (a,b) represent, respectively, the running time spectrum of f and the two pulses indicating the stage activation and arrest (see section 3.2.2 for details). Figure 4.9 (c) shows the evolution of $\Delta(t)$. In absence of forcing, the phase of the forcing remains constant and $\Delta(t)$ increases linearly at a rate equal to f_0. The insert at time $t = 1$ s shows in detail the variations of $\Delta(t)$ when the forcing starts. Our recording shows the presence of a transient over a finite period of time, in which the phase slowly decreases before $\Delta(t)$ reaches the steady state solution Δ_0.

From the phase difference $\Delta(t)$, recorded for each experiment within the synchronization region, we fit the experimental decay of the phase difference predicted by equation 4.8, in order to estimate the characteristic time scale of the transient $\tau = (\epsilon d\mathcal{Q}/d\Delta|_{\Delta_0})^{-1}$. For the experiment represented in figure 4.9, we find the duration of the transient to be $\tau = 172$ ms, corresponding to ≈ 9.5 periods of forcing motion. τ has an uncertainty of 1.1 ms due to the piezoelectric stage activation precision (details in section 3.2).

Fitting is, however, only possible when $\Delta(t)$ reaches the steady state towards an exponential decay, as in figure 4.10(b,d). If the flagella and the forcing are already in phase when the forcing starts, as in figure 4.10(c), we observe no transient and cannot fit the exponential decay (equation 4.8). Also, in many experiments, the initial phase difference $\Delta(t)$ is large and $\Delta(t)$ fluctuates before conveying to its steady state solution.
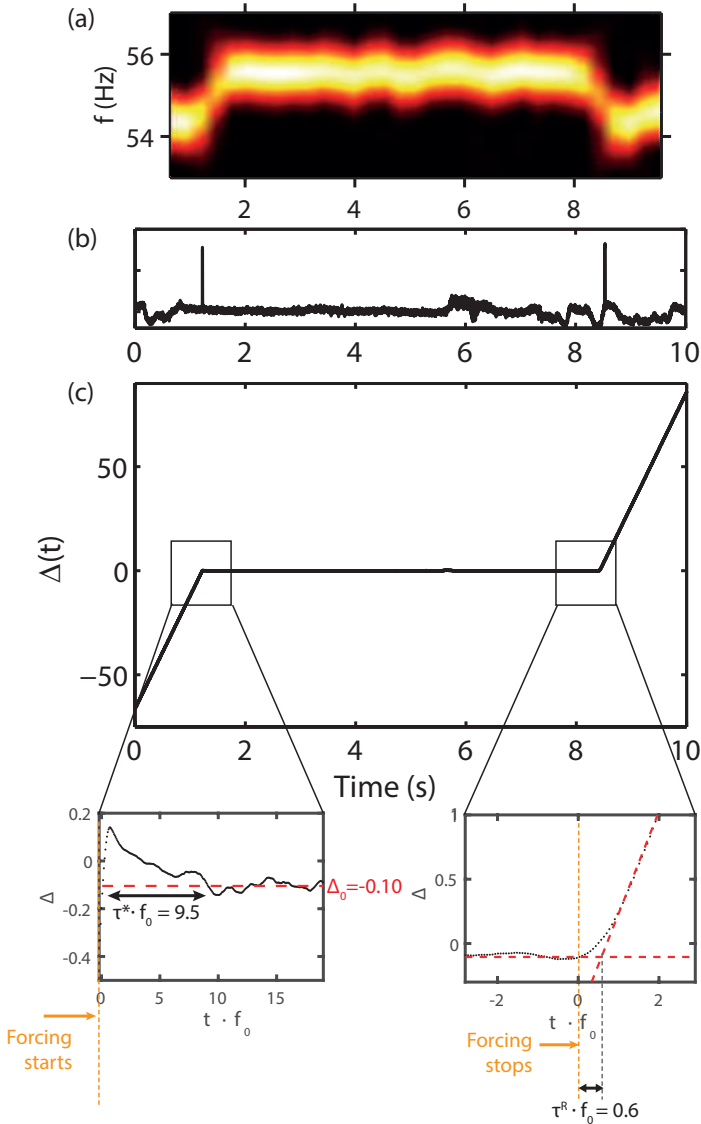
Figure 4.9: (a) Spectrogram of flagellar motion for $f_F = 55.6$ Hz and $U_F = 1071\ \mu m.s^{-1}$.**(b)** Signal extracted from the piezoelectric stage. The first peak indicates that the stage is activated, the second peak indicates that it is arrested. **(c)** Time variations of the phase difference $\Delta(t)$. Insets show respectively the time to reach constant phase $\tau* = 172$ ms and the time to recover to f_0, $\tau_R = 20m$s. Flagella are coupled with the forcing with a constant phase difference $\tilde{\Delta}(t) = -0.10$.

In this case, the exponential decay of $\Delta(t)$ does not begin instantaneously when the forcing is activated and cannot be fixed. Hence, we characterize the time scale of the transient by computing the total time $\tau*$ between the beginning of the forcing and the moment when phase locking is established. Phase locking is considered constant when $\Delta(t)$ shows fluctuations within ± 0.05. Considering all the experiments at $U_F = 670.3 \pm 74.8\ \mu m.s^{-1}$, the total time to reach the steady state is $\tau* = 202 \pm 114$ ms,

equivalent to 11 ± 6 flagella beating cycles. $\tau*$ has a large standard deviation among experiments, confirming that the flagellar phase angle $\phi(t)$ at the moment of forcing activation affects the time to reach a steady state [113].

To investigate whether $\tau*$ is influenced by the forcing amplitude, we tested, on the same cell, flows with a higher amplitude, i.e. $U_F = 680, 901, 1109, 1307 \; \mu\text{m.s}^{-1}$, and with a forcing frequency in the range $f_F = 49.9 - 58.5$ Hz. Figure 4.11(a) shows the average duration of the transient $\tau*$ at each of these forcing velocities. For each amplitude, the variation measured in $\tau*$ can be explained by the strong dependence of $\tau*$ on the initial phase difference. A key conclusion from figure 4.11(a) is that $\tau*$ significantly decreases at higher forcing velocities. It bears emphasis that the variance in the measured $\tau*$ is also significantly reduced. In detail, the median $(\tau*) \cdot f_0 \approx 10.7$ at $U_F = 680 - 901 \; \mu\text{m.s}^{-1}$ and decreases to $(\tau*) \cdot f_0 \approx 3.4$ at $U_F = 1109 - 1307 \; \mu\text{m.s}^{-1}$. Hence, for forcing velocities above 1 mm.s^{-1}, the cells synchronize with the external flow within $3 - 4$ oscillation periods, as confirmed by the lower standard deviation of $\tau*$. This outcome is consistent with the theoretical model of a self sustained oscillator forced externally, since, from equation 4.8, the transient duration $\tau*$ is expected to scale inversely proportional with the forcing strength ϵ.

THE STEADY STATE SOLUTION

We now turn our attention to the constant steady state phase difference Δ_0 reached by $\Delta(t)$ after the transient. Regarding the steady state, as discussed in subsection 4.2.1, if $f_F < f_0$, the theoretical model predicts Δ_0 to be positive, while, if $f_F > f_0$, Δ_0 is predicted to be negative.

Figure 4.10(b-d) shows the phase differences $\Delta(t)$ for 3 separate experiments on the same cell (with $f_0 = 54.4 \pm 0.2$ Hz) at constant forcing amplitude $A_F = 6.9 \; \mu\text{m}$. Experiments are performed for different values of the frequency detuning $\nu = -1.6, 0.3, 2.3$ Hz, and the corresponding phase dynamics are plotted in figure 4.10 (b, c, d), respectively. For all values ν, robust synchronization is established between the flagella and the forcing. In figure 4.10(b), the frequency detuning is $\nu = -1.6$ Hz, since the intrinsic frequency of the flagella is higher than that of the forcing. The inset of $\Delta(t)$ at center shows that the steady state phase Δ_0 is 0.15, corresponding to the flagella phase being ahead of the forcing. In figure 4.10(c), the forcing frequency is close to the intrinsic frequency, ν is 0.3 Hz, and synchronization is almost in phase with the steady state phase $\Delta_0 = 0.05$. Finally, when the intrinsic frequency is lower than the forcing, $\nu = 2.3$ Hz, and the phase of the flagella lags the phase of the forcing, $\Delta_0 = -0.12$ (see figure 4.10(d)). The dependence of the steady state phase difference on ν is clear from the images of the waveform; see right column of figure 4.10(b,c,d). Our observations are in agreement with the theoretical model. In fact, from the theoretical definition of the fixed point $0 = -\nu - \epsilon \mathcal{Q}(\Delta_0)$ in equation 4.5, we can directly infer the force of the coupling function $\mathcal{Q}(\Delta)$. To do this, we collected results for the steady state solution for 20 experiments on 3 cells at $U_F = 670.3 \pm 74.8 \; \mu\text{m.s}^{-1}$ (see figure 4.10(e)). We observe that phase-locking does not happen at every Δ_0; all steady state phase difference recorded experimentally are in the range $(-0.15, 0.38)$. Given these results, it seems not possible to reach a steady state solution where flagella are almost in anti-phase with the flow ($\Delta_0 \approx 0.5$).
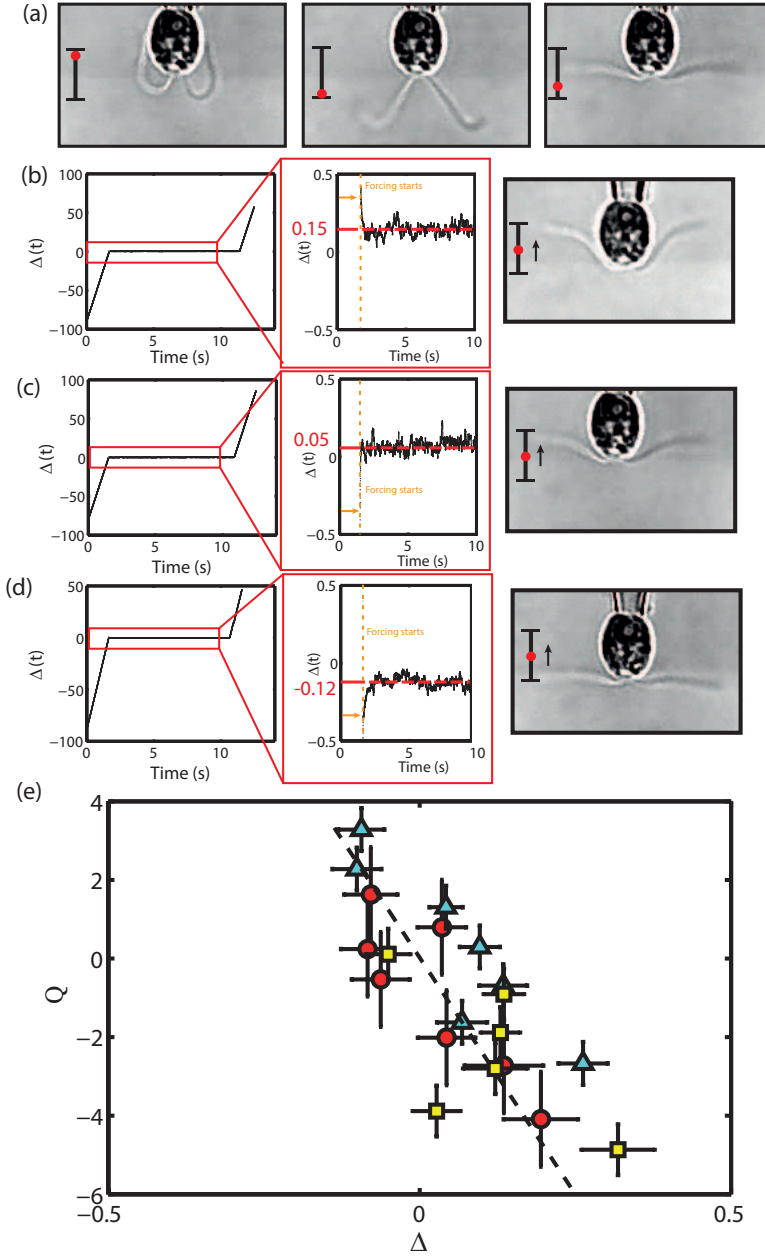
Figure 4.10: (a) Snapshots of flagellar beating cycle in the case of phase locking with $\Delta(t) = 0$. The dot represents the position of the stage, the bar delimits the amplitude of the stage motion, corresponding to $A_F = 6.9\ \mu$m. The time lapse between frames is 5 ms. **(b)** *Left* $\Delta(t)$ between flagella and background flow with $\nu = -1.6$ Hz and $\Delta_0 = 0.15$. *Center* Inset showing the steady state solution $\Delta_0 = 0.15$. At this Δ_0, flagella are coupled with the background flow moving slightly ahead of the stage displacement, as confirmed by the snapshot (*Right*). **(c)** $\Delta(t)$ for $\nu = 0.3$ Hz. In this experiment the steady state solution is $\Delta_0 = 0.05$, indicating that flagella are almost perfectly in phase with the background flow. **(d)** When ν is 2.3 Hz, Δ_0 is -0.12, suggesting that flagella are phase locked, lagging slightly behind the stage displacement. **(e)** Results for Δ_0 in (Δ,ν)-domain, different markers distinguish different cells. The solid lines on each marker represent $d\mathcal{Q}/d\Delta|_{\Delta_0}$. The dashed line is the slope of $\mathcal{Q}(\Delta) = -\alpha\Delta$ with $\alpha = 1/0.042 = 23.8$ from fitting.

An example of anti-phase coupling would be if flagella were in the recovery stroke while the stage displacement was at its maximum position. Figure 4.10(e) represents, for each experiment, ν as a function of the Δ_0 measured. From equation 4.5, $\nu = \mathcal{Q}(\Delta_0)$ and figure 4.10(e) approximates the function $\mathcal{Q}(\Delta)$. We find that $\mathcal{Q}(\Delta) = -\alpha\Delta$ with $\alpha = 23.8$.

THE TRANSIENT OUT OF SYNCHRONIZATION

In the same experiments discussed above, we also characterized the relaxation time (τ_R), defined as the time interval between when the forcing stops and the re-establishment of flagellar beating at a constant intrinsic frequency. As soon as the piezostage stops moving, the phase of the piezostage remains constant and no longer increases. As shown by the inset in figure 4.9(c), the phase difference $\Delta(t)$ resumes a linear increase, indicating that the intrinsic frequency has been restored. We estimate the relaxation time and the intrinsic frequency by fitting a line to $\Delta(t)$ and computing its intersection with the constant phase difference before synchronization is interrupted (see figure 4.9(c)). In this example, the intrinsic frequency is restored in less than one beating cycle ($\approx 0.6 \cdot f_0$).

We performed experiments at different forcing velocities on 7 cells (see figure 4.11 (c)). For $U_F = 680 - 1307$ μm.s^{-1}, we find $\tau_R \cdot f_0$ within 0.16 and 0.61. In separate experiments on different cells, we observe consistently that the intrinsic beating frequency is re-established within less than one beating cycle. The median value of τ_R is approximately constant among different velocities, suggesting that τ_R is independent of the forcing velocity.

This subsection concludes the results on the behaviour of the phase difference between flagella and forcing within the Arnold tongue. Our results show that the phase dynamics of the flagella of *C. reinhardtii* is very well modelled as that of an ideal self sustained oscillator subject to an external harmonic forcing. After a transient response, flagella steadily lock to the forcing frequency, and when the forcing ceases, they immediately re-establish their intrinsic frequency.

4.3.5 ADAPTATION IN FLAGELLAR BEATING FREQUENCY

Here we present results for experiments investigating changes to the intrinsic frequency of *C. reinhardtii* due to the external perturbation. We imposed a periodic background flow at $U_F = 1194 \pm 2.5$ μm.s^{-1} and $f_F = 56 - 58$ Hz; hence inside the synchronization region, in order to achieve phase locking. We imposed the forcing for long periods of time up to 608 s (equal to 10′8″) without interruption. We then measured the cell intrinsic frequency post forcing (f_0^{post}), and we compared it with the cell intrinsic frequency pre forcing (f_0^{pre}). Both f_0^{pre} and f_0^{post} have been extracted by computing the discrete Fourier transform as discussed in section 4.1.2. Figure 4.11(b) presents the results for $(f_0^{post} - f_F)/(f_0^{pre} - f_F)$ as a function of forcing duration. We observe that for the shorter experiments (≈ 7 s), the difference between the beating frequency before and after the synchronization period is small, and $f_0^{post} \approx f_0^{pre}$. When the duration of the experiment increases significantly (experiments lasting 310 s and
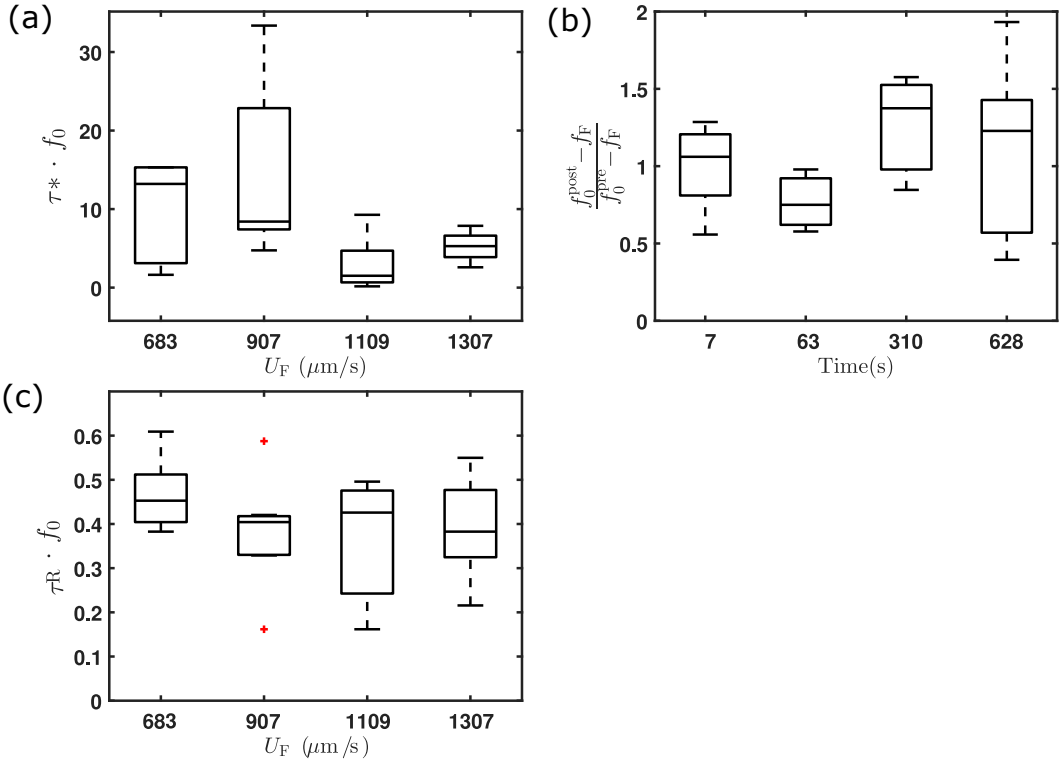
Figure 4.11: (a) Boxplots showing the time $\tau*$ to reach the steady state as a function of forcing velocity U_F. Forcing frequencies are all inside the synchronization region ($f_F = 49.9 - 58.5$ Hz). At the two lower forcing velocities considered, $\tau*$ is higher, with median $\tau * \cdot f_0 \approx 10.7$. At the two higher flow velocities $\tau * \cdot f_0 \approx 3.4$. **(b)** Relaxation time τ_R as a function of forcing velocity U_F. The median value of τ_R does not vary significantly when increasing U_F. **(c)** Results for $\left(f_0^{\text{post}} - f_F\right) / \left(f_0^{\text{pre}} - f_F\right)$ as a function of forcing duration. When the forcing duration increases, f_0^{post} is on average slightly higher than f_0^{pre}. However, this variation is within the limits of natural long range fluctuations in f_0 occurring in wt.

628 s) the difference between f_0^{post} and f_0^{pre} is on average larger. However, this difference in frequency before and after the forcing is no greater than 3 Hz. From our experiments, we find that *C. reinhardtii* wt show, over time, fluctuations in f_0 of about 3 Hz [75, 103]. Therefore, this mismatch f_0^{pre} and f_0^{post} in long recordings could be a natural adjustment of f_0 independent of the imposition of an external forcing. Based on this observation, there is no evidence that a forcing imposed for long times (i.e. longer than 600 s) systematically affects the intrinsic frequency of the cell.

4.4 CONCLUSIONS AND DISCUSSION

The algae *C. reinhardtii* has been the object of several studies aiming at understanding the details of its functioning and to clearly identify the mechanisms controlling flagellar synchronization. Given the synchronous beating of the flagella at an approximately constant frequency, *C. reinhardtii* is an example of biological oscillator.

We explored the possibility to entrain the biological oscillator *C. reinhardtii*. In the experiments described in this chapter, we imposed on a single cell periodic hydrodynamic forcing in an attempt to control externally the intrinsic frequency of the cell. The forcing imposed have controlled frequency and amplitude, and mimic the background flow generated by a freely swimming cell. The possibility of the cell to synchronize with this external flow yields insight not only on the nature of this biological oscillator, but also on the role of hydrodynamic forces in mediating flagellar synchronization.

4.4.1   C. REINHARDTII AS THE IDEAL BIOLOGICAL SELF SUSTAINED OSCILLATOR

The first important observation emerging from our experiments is that flagella from *C. reinhardtii* can be forced to beat at a different frequency by imposing an external hydrodynamic forcing. This consistent locking of *C. reinhardtii* to controlled external forcing has never been observed experimentally before. However, temporary changes in the intrinsic frequency have been reported in early studies by Rüffer and Nultsch [72, 73]. We observed that the cell is able to synchronize with the external flow within a certain range of forcing frequencies up to 6 Hz, and this frequency range is consistent among different cells (subsection 4.3.1). We modelled this phenomenon and compared our results with a model self-sustained oscillator coupled with an external forcing in the presence of noise. Our experiments define a synchronization region for *C. reinhardtii* having the shape of an Arnold tongue. By fitting the Adler equation [105] on the experimental data (equation 4.14), we show that the synchronization region for each cell can be modelled with three fitting parameters: the intrinsic frequency, the coupling strength, and the intensity of the Gaussian noise. The synchronization region was investigated for two forcing directions: axial flow (subsection 4.3.2), and cross flow (subsection 4.3.3). The latter flow direction delineates a less consistent coupling between flagella and external forcing. An explanation for this weak coupling of flagella with cross flow could be in the lower forces imposed on the flagella. To this purpose we provide, in the next chapter, a quantitative description of the forces imposed on flagella by axial flow and cross flow of equal forcing amplitude and frequency (see section 5.5). Within the synchronization region, we analysed the phase dynamics to address the analogy between wt and an ideal self sustained oscillator in more detail (subsection 4.3.4). Namely, we characterized the transient to synchronization and the steady state solution. We found that the forcing strength affects the transition time from intrinsic frequency f_0 to forcing frequency f_F. The duration of the transient varies significantly among experiments, hinting that the flagellar position when the forcing starts has an important role. Also, the forcing strength affects the time to reach the steady state, since for flow velocities above 1 mm.s^{-1} the transition to synchronization is 3 times faster. This behaviour is in agreement with the theoretical model described by the Adler equation.

The steady state solution is consistent with the theory of self-sustained oscillators: the phase of the flagella lags the phase of the forcing when the frequency of the forcing is higher than that of the flagella, while the phase of flagella is ahead of the phase of the forcing when the forcing frequency is lower than the intrinsic frequently (subsection 4.3.4). We also characterize the time interval between the arrest of the

forcing and the restoring of a constant intrinsic frequency. We find this time interval to be shorter than one beating cycle, showing that when the forcing is stopped, flagella return immediately to beat at their own frequency. We conclude the analogy with an ideal oscillator by considering the difference in cell beating frequency before and after imposing a forcing for 1, 5, and 10 minutes (subsection 4.3.5). Results indicate that the intrinsic beating frequency measured after imposing the forcing is always within 3 Hz from the frequency measured before the experiment, hence within the frequency fluctuations observed over time in wt.

The results presented in this chapter demonstrate that the behaviour of *C. reinhardtii* is in agreement with that of an ideal self sustained oscillator under external harmonic forcing.

4.4.2 SYNCHRONIZATION AND HYDRODYNAMIC FORCES

Above we discussed the analogy between the algae *C. reinhardtii* and a self sustained oscillator. Here we draw conclusions on the limitations in the model oscillator and on the implications of our study for the role of hydrodynamic interaction forces in mediating synchronization between the flagella. Our experiments demonstrate that eukaryotic flagella do respond to hydrodynamic forces and can be synchronized with an external flow.

As discussed in section 2.3, interflagellar synchronization in *C. reinhardtii* requires phase-locking between two flagella, whose intrinsic beating frequencies are reported to differ by as much as 30%, hence requiring coupling strengths $\epsilon \approx 15 - 20$Hz [114]. In contrast, in our experiments with the highest flow amplitude, $U_F \approx 10U_0$, the hydrodynamic forces on the flagella are an order of magnitude larger than those experienced for free-swimming cells, yet the flagella only synchronize to flows with forcing frequencies within 5 Hz of f_0. If the imposed frequency is more than 5 Hz apart from the intrinsic frequency, imposing the external flow has no effect on the cell behaviour. Based on our experimental results (see figure 4.8(a)), we can expect that in order to achieve synchronization at $15 - 20$ Hz from f_0, we should impose flows of over $30U_0 \approx 3300$ μm.s^{-1}. However, at such high flow intensity, abrupt and permanent changes in the cell have been reported, leading in some cases to deflagellation or cell death [115]. Another aspect of flagellar synchronization that emerged in our experiments is that only forcing at a frequency close to the *cis*-flagellum intrinsic frequency (≈ 53 Hz) can trigger synchronization. A forcing at a frequency close to the frequency of the *trans*-flagellum has no effect. This suggests that the *trans*-flagellum is strongly locked to the *cis*-flagellum, since its dynamics is not affected by a strong external hydrodynamic forcing close to its intrinsic frequency at about 70 Hz.

IMPLICATIONS FOR THE ROLE OF HYDRODYNAMIC FORCES

As stated in section 2.5, exploring the role of hydrodynamic forces on flagellar synchronization is the primary goal of this thesis. A large number of theoretical and experimental studies supported the dominant role of hydrodynamic interaction forces in mediating interflagellar synchronization (see section 2.4 for details). As discussed in

section 2.3.2, a recent experimental study provides evidence of established synchronization through hydrodynamic interactions between two isolated flagella of Volvox, whose intrinsic beating frequencies differ by $\sim$ 10% [12]. Volvox and *C. reinhardtii* are different organisms, and the synchronization modes observed in [12] are different from the symmetric breaststroke of wt *C. reinhardtii* investigated here. In our experiments on *C. reinhardtii*, even at flows $U_F \approx 10U_0$, flagella do not synchronize to the background flow when f_F is outside of the synchronization region. This means that, although the velocity field around the cell due to the periodic background flow is 10 times larger than what would be expected in free swimming conditions, the flagella still remain phase locked with each other, but do not couple with the external hydrodynamic forcing. This observation warrants a thorough investigation into how much hydrodynamic interactions contribute to interflagellar synchronization in wt *C. reinhardtii* performing breaststrokes. A more accurate quantification of the hydrodynamic forces at play is needed. In chapter 5 we describe a combined experimental/numerical approach to quantify and compare the hydrodynamic force applied on the flagella due to (1) the external background flow in our experiments, and (2) the flow generated by one flagellum on the other one. In parallel, we seek to characterize other potential synchronization mechanisms to explain the strong locking observed between the two flagella. As discussed in section 2.3, preliminary studies on *C. reinhardtii* suggested that the distal striated fiber, connecting mechanically the two flagella [65], could mediate synchronization [69, 116]. Indeed, if we consider a force balance on one flagellum, the total hydrodynamic force exerted by the flagellum on the surrounding fluid is exactly balanced by the direct mechanical force the same flagellum exerts on the basal apparatus. As a result, strong mechanical stress concentration is expected in the region of the cell cortex around the basal apparatus of the flagella, which by far exceeds the viscous stresses inside the fluid. Synchronization is therefore more likely mediated by elastic stresses, which are conservative and act over an interflagellar distance of only $\sim$ 200 nm in the distal fiber, rather than viscous stresses, which are dissipative and act over an interflagellar distance of $\sim$ 10 μm in the fluid. To address the role of the distal fiber in mediating flagellar coupling, we performed additional experiments on mutants, presented in the following chapter.

5

HYDRODYNAMIC FORCES ON FLAGELLA AND FLAGELLAR COUPLING

In chapter 4, we focused on the synchronization of flagella with an external flow. A question of greater biological significance is related to the origin of the synchronization between the flagella. Though these are two different problems, our results presented in chapter 4 have implications regarding interflagellar synchronization. In chapter 5, we present experimental results that shed new light on interflagellar synchronization and hydrodynamic forces.

Following chapter 4, we first quantify the strength of the hydrodynamic forces experienced by *C. reinhardtii* in our experiments. Namely, we are interested in characterizing the strength of the viscous forces imposed by the external flow on the flagella and how they compare with the viscous forces imposed by one flagellum onto the other during free swimming. To this purpose, we tracked the waveforms of the flagella and precisely computed numerically the flow velocity fields generated around the cell as well as the hydrodynamic forces on the flagella during our experiments (section 5.2).

We apply this methodology to both wt *C. reinhardtii* and mutant *ptx1*. In fact, recent work has suggested that antiphase synchronization observed in the mutant *ptx1* (see figure 2.7) is caused by hydrodynamic interactions [83]. The flagella of *ptx1* beat in opposite directions, see sections 2.3.1 and 2.4. By imposing a hydrodynamic forcing on wt and *ptx1* cells and by quantifying the viscous forces involved in in-phase and antiphase beating, we explore the role of hydrodynamics in mediating this beating pattern (section 5.3). An alternative mechanism at the origin of flagellar synchronization involves the mechanical coupling of the flagella inside the cell membrane. It has been observed that wt basal bodies are connected via distal striated fibers, and these structures have been suggested to play a role in flagellar synchronization [81, 82] (for details see section 2.3.1). Further investigation of this mechanism is needed. A mutant of *C. reinhardtii* lacking this structure is the *vfl3* mutant (see section 2.3.1 for details). We investigate the behaviour of *vfl3* under the same experimental conditions as wt (see chapter 4), and we observe how the lack of functioning distal fibers affects flagellar motility (section 5.4).

One final aspect of interflagellar synchronization often discussed in the literature is the fundamental asymmetry in behaviour between the *cis-* and the *trans-* flagella. In this chapter we attempt to probe separately the response of the *cis-* and the *trans-* flagella to the effect of an external forcing, by selectively perturbing each of the two flagella with different intensity. We achieve this by imposing an external flow that generates asymmetric forces on the two flagella (section 5.5).

Regarding the outline of this chapter, in section 5.1 we detail the image processing method developed to track the deformations of the flagella during a beating cycle. Afterwards, all the results are presented. In section 5.2, we characterize the viscous forces acting on wt during breaststroke. In section 5.3, we present the experiments on *ptx1* mutants and discuss the role of hydrodynamics by computing the viscous forces involved in antiphase beating. In section 5.4, we discuss experiments on the mutant *vfl3*, that highlight the importance of intracellular coupling and the limits of hydrodynamics in flagellar synchronization. Finally, in section 5.5, we analyse the experiment used to selectively force one flagellum rather than the other and the observations on the *cis-trans* coupling mechanism.

5.1   METHOD   FOR   FLAGELLA   TRACKING   AND   FLOW   FIELD   COMPUTATION

In this section, we detail the methodology used to track the flagellar motion in each acquired video frame and the computational method used to evaluate the velocity field around the cell as well as the forces on the flagella. The methodology described in the previous chapter (section 4.1.2) and based on the 'interrogation windows' is not adequate. In chapter 4, the phase dynamics of flagella is inferred from an image analysis method relying on the periodic sweeping of flagella through an interrogation window. This method provides no information regarding the details of the deformation and stroke patterns of the flagella. In addition, phase fluctuations within one beating cycle are not resolved either. To resolve the velocity field and compute the viscous forces imposed on the flagella, we need to track accurately the motion of the flagella during each beating cycle. Hence, we need to develop the tools to characterize the whole flagellar waveform in each video frame. Other recent studies on cilia and flagella motility adopted a similar tracking approach [75, 117, 118].

5.1.1   IMAGE PROCESSING ALGORITHM

We implemented a custom made image processing method to detect the slope of the flagella in each frame and a consistent description of flagellar waveforms allowing to compare the strokes of different cells. The implementation is summarized hereafter and includes details on: flagella discretization, image enhancement, and flagella shape reconstruction.

Discretization of the flagellum
In order to compare shapes among different cells and datasets, we represent the flagellar waveforms with the curvature of the centerline of the flagella $\kappa(s)$ as a function of the arc-length s, where $s = 0$ is at the base of the flagellum, as shown in figure 5.1. For each flagellum, the curvature $\kappa(s)$ uniquely describes the flagellum shape to the initial tangent angle θ_0 at the base of the flagellum. The flagellum is discretized in N elements of equal length ds, separated by $N + 1$ nodes located at the arclength $s_i = i \cdot ds$, for $i = 0...N$ see figure 5.1. The curvature at the end of the flagellum is $\kappa_{N+1} = 0$, assuming a free end. The curvature is expressed in the dimensionless form

$\tilde{\kappa}_i = \kappa_i \cdot l_f$, where l_f is the flagellum length in micron. For each frame, the flagellar shape is therefore described by a shape vector $\mathbf{k}$ of dimension $N + 1$, where the first entry is the initial tangent angle θ_0 and the other N following are the curvatures at nodes $s_0...s_{N-1}$, such that $\mathbf{k}=(\theta_0, \kappa_0, ..., \kappa_N)$ at each node. The position vector along the centerline of the flagella $\mathbf{r}(s_i) = (x_i, y_i)$ is reconstructed by numerical integration of the curvature. The main aspects of the processing algorithm are outlined hereafter. For details about the implementation, the reader is referred to [115].
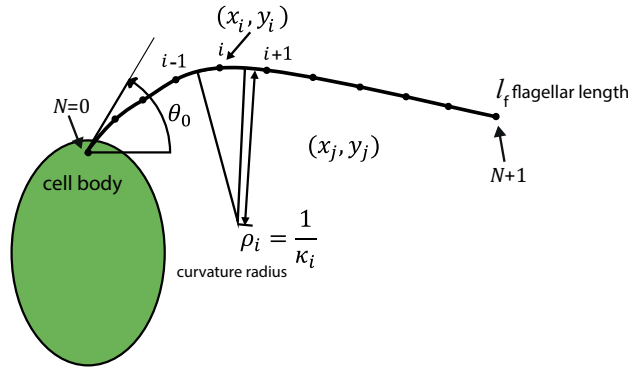
Figure 5.1: Flagella shapes are described by N (with $N = 10$) curvature values along the flagellum. In the sketch are also shown the tangent angle at flagellum base and the Cartesian coordinates of each node. Adapted from [115].

Image enhancement

The high level of noise in the recorded images (due to low light levels) requires to extensively process the images before tracking the flagella. First, the pipette vibration is suppressed as discussed in 3.3. Then, the contrast of the images is improved and a Wiener filter is applied to remove Gaussian noise [119]. The image quality is hence improved, and flagellar shapes can be extracted.

Flagella shape reconstruction A flagella shape detection based on the variation of pixel intensity in grayscale proved not to be robust. This method was used to detect the flagella beating frequency as discussed in subsection 4.1.2, but is not appropriate to track accurately the entire flagellum shape. As shown in figure 5.2(a), for a typical recording, one flagellum goes temporarily out of the focal plane during the beating cycle. This causes the pixel intensity to abruptly invert along the flagellum. To overcome this issue we derived a method that was more effective in cases where the grayscale of the flagella varies from one video frame to the next. This method for flagellar tracking is based on Gaussian background modeling [120]. It is a motion tracking algorithm that extracts the moving foreground of each frame by approximating the stationary background over a series of frames.

This assumes that the light intensity around each pixel in different frames can be described as a Gaussian distribution with mean m and standard deviation σ [121]. Based on the value of m and σ, a pixel is classified into either background or foreground. The underlying assumption is that the background intensity remains constant among

different frames. Since, in reality, the pixel intensities change among frames, m and σ for the background pixels are updated between two consecutive frames based on a learning rate factor empirically chosen [122]. In the original algorithm, the result of this background modelling is a binary image where the foreground pixels are black ($I = 0$), while the background pixels are white ($I = 1$). However, we experienced that such binary classification causes loss of details about the probability that a pixel would belong to the foreground or to the background. Hence, instead of this binary segmentation, our classification is based on the scaled distance $\tilde{d}$ from the mean m, defined as $\tilde{d} = |I_i - m_{i+1}|/c$, where $c = 0.1$ represents an empirically chosen scaling factor. Pixels with larger $\tilde{d}$ are more likely to belong to the foreground. By inverting $\tilde{d}$, we obtain an image with minimum cost for the foreground, as the one shown in figure 5.2(b).
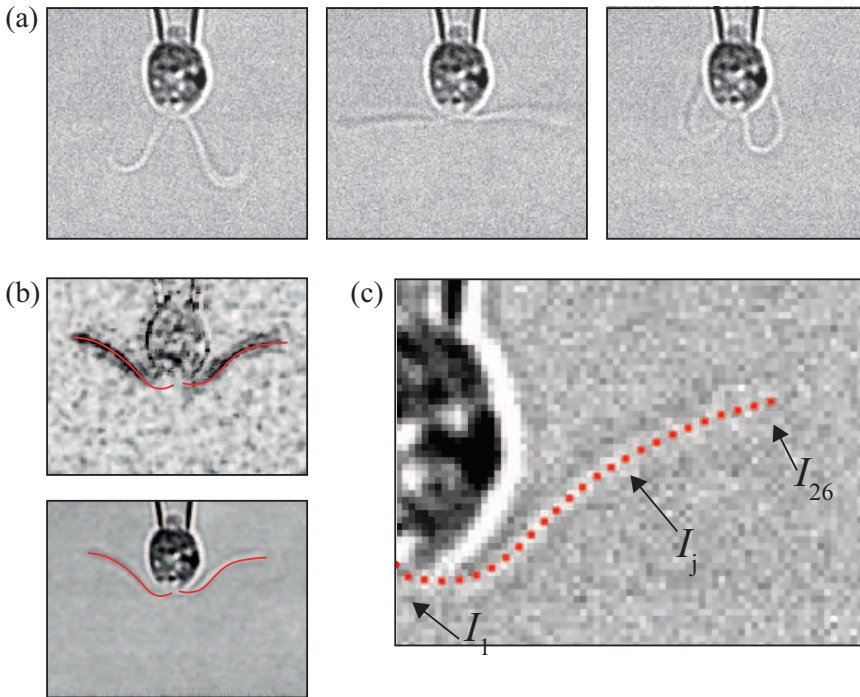
Figure 5.2: (a) Snapshots showing color inversion during flagellar beating cycle. At the begin of the recovery stroke, both flagella are bright with respect to the background, but 4 frames further, one flagellum becomes dark. **(b)** The top image shows the result of Gaussian background representation. The foreground is shown in black corresponding to low pixel intensity. The red line is the flagellar shape guess. The bottom image represents the original grayscale video frame. **(c)** Image illustrates tracking of one flagellum with N equidistant nodes. In this case $N = 26$. The pixel intensity of the image at each node I_j is used to compute the shape cost C.

The shape of the flagella is extracted from this image by minimization of a cost function C associated with a particular vector. The formulation for the cost function is the following:

$$C = w_1 \frac{1}{N} \sum_{j=1}^{N} I_j + w_2 \int_0^{l_f} \tilde{\kappa}^2 ds, \qquad (5.1)$$

where I_j represents the pixel intensity at the jth node and is computed by interpolation of the foreground image at that node. w_1 and w_2 are two weighting parameters. This cost function is the sum of two contributions. The first term is the image intensity contribution $1/N \sum_{j=1}^{N} I_j$. This term represents the average pixel intensity over the N nodes of the shape (shown in figure 5.2(c)). The second term in equation 5.1 ($\int_0^{l_f} \tilde{\kappa}^2$) is the bending energy of the shape guess. The shape cost function C is minimal when the pixels delimiting the shape are black ($I_j = 0$) and the curvature is low (low bending energy). Therefore, as shown in figure 5.2(c), the minimal cost function is obtained in the darkest part of the image, while the bending energy term penalizes high curvature shapes. This penalty on bending prevents the algorithm from converging towards local optimal shapes characterized by kinks and loops. The weighting factors w_1 and w_2 allow a correct balance between fitting the details of the flagellum shape and obtaining a smooth flagellar shape. In addition, the following constraints are imposed to avoid unlikely waveforms: (1) the smallest curvature radius is set to $1/50$ μm, (2) the tangent angle of each flagellum is constrained between $\pi/6$ and $3\pi/4$ (this range includes all the flagellar shapes observed in experiments), and (3) the flagellum is not allowed to intersect the cell body. An example of flagella shape reconstruction over a beating cycle is shown in figure 5.3.

5.1.2   FLOW FIELD COMPUTATION

Once the flagella are tracked, the time dependant deformations of the flagella can be deduced. Using these deformations as boundary conditions, the hydrodynamic forces acting on the flagella during beating can be computed by numerical tools. To this purpose, the flow field around the cell and the micropipette is computed by solving the Stokes equations (2.4-2.5) subject to a no slip boundary condition at the surface of the micropipette, the cell body, and the deformable flagella. Our numerical approach combines a boundary element method (BEM) formulation for the pipette and the cell body, together with slender body theory for the deformed flagella.

Cell body and pipette
To represent the cell body and the pipette, we use a boundary integral representation derived from the Stokes equations [123]. Such formulation reduces the complexity of the numerical approach. Instead of solving a three dimensional flow field, we compute a singularity distribution on the boundary of the object. Our numerical approach uses the completed double-layer boundary integral equation introduced by Power and Miranda [123], which numerically solves an integral equation of the second kind (Keaveny and Shelley [124]). In this approach, Stresslets are distributed over the surface of the cell and the pipette.
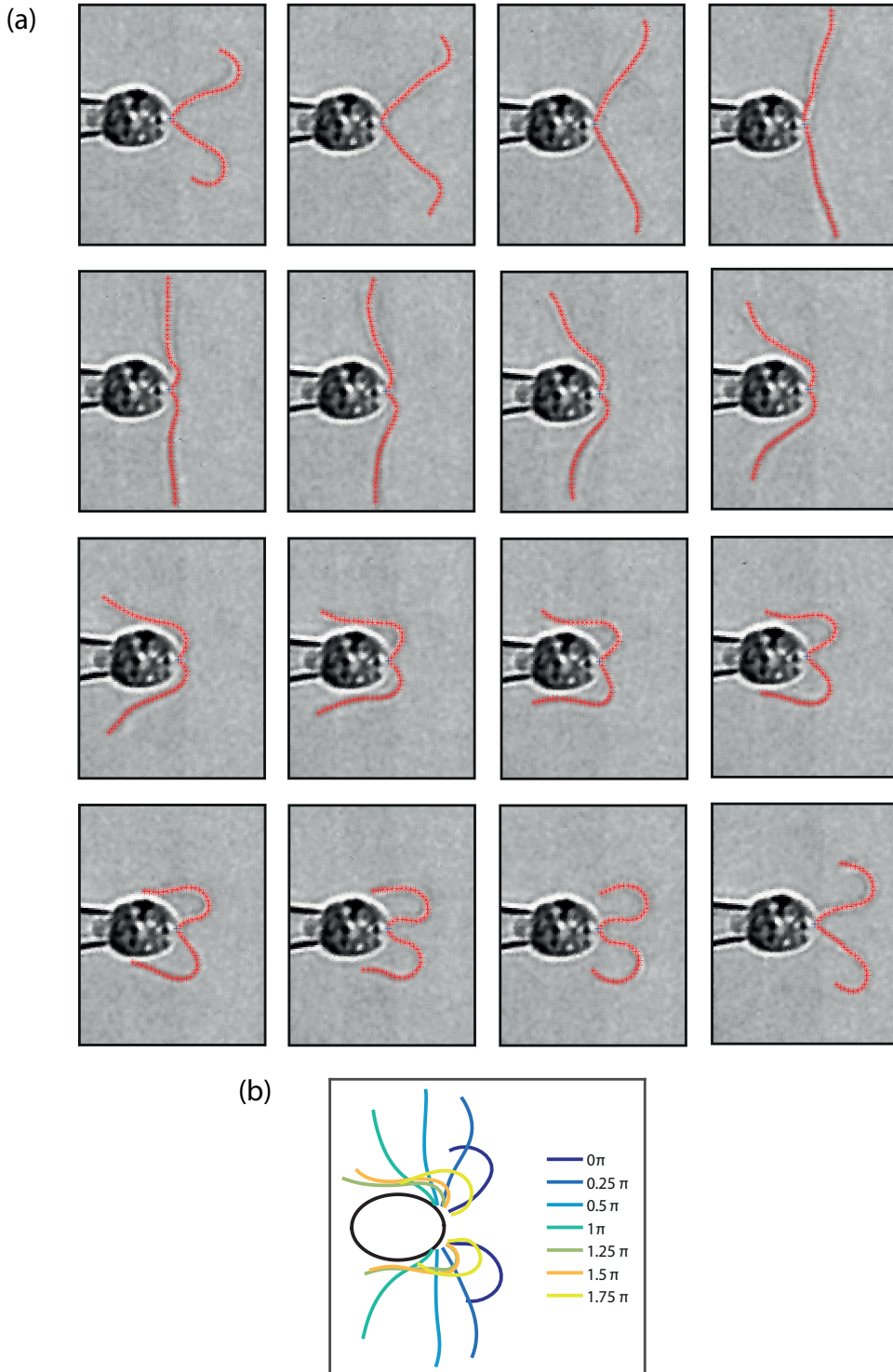
Figure 5.3: (a) Snapshots of one cell beating cycle where flagella shape was reconstructed with the cost function minimization. **(b)** Superposition of several flagellar shapes and their tangent angle at the flagellum base.

The superposition of singularities results in a total surface velocity u^s equal to the velocity prescribed at the boundary. Since a stresslet cannot produce a net force or torque (as discussed in 2.2.1), Power and Miranda added a point Stokeslet and rotlet at the center of the object, inside the closed boundary, to account for the net force produced by an arbitrary flow over the object. In our case, the elongated geometry of the pipette leads to poor conditioning of the numerical problem when using the formulation from Power and Miranda with a point singularity inside the boundary. To prevent this issue, we use instead a line distribution of Stokeslets and rotlets, along the axis of axisymmetry of the object, following Keaveny and Shelley [124]. The surface velocities and the stresslet distribution are related by the integral equation:

$$u_i^s(\mathbf{x}) = \frac{1}{2\mu}\Psi_i(\mathbf{x}) + n_k(\mathbf{x})\int_D \mathbf{T}_{ijk}(\mathbf{y} - \mathbf{x})\Psi_j(\mathbf{y})dS_{\mathbf{y}} + v_i^T[\mathbf{\Psi}](\mathbf{x}), \qquad (5.2)$$

where D represents the surface of the cell and the pipette, and $\mathbf{x}$ is on the surface D. Here u^s is the known velocity on the boundary of the cell and the pipette, Ψ is the double layer density, $\mathbf{n}$ is the surface normal vector, $\mathbf{T}$ is the stresslet tensor:

$$\mathbf{T}_{ijk}(\mathbf{x} - \mathbf{y}) = \frac{3}{4\pi\mu}\frac{(x_i - y_i)(x_j - y_j)(x_k - y_k)}{|\mathbf{x} - \mathbf{y}|^5}. \qquad (5.3)$$

v^T is the adjoint of the completion flow:

$$v_i^T[\mathbf{\Psi}](\mathbf{x}) = \int_D \mathbf{G}_{ij}(\mathbf{y} - \mathbf{X}(\mathbf{y}))\Psi_j(\mathbf{y})dS_{\mathbf{y}} + \epsilon_{ijk}(x_k - X_k(\mathbf{x}))\int_D \Psi_l(\mathbf{y})\mathbf{R}_{ij}(\mathbf{y} - \mathbf{X}(\mathbf{y}))dS_{\mathbf{y}}, \qquad (5.4)$$

where, for all $\mathbf{y} \in D$, $\mathbf{X}(\mathbf{y})$ are points along the axis of axisymmetry in the interior of the body over which the Stokeslets and rotlets are distributed [124]. $\mathbf{G}_{ij}$ and $\mathbf{R}_{ij}$ represent the Stokeslet and rotlet kernels:

$$\mathbf{G}_{ij}(\mathbf{x}) = \frac{1}{8\pi\mu}\left(\frac{\delta_{ij}}{|\mathbf{x}|} + \frac{x_i x_j}{|\mathbf{x}|^3}\right) \qquad (5.5)$$

$$\mathbf{R}_{ij}(\mathbf{x}) = \frac{1}{8\pi\mu}\left(\frac{\epsilon_{ijk}x_k}{|\mathbf{x}|^3}\right) \qquad (5.6)$$

Flagellum

We use slender body theory to avoid the discretization of the slender flagella surface which would require a large number of small discrete elements and would significantly increase the computational cost. We model flagella with slender-body theory [125]. This method is suited for long and slender geometries. We implement the integral formulation from Keller & Rubinow [126]. In this formulation, Stokeslet and Stokes doublets are distributed along the centerline of the flagella to satisfy the no-slip boundary condition imposed on the surface of the flagella [127]. The integral equation for the velocity $\mathbf{U}$ at the centerline is:

$$\mathbf{U}(s) = \mathbf{\Lambda}(s)\mathbf{f}(s) - \int_0^{2L}[\mathbf{G}_{ij}(\mathbf{r}(s) - \mathbf{r}(\tilde{s}))\mathbf{f}(\tilde{s}) - \left(\frac{\delta_i + t_i(\tilde{s})t_j(\tilde{s})}{|s - \tilde{s}|}\right)\mathbf{f}(\tilde{s})]d\tilde{s}, \qquad (5.7)$$

where $\mathbf{t}(s)$ is the vector tangent to the flagellum centerline at arclength s, $\mathbf{r}(s)$ is the position vector at s, $\mathbf{U}(s) = \dot{\mathbf{r}}(s)$ the velocity at the centerline, and $\mathbf{f}(s)$ the distribution of hydrodynamic forces per unit length acting on the flagellum. $\mathbf{\Lambda}(s)$ is a linear operator defined as:

$$\mathbf{\Lambda}(s) = \frac{1}{8\pi\mu}\left(\ln(\kappa^2 \exp(1))[\delta_{ij} + 2t_i(s)t_j(s)] - 2[\delta_{ij} - t_i(s)t_j(s)]\right). \tag{5.8}$$

Discretization

The cell body and pipette are meshed as a whole by means of an unstructured triangular mesh of about 1500 elements, with grid size refinement on the cell body, as shown in figure 5.4(a). The pipette has the shape of a cone with a half angle of 5.5° corresponding to the geometry of the tip of the pipette. We truncated the pipette 80 μm away from the cell to decrease the computational cost. Flagella are discretized in linear elements equally spaced along the arclength of the flagellum. We use the same discretization as the one used for the shape tracking algorithm; see section 5.1.1. A small gap of ≈ 1 micron is left between the cell body and the flagella, as shown in figure 5.4(b). Leaving this small gap allows a better conditioning of the numerical problem. The no-slip boundary condition is imposed on the surface of the cell body and the pipette at collocation points. The collocation points are the centers of gravity of each triangular element; see figure 5.4(a). Imposing the no-slip boundary condition at the surface of the flagella requires knowledge of the displacement of the flagella and in particular of the velocity $\mathbf{U}(s)$ at the centerline. Here, $\mathbf{U}(s)$ is obtained by our experiments and the tracking of the flagella. The velocity $\mathbf{U}(s)$ is computed at the center of each linear element of the flagellum. This velocity is computed by a numerical differentiation of the time dependent position at each node on the flagellum by means of a five point Savitzky-Golay Digital Differentiator [128, 129].

The discretization of the integral equation for the cell body and the pipette, equation 5.4, together with the integral equation for the flagellum, equation 5.7, leads to a linear system that is solved for the surface distribution $\mathbf{\Psi}(\mathbf{x})$ of stresslet for $\mathbf{x}$ on D and the line distribution $\mathbf{f}(s)$ of Stokeslet along the flagellum. The flow velocity field $\mathbf{U}$ can be computed from the distribution of singularity $\mathbf{\Psi}$ and $\mathbf{f}$ at any location $\mathbf{x}$ in the bulk of the flow by superposition.

An example of velocity field reconstruction from an experiment is shown in figure 5.4 (c). In this example there is no background flow. The colormap represents the amplitude of the flow field generated by the motion of flagella.

5.1.3   FORCE AND POWER ASSOCIATED WITH FLAGELLAR BENDING

The numerical approach outlined in section 5.1.2 yields the distribution of Stokeslets $\mathbf{f}(s)$ along the flagella, which represents the distribution of hydrodyanmic forces exerted by the surrounding fluid on the flagella. This allows us to directly investigate forces applied on the flagella. In particular, we compute the total force on a flagellum as:

$$\mathbf{F} = \int_0^{l_F} \mathbf{f}(s)ds, \tag{5.9}$$

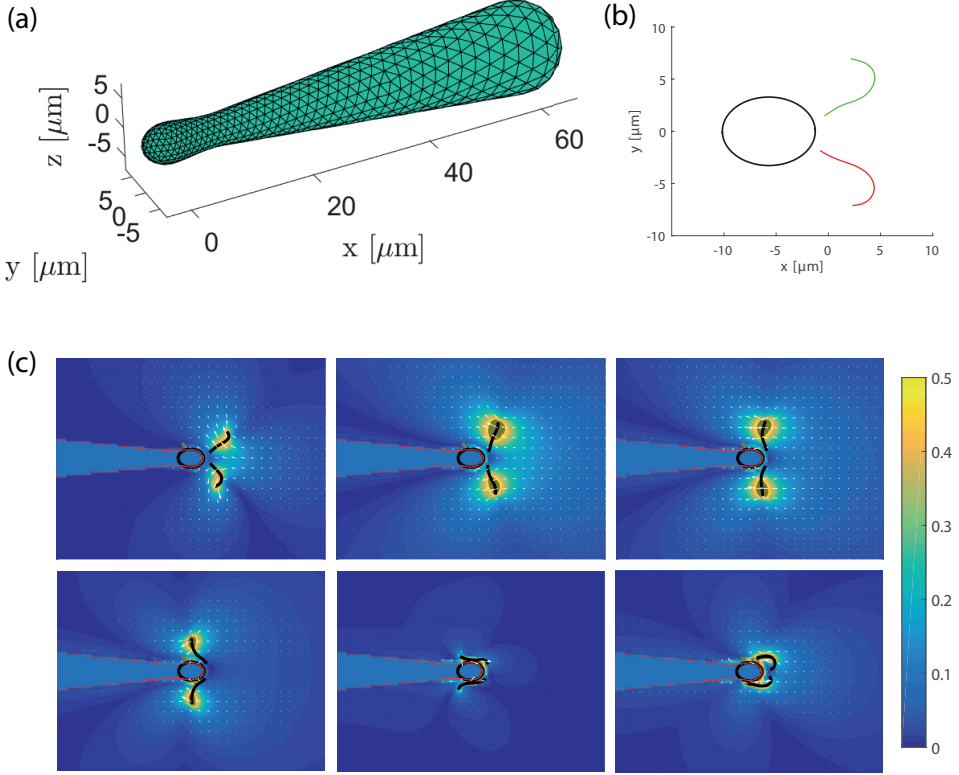**Figure 5.4: (a)** Mesh of cell body and pipette obtained with Matlab mesh generator by Persson and Strang [121]. **(b)** Gap between cell body and flagella to prevent numerical instability. Adapted from [115]. **(c)** Frame sequence showing the velocity field in an experiment without external flow. The vectors show the flow field generated by flagellar beating at different phases of the beating cycle.

and call $\mathcal{F} = |\mathbf{F}|$ the magnitude of the force. The non dimensional total force is obtained as:

$$\tilde{\mathcal{F}} = \frac{\mathcal{F}}{\mathcal{F}_0} = \frac{\mathcal{F}}{6\pi\mu a U_0}, \tag{5.10}$$

where $\mathcal{F}_0$ is the Stokes drag on a sphere moving at the cell free swimming velocity $U_0 = 110 \pm 12 \ \mu\text{m.s}^{-1}$ and $a = (a_{maj} \cdot a_{min})^{0.5}$ is the cell radius, computed as the geometric average of the major and minor cell radii.

The viscous power, namely the rate of work of the flagella against viscous forces, is obtained as:

$$\mathcal{P} = \int_0^{l_{\mathrm{F}}} \mathbf{f}(s) \cdot \mathbf{U}(s) ds, \tag{5.11}$$

where $\mathbf{U}(s)$ is the velocity of the centerline of the flagella. Similarly to the force, also the magnitude of the viscous power is expressed in non dimensional form as:

$$\tilde{\mathcal{P}} = \frac{\mathcal{P}}{\mathcal{P}_0} = \frac{\mathcal{F}}{6\pi\mu a U_0^2}. \tag{5.12}$$

The elastic power is the rate of work of elastic stresses due to the deformation of the flagella. It can be computed assuming classical Euler-Bernoulli beam theory as:

$$\mathcal{P}_e = \frac{EI}{2}\frac{d}{dt}\int_0^{l_F} \kappa(s)^2 ds, \tag{5.13}$$

where E and I are respectively the Young's modulus and the area moment of inertia of the flagellum, and determine the bending stiffness of the flagella. We used an oft-quoted value for the eukaryotic flagella bending stiffness, equal to $EI = 0.9 \cdot 10^{-21}$ Nm^{-2} [130]. This stiffness was measured in sea urchin sperm in relaxed state. Similarly, to the viscous power, the elastic power magnitude is expressed in nondimensional form:

$$\tilde{\mathcal{P}}_e = \frac{\mathcal{P}_e}{\mathcal{P}_0}. \tag{5.14}$$

5.2 HYDRODYNAMIC FORCES ACTING ON THE FLAGELLA OF WT C. REINHARDTII

In this section, we quantify the effects of fluid flow on a flagellum of wt *C. reinhardtii* during breaststroke, both in the absence and in the presence of an external hydrodynamic forcing. The effects of hydrodynamic forces due to hydrodynamic interactions between the flagella are compared with the forces due to the external flow by looking at three different experiments:

1. wt *C. reinhardtii* motility in the absence of flow.

2. wt *C. reinhardtii* motility in the presence of a background flow right outside the synchronization region ($f_F = 58.2$ Hz and $A_F = 10.3$ μm).

3. wt *C. reinhardtii* motility in the presence of a background flow inside the synchronization region ($A_F = 14$ μm, $f_F = 58.2$ Hz).

In each of these experiments, the effects of fluid flow are characterized by using the experimental approach detailed in section 5.1. This approach is used to compute the total hydrodynamic drag force $\mathbf{F}$ imposed on the flagellum (equation 5.9), the rate of work of the drag force $\mathcal{P}_v$ (equation 5.11). Snapshots of the velocity field in the three experiments are shown in figure 5.5. In our experiments, the total drag force on a flagellum is due to the flow around the flagella. Here, the flow has three distinct origins: first the motion of the flagellum itself, second the motion of the other flagellum, and third the background flow. From the linearity of Stokes equations, the flow velocity field can be computed as the superposition of the three components. As a
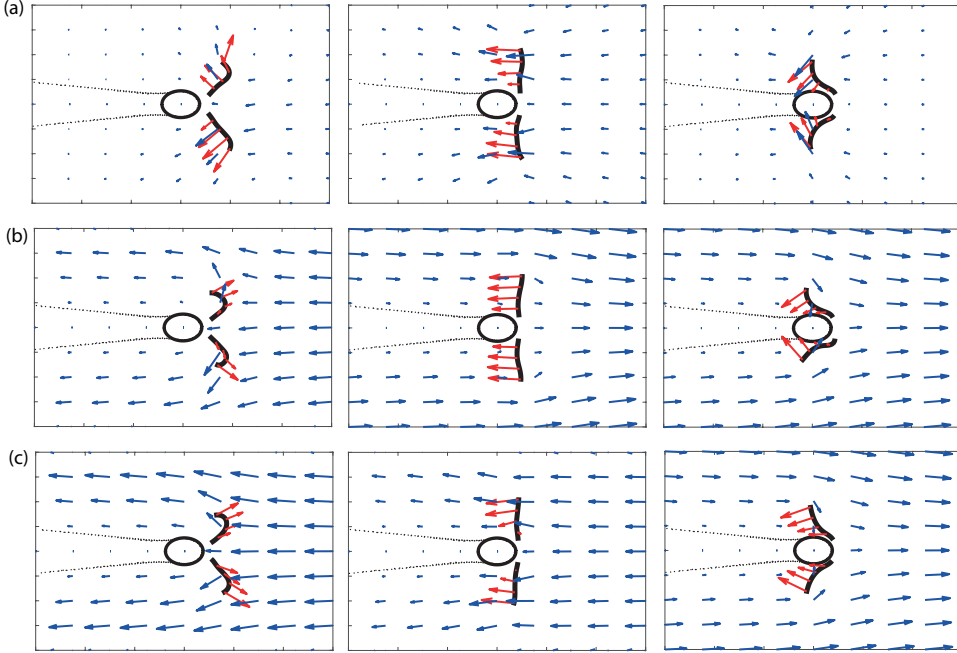
Figure 5.5: Examples of numerical computation of the flow field. The blue vectors describe the flow velocity field, while the red vectors indicate the distribution of singularities on the flagella. **(a)** Snapshots of the flow field around a cell in absence of external flow. **(b)** Snapshots of the flow field for a cell beating in antiphase with the flow. The flow imposed is axial flow at $U_F = 1.19$ mm.s^{-1}, $A_F = 10.3$ μm, $f_F = 58.2$ Hz. **(c)** Snapshots of the flow field during an experiment where the flagella are synchronized in phase with the background flow. The imposed flow is axial flow at $U_F = 1.63$ mm.s^{-1}, $A_F = 14$ μm and $f_F = 58.2$ Hz.

consequence, the total hydrodynamic drag force **F** on a flagellum can be written as the linear superposition of three components:

$$\mathbf{F} = \mathbf{F}_{\text{motion}} + \mathbf{F}_{\text{int}} + \mathbf{F}_{\text{flow}} \tag{5.15}$$

where $\mathbf{F}_{\text{motion}}$ is the force due to the flow generated by the motion of the flagella, $\mathbf{F}_{\text{int}}$ is the hydrodynamic interaction force due to the motion of the other flagellum and $\mathbf{F}_{\text{flow}}$ is the force due to the external background flow.

In addition, we compute the rate of work associated with each of the three components of the drag force corresponding to the flagellar motion $\mathcal{P}_{\text{motion}}$, the flagella hydrodynamic interaction $\mathcal{P}_{\text{int}}$ and the external flow $\mathcal{P}_{\text{flow}}$.

5.2.1   NO FORCING

Forces and rates of work for an average beating cycle

We start by discussing an experiment performed in the absence of external forcing. We tracked the shape of the flagella in each frame of the recording for over one second corresponding to ≈ 1000 consecutive frames. We computed the distribution $\mathbf{f}(s)$ of

CHAPTER 5

hydrodynamic forces and deduced the total force **F** acting on the flagella and the rate of work $\mathcal{P}$ of hydrodynamic forces. Furthermore, we also computed the elastic power $\mathcal{P}_e$. Figure 5.6 presents our results for the three quantities $\mathcal{F} = |\mathbf{F}|$, $\mathcal{P}$, $\mathcal{P}_e$ for one flagellum (black line). These results correspond to a single period averaged over 14 beating cycles. The total hydrodynamic force $\mathcal{F}$ (figure 5.6(a)) and the rate of work $\mathcal{P}$ (figure 5.6(b)) present two local extrema. The first and largest one, when the flagellar phase is $\approx \pi/4$, corresponds to the power stroke. The second one, when the phase is $\approx 3\pi/4$, corresponds to the recovery stroke. The maximum force magnitude is $\mathcal{F} = 5.1\ \mathcal{F}_0$. The maximum rate of work is $\mathcal{P} = 63\ \mathcal{P}_0$. The maximum value corresponds to the power stroke, when the cell generates a net thrust on the surrounding fluid and moves forward. The rate of work produced reaches its minimum at $\phi \approx \pi$ and $\phi \approx 2\pi$, which correspond to the end of the power and the end of the recovery stroke respectively, when the direction of motion of the flagella changes. The elastic power accounts for changes in stored elastic energy, as the flagella deform (figure 5.6(c)). It is negative between the end of the recovery stroke and the begin of the power stroke ($\phi \approx 2\pi$), when the flagella extend and the curvature along the flagella decreases to zero. Instead, during the power stroke and the begin of the recovery stroke, $\mathcal{P}_e$ is positive, which corresponds to the flagella actively bending through the action of molecular motors. Flagellar bending in *C. reinhardtii* is the result of sliding among the microtubule filaments composing the axoneme (as discussed in section 2.3).

Force and power across multiple beating cycles

We now consider force and rate of work over several beating cycles, and we write these quantities as a function of the unwrapped flagella phase ϕ. Figure 5.5 (a) represents the flow velocity field around the flagella in absence of external forcing. In figure 5.7 (b), the black trace represents $\mathcal{F}/\mathcal{F}_0$ on flagella during a typical experiment in the absence of flow. $\mathcal{F}$ is clearly periodic, and the fluctuations between consecutive strokes are small. The average value for the force is $\mathcal{F}/\mathcal{F}_0 = 3.5 \pm 0.6$. We decomposed the hydrodynamic force into the three different contributions from equation 5.15. Figure 5.7(d) represents $\mathcal{F}_{\text{motion}}$ and figure 5.7(e) represents $\mathcal{F}_{\text{int}}$. In experiments without forcing there is no contribution of the external flow and $\mathcal{F}_{\text{flow}} = 0$. We find $\mathcal{F}_{\text{motion}}$ to be one order of magnitude larger than $\mathcal{F}_{\text{int}}$ and hence, in absence of forcing, the total hydrodynamic viscous force $\mathcal{F}$ only depends on the force generated by flagellar active motion.

We also computed $\mathcal{P}$ in absence of forcing, shown in figure 5.8(a) (black trace), and represent the different contributions separately . Our results are similar to those for $\mathcal{F}$. The rate of work of the force due to the motion of the flagellum is $\mathcal{P}_{\text{motion}}/\mathcal{P}_0 = -39.6 \pm 9.8$ on average. On the other hand, the average rate of work due to the hydrodynamic interaction of one flagellum with the other one is 3 orders of magnitude smaller: $\mathcal{P}_{\text{int}}/\mathcal{P}_0 = 0.03 \pm 0.77$. In experiments without external forcing, the rate of work of the hydrodynamic forces is almost entirely due to the motion of the flagellum. Furthermore, $\mathcal{P}$ remains negative all the time during the flagellar beat, indicating that the eukaryotic flagella, when moving, are always working against hydrodynamic forces.

From the experiments without external forcing, we learn that the rate of work and viscous forces due to hydrodynamic interaction between the flagella are negligible with
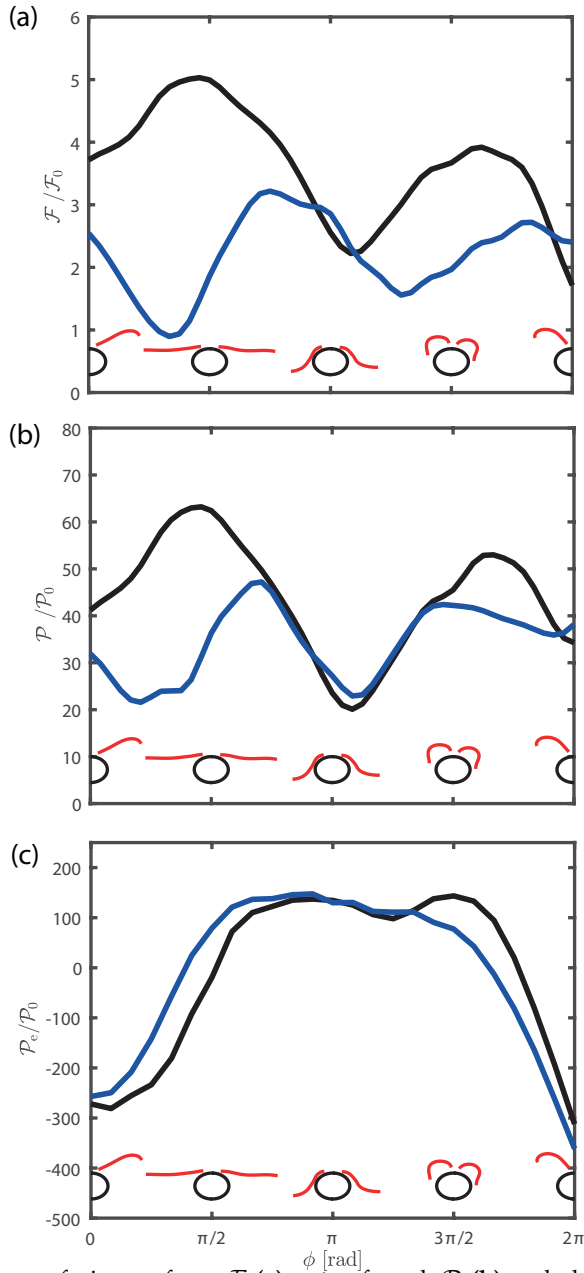
Figure 5.6: Comparison of viscous force $\mathcal{F}$ **(a)**, rate of work $\mathcal{P}$ **(b)** and elastic power $\mathcal{P}_e$ **(c)** on a flagellum averaged over one beating cycle. Comparison between experiment without external forcing (black line) and with a forcing $U_F = 1.63$ mm.s^{-1} causing phase locking (blue line).

respect to the forces and rate of work generated by the flagellum during its motion. In the next two paragraphs we compare the force and rate of work in presence of an external forcing.
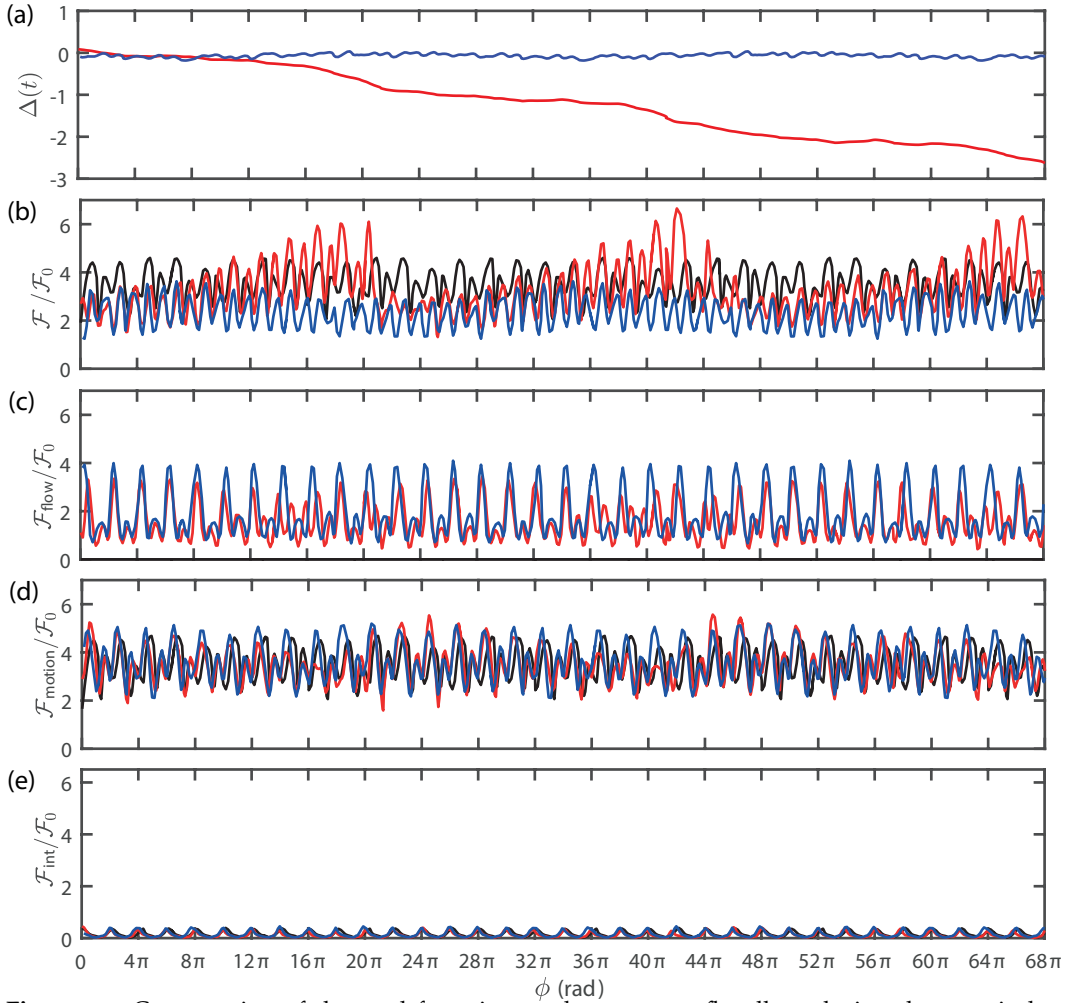
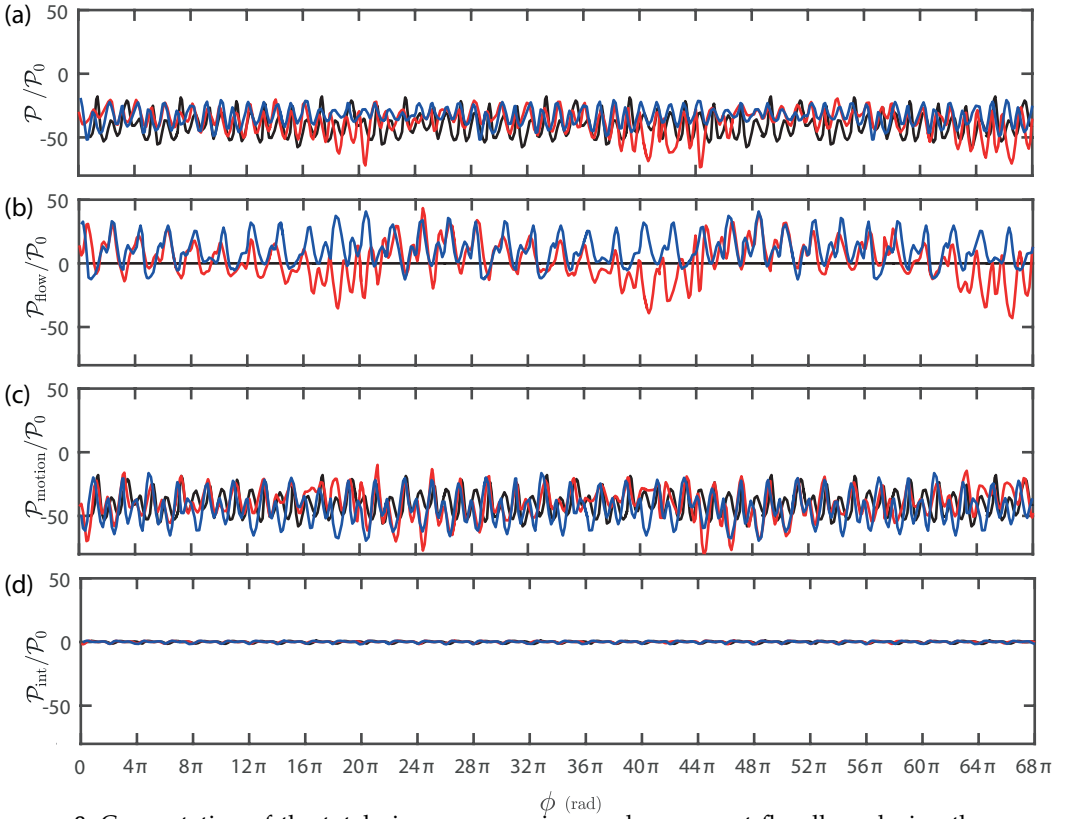**Figure 5.7:** Computation of the total force imposed on one wt flagellum during three typical experiments and separation of effects. **(a)** Phase difference between flagella and forcing as a function of the unwrapped flagella phase ϕ. Comparison between the experiment with axial flow at $U_F = 1.19$ mm.s^{-1} (red line) and the experiment with axial flow at $U_F = 1.63$ mm.s^{-1} (blue line). At the lower flow velocity, the cell does not synchronize with the background flow and the phase difference is constantly decreasing (red line). At the higher flow velocity, the cell is always synchronized with the external flow. **(b)** Total non dimensional force $\mathcal{F}/\mathcal{F}_0$ measured on one flagellum as a function of the unwrapped phase ϕ. Comparison among an experiment without forcing (black line), an experiment with non synchrony-inducing flow (red line) and an experiment with synchrony inducing flow (blue line). **(c)** Contribution to the total force on one flagellum due to the periodic background flow $\mathcal{F}_{\text{flow}}$. **(d)** Force contribution on one flagellum due the flagellar motion $\mathcal{F}_{\text{motion}}$. **(e)** Force contribution on one flagellum due to hydrodynamic interaction between the two flagella $\mathcal{F}_{\text{int}}$.

5.2.2   FORCING WITH SYNCHRONY

We imposed on the same cell axial flow at $U_F = 1.63$ mm.s^{-1} and $f_F = 58.2$ Hz. This frequency value is approximately in between what is thought to be the beating

Figure 5.8: Computation of the total viscous power imposed on one wt flagellum during three typical experiments and separation of the different contributions. **(a)** Magnitude of the total non dimensional rate of work $\mathcal{P}/\mathcal{P}_0$ measured on one flagellum as a function of the unwrapped phase ϕ for an experiment without external flow (black line), an experiment with axial flow at $U_F = 1.19\ \mu\text{m.s}^{-1}$ (red line) and an experiment with axial flow at $U_F = 1.63\ \mu\text{m.s}^{-1}$ (blue line). **(b)** Rate of work on one flagellum due to the external forcing $\mathcal{P}_{\text{flow}}$. **(c)** Rate of work generated by the flagellum motion $\mathcal{P}_{\text{motion}}$. **(d)** Rate of work due to flagellar hydrodynamic interaction $\mathcal{P}_{\text{int}}$.

frequency of the *cis-* and the *trans-* flagella, as discussed in section 2.3. At this flow velocity, we observe frequency locking for the whole recording time, and the flagella beat in phase with the flow (see flow field snapshots in figure 5.5(c)).

Force and power per beating cycle

Figure 5.6 shows the total force $\mathcal{F}$ (figure 5.6(a) blue line), the rate of work of hydrodynamic forces $\mathcal{P}$ (figure 5.6(b) blue line), and the elastic power $\mathcal{P}_e$ (figure 5.6(c) blue line) averaged over several beating cycles. The magnitude of the total hydrodynamic force **F** reaches two extrema per beating cycle: one during the power stroke and one during the recovery stroke. The maximum force is exerted for $\phi \approx 3\pi/2$; hence, later in the beating cycle than when there is no flow. Under the external forcing the cell is beating in phase with the flow; hence, the maximum force is imposed on the flagella towards the end of the power stroke, when the flagella are

more bent. Furthermore, the magnitude of the hydrodynamic force when the flagella synchronize with the flow is lower than in the absence of flow throughout the entire power-recovery stroke. The maximum force magnitude is $3.2\mathcal{F}_0$, and therefore 37% smaller than when there is no flow. Similarly, the viscous rate of work is maximum in the same flagellar phase and equal to $\mathcal{P} = 47\mathcal{P}_0$; therefore it is $\approx 25\%$ smaller than in the absence of flow. This lower force and rate of work, compared to those in absence of flow, are a consequence of phase locking between the flagella and the forcing. The flagella, by beating in phase with the forcing, exploit the drag generated by the external flow to propel, and the force exerted by the fluid is smaller. In fact, in figure 5.6(b), the area between the black line (rate of work in the absence of flow) and the blue line (rate or work for a synchrony-triggering external flow) corresponds to the positive work produced by the flow on the flagella during one beating period. The elastic power does not differ significantly in the two cases (see figure 5.6(c)). This indicates that the elastic deformations of flagella are not significantly affected by the flow. In other words, the flagellar shape and waveforms in the two experiments are approximately the same, as shown also in the snapshots in figure 5.5(a,c).

Force and power across multiple beating cycles

Figure 5.7 represents the hydrodynamic force as a function of the unwrapped phase for a synchrony-inducing flow (blue trace). The magnitude of $\mathcal{F}$ is approximately constant across subsequent beating cycles.

We decompose the hydrodynamic force into its three components. $\mathcal{F}$ is lower compared to experiments without flow. This decrease of total force is a direct consequence of the action of the external flow. Indeed, $\mathcal{F}_{\text{motion}}$ remains mostly unchanged (see figure 5.7(d)), although it is slightly larger than in the absence of flow. This indicates that the waveform is mostly unaffected by the flow. The moderate increase in $\mathcal{F}_{\text{motion}}$ is due to the fact that the amplitude of the flagellar motion increases slightly for a synchrony-inducing flow, which drags the flagella further in their direction of motion during the power recovery stroke. $\mathcal{F}_{\text{flow}}$, on the other hand, becomes significant (see figure 5.7(c)). The highest value for $\mathcal{F}_{\text{flow}}$ is reached during the power stroke, with a second lower peak recorded during the recovery stroke. The significant amplitude of $\mathcal{F}_{\text{flow}}$ is the cause for the overall decrease in the amplitude of the hydrodynamic force $\mathcal{F}$. The role of the three components $\mathbf{f}_{\text{flow}}$, $\mathbf{f}_{\text{motion}}$ and $\mathbf{f}_{\text{int}}$ is clearer when considering the rate of work of each of them separately. The rate of work of $\mathbf{f}_{\text{motion}}$ is always negative, indicating that the flagella always have to produce work in order to move, both in the presence and in the absence of flow. In the presence of synchrony-inducing flow, the rate of work of $\mathbf{f}_{\text{flow}}$ is always positive. This confirms that for synchrony-inducing flows, the background flow produces positive work (see figure 5.8(c)). The figure highlights that positive work is produced both during the power stroke (large peak) and during the recovery stroke (small peak). The rate of work of $\mathbf{f}_{\text{int}}$ is $\mathcal{P}_{\text{int}}/\mathcal{P}_0 = -0.02 \pm 0.9$, similar to the rate of work measured in absence of flow (equal to $\mathcal{P}_{\text{int}}/\mathcal{P}_0 = 0.03 \pm 0.77$).

5.2.3   FORCING WITH NO SYNCHRONY

We imposed, on the same cell discussed above, axial flow at $U_F = 1.19$ mm.s^{-1} and $f_F = 58.2 Hz$. This flow velocity is at the edge of the Arnold tongue, and corresponds to point 3 in figure 4.4. The amplitude chosen $A_F = 10.22$ μm is lower than the amplitude of the synchrony-inducing flow, but it is the highest possible at this frequency without the occurrence of frequency locking. Figure 5.7(a) shows the phase difference $\Delta(t)$ between the flagella and the flow (red trace). In this experiment, $\Delta(t)$ has the typical trend of a synchronization transition (for details see section 4.2.1). Periods where the phase is almost constant indicate that flagella are approaching synchronization with the flow ($\Delta \equiv 0$ mod 1). This happens for example in figure 5.7(a) when ϕ is between 0 and 8π. Instead when ϕ is between 16π and 22π, the phase difference is decreasing more rapidly, and the flagella even beat at some point in antiphase with the flow ($\Delta \equiv 0.5$ mod 1).

We compute the amplitude of $\mathcal{F}/\mathcal{F}_0$ for this non synchrony-inducing external flow. In this experiment, $\mathcal{F}$ shows changes in amplitude from one stroke to the other. The hydrodynamic force has a higher amplitude for beating cycles in which flagella are in antiphase with the flow ($\Delta \equiv 0.5$ mod 1), as shown in the snapshots in figure 5.5(b). Instead, $\mathcal{F}$ has a lower amplitude when the flagellar phase is very close to the phase of flow ($\Delta \equiv 0$ mod 1). We computed $\mathcal{F}/\mathcal{F}_0 = 2.7 \pm 0.6$ when $\Delta \equiv 0$ mod 1 and $\mathcal{F}/\mathcal{F}_0 = 4.3 \pm 0.7$ when $\Delta \equiv 0.5$ mod 1. When the forcing is in phase with the flagellar beating, it entrains the flagellar motion by reducing the total viscous force acting on the flagellum. As a consequence, if we compare the amplitude of $\mathcal{F}$ when $\Delta \equiv 0$ mod 1 with that in absence of flow, we find it to be 23% smaller. In figure 5.7(b), the modulations in the amplitude of $\mathcal{F}$ occur at a beat frequency of $2 - 3$ Hz, which agrees with the difference in frequency between the two interacting oscillators: the external flow and the flagella. The flagella beat briefly in antiphase $2 - 3$ times per second. During these time intervals, the maximum hydrodynamic force acting on the flagella is reached, during the power stroke, at about $\mathcal{F} \approx 6\mathcal{F}_0$. If we consider the separate contributions in $\mathbf{F}$, we find $\mathcal{F}_{\text{motion}}/\mathcal{F}_0$ and $\mathcal{F}_{\text{int}}/\mathcal{F}_0$ in the same range as in the experiment with no flow. The difference in $\mathcal{F}/\mathcal{F}_0$ is entirely due to the hydrodynamic force imposed by the flow, $\mathcal{F}_{\text{flow}}/\mathcal{F}_0$.

We also computed $\mathcal{P}$ (figure 5.8(a)), and separated the three contributions: $\mathcal{P}_{\text{flow}}$ (figure 5.8(b)), $\mathcal{P}_{\text{motion}}$ (figure 5.8(c)), and $\mathcal{P}_{\text{int}}$ (figure 5.8(d)). The same trend in amplitude observed in $\mathcal{F}$ appears also in $\mathcal{P}$. We focus on the rate of work of the force due to the external flow $\mathcal{P}_{\text{flow}}$. When the flagella are beating in phase with the flow ($\Delta \equiv 0$ mod 1), the rate of work $\mathcal{P}_{\text{flow}}$ is positive, meaning that the external flow is promoting flagellar beating, by providing positive work to the flagella. This is similar to what we discussed in section 5.2.2. When the flagella are in antiphase with the flow, $\mathcal{P}_{\text{flow}}$ is negative, indicating that, in this case, the flagella have to provide additional work to beat against the external flow. The average rate of work per period during in phase beating is $\mathcal{P}_{\text{flow}}/\mathcal{P}_0 = 5.2 \pm 11.0$, while in antiphase is $\mathcal{P}_{\text{flow}}/\mathcal{P}_0 = -12 \pm 15.3$. Instead, the average rate of work per period due to the motion of flagella is $\mathcal{P}_{\text{motion}}/\mathcal{P}_0 = -39.5 \pm 12.3$ during in phase beating and $\mathcal{P}_{\text{motion}}/\mathcal{P}_0 = -36.6 \pm 11.3$ during antiphase beating. Similar to the other flow conditions discussed in sections 5.2.1 and 5.2.2, $\mathcal{F}_{\text{int}}$ is an order of magnitude smaller that $\mathcal{F}_{\text{flow}}$ and $\mathcal{F}_{\text{motion}}$.

CHAPTER 5

Additionally, the rate of work of the hydrodynamic interaction force $\mathcal{P}_{\text{int}}/\mathcal{P}_0 = -0.02 \pm 0.76$ is three orders of magnitude smaller than $\mathcal{P}_{\text{flow}}$ and $\mathcal{P}_{\text{motion}}$.

5.2.4 DISCUSSION

In the present section, we quantified the strength of the viscous forces imposed by the external flow on the flagella with respect to the viscous forces generated during flagellar hydrodynamic interactions. The main results of this characterization are summarized below.

Hydrodynamic interaction forces

We end this section with a discussion over the implications of our work on the mechanism at the origin of synchronization between the flagella, and in particular on the role of hydrodynamic interaction forces. To this purpose, we compare the results of our experiments performed with an external background flow of frequency $f_{\text{F}} = 58.2$ Hz. When the velocity of the background flow is $U_{\text{F}} = 1.19$ μm.s^{-1}, the hydrodynamic force exerted by the flow is too low to induce synchronization. However, for a slightly higher flow velocity of $U_{\text{F}} = 1.63$ μm.s^{-1}, the flagella do synchronize with the background flow. From our data analysis, combining image processing and computational fluid dynamics, we estimate the hydrodynamic force imposed by the external flow. We find that, for the non synchrony-inducing weaker flow, the hydrodynamic force exerted by the external flow is $\mathcal{F}_{\text{flow}}/\mathcal{F}_0 = 1.6 \pm 0.8$, corresponding to $\mathcal{F}_{\text{flow}} = 10.6 \pm 5.3$ pN (see figure 5.7(c) red trace). At the same frequency, synchronization is induced when the hydrodynamic force exerted by the external flow is $\mathcal{F}_{\text{flow}}/\mathcal{F}_0 = 1.9 \pm 1.0 = 12.6 \pm 6.6$ pN (see figure 5.7(c) blue trace). We deduce that an average hydrodynamic force of magnitude ≈ 12 pN is required to trigger synchronization. In addition, a hydrodynamic force of this amplitude is only sufficient to trigger synchronization at a frequency relatively close to the intrinsic beating frequency of the cell. Indeed, in our experiments, $f_{\text{F}} = 58.2$ Hz, which is only a few hertz different from the cell intrinsic frequency $f_0 = 53.2$ Hz. For comparison, the difference in intrinsic frequency between the two flagella is thought to be on the order of ≈ 20 Hz (see section 2.3).

The hydrodynamic force due to the interaction between the flagella can also be estimated from our procedure, and it is found to be orders of magnitude lower ($\mathcal{F}_{\text{int}} = 0.6 \pm 0.5$ pN). Since the hydrodynamic force due to flagellar interaction is orders of magnitude lower than the hydrodynamic force required for synchronization in our experiments, we conclude that hydrodynamic interactions between flagella are too small to be responsible for flagellar synchronization in wt *C. reinhardtii*. The hydrodynamic forces generated by the 'cell-body rocking' mechanism [76] (discussed in section 2.4), are also significantly lower than the hydrodynamic forces generated by the external flow and therefore are likely not at the origin of flagellar synchronization.

Similarly, we computed the rate of work against hydrodynamic forces in the presence and in the absence of forcing. We consider the external forcing where $U_{\text{F}} = 1.19$ μm.s^{-1}, and synchronization with the flagella is not triggered. As we have just discussed, the hydrodynamic force due to the external flow is significant (10.6 ± 5.3 pN). However, since the phase is not locked, the flagella will be

alternatively in and out of phase. When flagella are in phase with the forcing, the rate of work exerted by the flow is $\mathcal{P}_{\text{flow}} = 3.8 \pm 8.0$ fW, while in antiphase it is $\mathcal{P}_{\text{flow}} = -8.8 \pm 11.2$ fW. The flagella do not synchronize with the external flow when they receive work from the flow and they continue beating when they have to produce, instead, rate of work against the flow. The rate of work of hydrodynamic interaction force between the flagella is $\mathcal{P}_{\text{int}} = -0.01 \pm 0.5$ fW. It is much smaller than the rate of work generated against the external flow. The negative sign also indicates that the flagella have to produce work against the hydrodynamic interaction force. Our quantitative results strongly suggest that hydrodynamic interactions are not at the origin of interflagellar synchronization, which instead relies on a different, much stronger, physical mechanism.

Maximum force and maximum power

Applying external hydrodynamic loads on the flagella under different flow conditions allows us to estimate how much mechanical force the flagella can exert. The maximum total hydrodynamic force in our experiments measures $\mathcal{F} = 44.2$ pN in the experiment with a non synchrony-inducing flow with velocity $U_F = 1.19$ mm.s^{-1}. In that experiment, the maximum rate of work of the hydrodynamic force is $\mathcal{P} = 60.1$ fW. In comparison, in the experiment without external forcing we find the minimum and maximum rate of work per beating cycle to be within 15.3 fW and 46.2 fW respectively. The viscous swimming power generated by a free swimming cell has been computed previously by Guasto *et al.* [87]. The maximum power found in their study is 15 fW. This discrepancy can be explained by the fact that the measured rate of work is estimated from viscous dissipation taking only into account the far-field flow generated by the cell. The flow was measured using tracer particles with 1 μm diameter. The flow field resolution was not sufficient to capture the flagella-body interactions. By computing the flow field numerically, we resolve details of the flow field around the cell body and the flagella, and we find this near field interactions to be important for the total rate of work produced by flagella. Furthermore, the rate of work that we compute is always significantly larger than zero, while in Guasto *et al.*'s study, the viscous power approaches zero between the power and recovery stroke. Even though the flow field around flagella is almost zero between the power and the recovery stroke, the flagella remain in motion, and the power generated is larger than zero. However, when the velocity of the free swimming organism approaches zero, while the stroke transitions from power to recovery, the far-field flow is almost zero, causing the rate of work to drop [87]. Finally, this study [87] focuses on a free swimming cell while we considered a cell constrained at the tip of the micropipette. It is possible that the oscillatory flows in this two different configurations are fundamentally different, which would also affect the viscous forces measured on flagella.

Energetics of flagellar bending

The total rate of work involved in flagellar bending is a combination of active flagellar deformation, initiating bending and passive resistive deformation due to the viscous forces imposed externally by the fluid. We computed the local moment along flagella associated with these two components and found that the energy consumption

required for flagellar bending is by far larger than the energy required to overcome viscous dissipation in the beating of *C. reinhardtii*. Previous studies on wave propagation in sperm cell flagella [131, 132] have shown that the largest amount of power consumption is due to viscous dissipation and a small amount is involved in elastic deformation, contrary to our observation. An explanation for this discrepancy could be in the difference in motility between sperm cell and *C. reinhardtii*. The former displays beating patterns with long waveforms and low curvature, which stores less elastic energy compared to *C. reinhardtii*, which presents short waveforms instead with higher curvature and requires an higher energy intake.

Given that the elastic rate of work is conservative, the total work of elastic forces is zero over one period. On the other hand, the viscous forces are dissipative and require net energy consumption. The energetic cost increases when the forcing is activated, since the rate of work is on average 10% higher in presence of external flow during antiphase beating. The fact that the rate of work increases when the cell beats in antiphase with the flow, suggests that the cell does not normally beat at its maximum power output. Studies on wt beating in medium of increasing viscosity reported a similar finding: in a certain range of viscosity, the increase of medium viscosity leads to an increased propulsive force by the cell [133]. Another recent study on wt reported increased swimming speed for a certain range of increased external load [117]. But when the external load is increased further, the speed decreases until it reaches a stalling point. We did not observe stalling even when we explored waveforms with an amplitude up to 3 mm.s^{-1}. However, we observed reduced stroke for a flow velocity above 2.5 mm.s^{-1}. For details the reader is referred to [115].

5.3 HYDRODYNAMIC FORCES ACTING ON FLAGELLA OF PTX1, MUTANT OF C. REINHARDTII

The mutant *ptx1* displays a peculiar beating pattern, named AP, where flagella synchronize in antiphase with each other. This beating pattern is named AP (antiphase) mode after Leptos *et al.* [83]. The other beating pattern observed in *ptx1* is the in-phase (IP) beating analogous to breaststroke in wt. AP beating resembles the wavelike beating observed in cilia [61, 77, 83], and several models suggest that ciliary coupling is a consequence of hydrodynamic interactions [44, 83]. It has been suggested that AP beating in *ptx1* is generated by hydrodynamic interactions between flagella [83, 84]. Further understanding of *ptx1* beating dynamics is therefore needed. In this section we investigate the effects of hydrodynamics on AP synchronization, at first by characterizing the beating dynamics of *ptx1* at the tip of a micropipette without external flow, and subsequently by investigating the behaviour of *ptx1* under external hydrodynamic forcing. From both experiments we compute the hydrodynamic forces similarly to the previous section 5.2.

5.3.1 FLAGELLAR SYNCHRONIZATION IN PTX1

RESULTS IN ABSENCE OF FLOW

In the mutant *ptx1*, the switch between IP and AP beating mode is stochastic. The AP stroke is shown in figure 5.9(a). The IP beating mode resembles the breaststroke in wt, while the AP stroke has some features of the slip in wt [83]. In the AP beating, power and recovery strokes are clearly distinguished for each flagellum as in the wt breaststroke. The main difference is that, in the AP, one flagellum executes the power stroke while the other one executes the recovery stroke. When the cell switches from IP to AP, the phase difference Δ between the two flagella increases by 0.5, corresponding to a half flagellar beating cycle [83]. Instead, when the cell transitions from AP to IP, the interflagellar phase difference decreases by 0.5. In the example shown in figure 5.9(a-c), the cell beats normally at the frequency $f_{\mathrm{IP}} = 49.6 \pm 3$ Hz, while, during AP beating, flagella beat at $f_{\mathrm{AP}} = 74.5 \pm 1$ Hz, in agreement with [83]. Here, we computed the interflagellar phase difference between the *cis-* and *trans-* flagella as $\Delta_{\mathrm{f}}(t) = (\phi_{\mathrm{cis}}(t) - \phi_{\mathrm{trans}}(t))/2\pi$ for *ptx1* (similar analysis for wt is presented in Appendix B). Transitions from IP to AP beating are recognizable in the spectrogram, where the detected beating frequency suddenly jumps. In figure 5.9(b), such frequency jump can be seen after 2 seconds and 8 seconds from the start of the experiment. During the switch to AP, the interflagellar phase difference $\Delta_{\mathrm{f}}(t)$ increases by half integer. This increment in $\Delta_{\mathrm{f}}(t)$ indicates that the AP beating is initiated by the *cis*-flagellum (upper flagellum in Fig.5.13(a)) and immediately followed by the *trans*-flagellum. Results on the interflagellar phase difference in absence of external flow for 6 cells in 44 recordings show that the cells beat in IP $67 \pm 30\%$ of the time. The large standard deviation implies that some *ptx1* cells did not show AP beating at all in some recordings. Overall there is a large fluctuation in transitions to AP, but most cells beat their flagella in IP more frequently than in AP, in agreement with [83]. Moreover, the ratio between the average frequency during AP and IP is $\approx 3/2$, in agreement with what is found in the literature. In our experiments, the cells were recorded under the same light conditions used for wt experiments (discussed in 3.2.2) in order to avoid triggering the photoresponse in the cell by changes in light conditions as in other previous works [61, 77].

RESULTS WITH BACKGROUND FLOW

After monitoring *ptx1* beating in absence of any external forcing, we imposed an axial flow at frequency in the range $f_{\mathrm{F}} = 45 - 80$ Hz and velocity $U_{\mathrm{F}} = 100 - 1600$ μm.s^{-1}. Results were collected for 5 cells and a total of 221 recordings. In these experiments, we measured the time fraction in which *ptx1* is frequency locked with the external forcing, and the results are shown in figure 5.9 (d), similarly to the characterization for wt discussed in section 4.3.2. The behaviour of the mutant *ptx1* is less consistent than that of wt. For example, at $U_{\mathrm{F}} = 900$ μm.s^{-1} for wt we always observed phase locking for a forcing frequency f_{F} within ≈ 4.5Hz from f_0 (results in figure 4.8(a)). For *ptx1*, even at $f_{\mathrm{F}} \approx f_0$, we occasionally observe no phase locking or very short phase locking events (see figure 5.9 (d)).
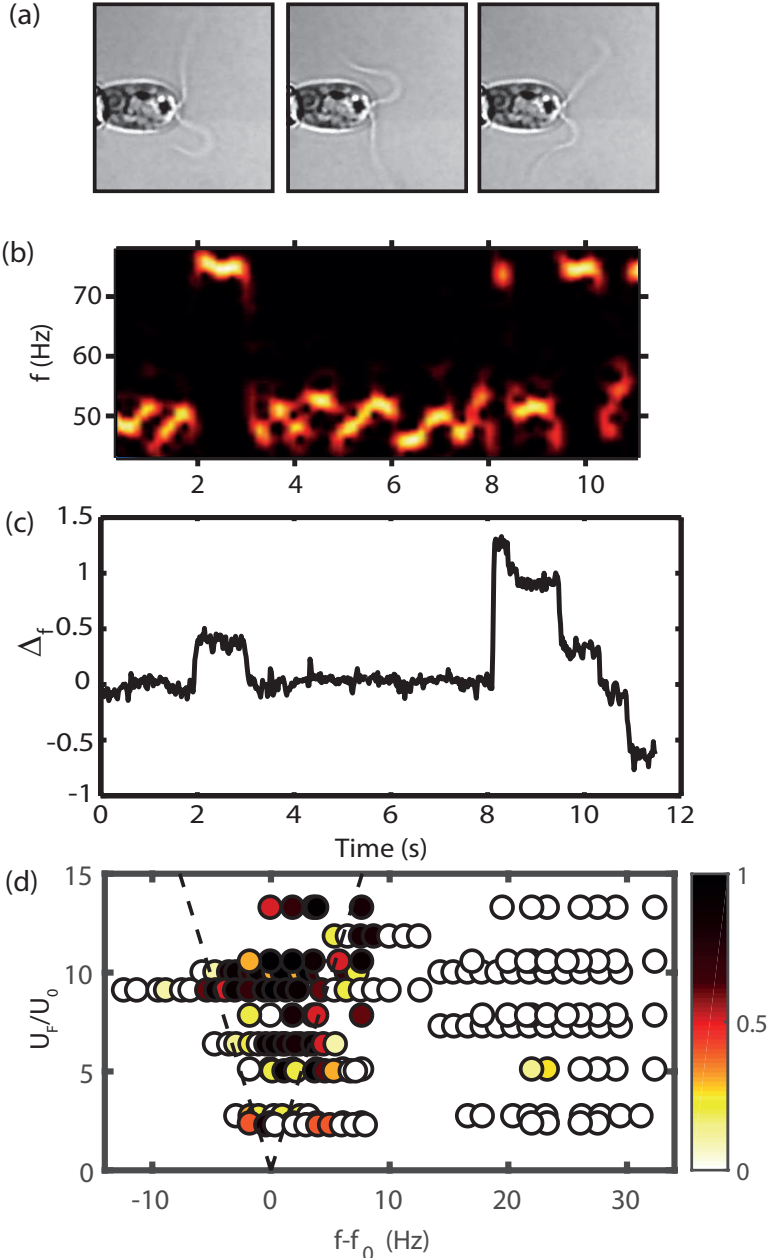
Figure 5.9: (a) Snapshots showing AP beating in *ptx1*. **(b)** Spectrogram of flagellar beating frequency during an experiment in absence of forcing. The higher frequency correspond to AP beating. **(c)** Phase difference between flagella in the same experiment as **(b)**. Switches to AP correspond to increments in interflagellar phase difference Δ_f by 0.5 corresponding to half beating cycle. **(d)** Synchronization region in (f_F, U_F)-domain for *ptx1* under axial flow. Each marker represents a separate recording. U_F ranges from 100 μm.s^{-1} to 1600 μm.s^{-1}. $U_0 = 110 \pm 12$ μm.s^{-1} is the free swimming velocity in wt. Colormap represents the time fraction when flagellar beating is phase-locked with external flow. It is equal to 1 (black) when phase-locking is observed for the entire time of recording, while it is 0 (white) when phase-locking is never observed.

One possible explanation for this lower incidence of synchronization with the forcing is the stochastic switching between IP and AP. When beating in AP, the cell has a frequency ≈ 20 Hz higher than the forcing. Therefore, it cannot synchronize with a forcing in the range $45 - 60$ Hz. To investigate whether synchrony could occur during AP stroke, we imposed a forcing frequency up to 80 Hz. As shown in figure 5.9 (d), synchronization with the background flow during AP is a rare event. Only two experiments at $f_F = 70 - 71$ Hz and $U_F = 560$ μm.s^{-1} show few periods of phase locking. Apart from these 2 experiments, we also recorded phase locking in AP in 3 recordings where the forcing frequency was $f_F = 49, 54, 57$ Hz. During these events, AP beating occurred at frequencies in the range of IP beating. This suggests that the frequency at which the AP stroke occurs can vary significantly (up to ≈ 20Hz) among cells and also in different recordings of the same cell. The most important finding from the experiments with external forcing is that phase locking between the flow and the cell during AP is an extremely rare event (5 experiments out of 221). Therefore, it seems that the cell during AP stroke is poorly influenced by hydrodynamic forces. Further evidence on the effect of hydrodynamic forces on *ptx1* is discussed in the next paragraph.

5.3.2   HYDRODYNAMIC DRAG FORCE WITH AND WITHOUT BACKGROUND FLOW

To gain insights about the strength of hydrodynamic interaction in AP stroke, we consider an experiment on *ptx1* without any forcing and compare it with an experiment on the same cell with $f_F = 49$ Hz and $U_F = 900$ μm.s^{-1}. From both experiments we tracked 10 beating cycles of the AP stroke. Experiments were limited to about 10 consecutive periods, because in the experiment with background flow the flagella rarely beat in antiphase and only for short periods of time. In this experiment, IP beating was observed for 95% of the recording, and during IP beating, flagella were phase locked with the flow. The velocity of the flow field during one beating cycle in AP is shown in the snapshots from figure 5.10(a). The reference phase $\phi = 0$ is the configuration in the first snapshot in figure 5.10(a).

Rate of work in AP beating in absence of forcing
We computed the total rate of work of *cis*-flagellum ($\mathcal{P}^{cis}$) and *trans*-flagellum ($\mathcal{P}^{trans}$), during AP beating (see figure 5.10(b), black line). The rate of work of the hydrodynamic force on the *cis*- flagellum is $\mathcal{P}^{cis}/\mathcal{P}_0 = 23.3 \pm 4.0$. Similarly to the characterization on wt (section 5.2), we separated the hydrodynamic force on the flagella in different components. We find that the rate of work of the hydrodynamic interaction force is $\mathcal{P}^{cis}_{int}/\mathcal{P}_0 = 0.016 \pm 0.2$. This value is three orders of magnitude smaller than $\mathcal{P}^{cis}/\mathcal{P}_0$. Therefore, in absence of forcing, the rate of work of the hydrodynamic force is entirely due to the flagellar motion, and $\mathcal{P}^{cis}_{motion}$ is equal to the total rate of work. Comparing these results with our results from wt, we find that $\mathcal{P}_{motion}$ in *ptx1* is 41% lower than in wt. The smaller rate of work can be explained by the difference in waveform displayed during AP beating. AP beating is characterized by a reduced stroke amplitude (as shown in figure 5.9(a) with respect to figure 2.1(c,d)). We also find the rate of work of the hydrodynamic interaction force $\mathcal{P}^{cis}_{int}$ to be approximately 33% smaller for AP beating in *ptx1* compared to wt. The forces

measured on the *trans*-flagellum have the same magnitude, but a lag in phase equal to $\Delta \equiv 0.5 \mod 1$ and are shown for comparison in figure 5.10(b-d).
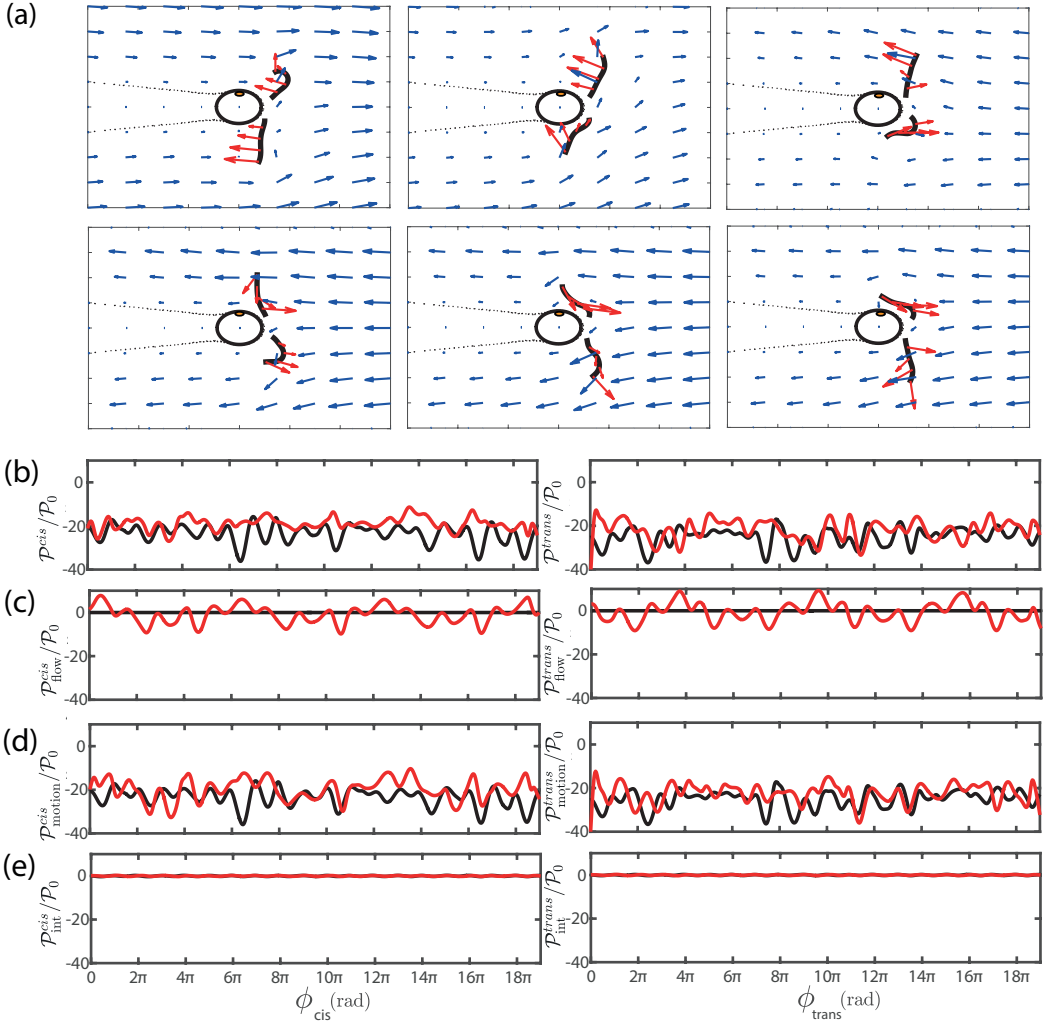

Figure 5.10: Rate of work imposed on *ptx1* flagella during AP beating. **(a)** Snapshots of the computed velocity field for a cell in presence of axial flow at $U_F = 900$ μm.s^{-1} and $f_F = 49 Hz$. **(b-e)** Adimensional rate of work on the *cis*-flagellum (left) and *trans*-flagellum (right) as a function of the unwrapped phase ϕ. Experiment without external flow (black line) is compared with experiment with axial flow at $U_F = 900$ μm.s^{-1} (red line). The total rate of work $\mathcal{P}^{cis}/\mathcal{P}_0$ and $\mathcal{P}^{trans}/\mathcal{P}_0$ in **(b)** is the sum of three contributions: the rate of work due to the external flow **(c)**, the rate of work due to flagellar motion **(d)** and the rate of work due to flagella hydrodynamic interactions **(e)**.

Rate of work in AP beating in presence of forcing

We now consider experiments with an external flow to which *ptx1* synchronizes in the IP stroke. We focus on the time intervals when the AP stroke is established. We find that the rate of work due to hydrodynamic interactions is equal to the experiment

without flow and therefore negligible. The nondimensional rate of work of the hydrodynamic force ($\mathcal{P}^{cis}_{flow}/\mathcal{P}_0$) ranges from -9.7 to 7.8. Similarly to wt, when the rate of work is negative, the external flow works against the flagellar beating, whereas when it is positive, the external flow provides useful work to the flagella. It must be noted that the maximum rate of work due to hydrodynamic interaction between flagella in AP is $\mathcal{P}^{cis}_{int}/\mathcal{P}_0 = -0.02 \pm 0.1$. Therefore, its contribution appears to be irrelevant to the total force.

5.3.3   DISCUSSION

In section 5.2, we showed that the symmetric breaststroke in *C. reinhardtii* is not a consequence of hydrodynamic interaction between the flagella. Here, we investigated whether the AP beating mode observed in the mutant *ptx1* can instead be induced by hydrodynamic interactions. By separating contributions, we computed the hydrodynamic force applied on one flagellum due to the motion of the other one. In AP stroke, this interaction force is even smaller than in wt due to the scarce interaction between the flagella that are always at a different phase of the beating cycle. Furthermore, in our experiment, the cell is synchronized in IP stroke with the background flow for most of the time. In this experiment, during AP, the rate of work of the hydrodynamic force due to the external flow is 3 orders of magnitude larger than the rate of work of the hydrodynamic interaction force. The fact that the cell is able to interrupt IP, phase locked with the external flow, and switch to AP implies that AP synchrony is not sustained by hydrodynamic forces since the hydrodynamic force imposed by the flow would induce the cell to continue IP in order to minimize viscous drag. The observation that *ptx1*, regardless of the strong external forcing, can switch to AP suggests that hydrodynamic forces have neither effect on the AP beating nor on the switching between IP and AP, as suggested by Leptos *et al.* [83].

To conclude, the detailed quantitative investigation of the hydrodynamic forces and the magnitude of the hydrodynamic interaction force in *C. reinhardtii* wt (section 5.2) and *ptx1* (this section) leads to the conclusion that, in *C. reinhardtii*, hydrodynamic interaction between flagella plays no role in flagellar synchronization. The viscous force imposed by the flow is one order of magnitude larger than the force due to interflagella hydrodynamic interactions. The cell can overcome the hydrodynamic viscous forces imposed by the flow by not synchronizing in the case of wt and by switching to AP in the case of *ptx1*.

5.4   IMPORTANCE OF INTRACELLULAR COUPLING: EXPERIMENTS ON THE VFL3 MUTANT

A possible synchronization mechanism, suggested in previous studies, is coupling through elastic forces through the distal striated fiber, see section 2.3. The distal striated fibers mechanically connect the basal bodies of the two flagella [65] (see sketch in figure 5.11(a)). This mechanical connection could play a major role in the flagellar synchronization for *C. reinhardtii*, also discussed in [69, 116]. Indeed, if we consider a force balance on one flagellum, the total hydrodynamic force exerted by the flagellum

on the surrounding fluid is exactly balanced by the direct mechanical force the same flagellum exerts on the basal apparatus. As a result, strong mechanical stress concentration is expected in the region of the cell cortex around the basal apparatus of the flagella, which far exceeds the viscous stresses inside the fluid. Synchronization is therefore more likely mediated by elastic stresses, which are conservative and act over an interflagellar distance of only $\sim$ 200 nm in the distal fiber (see figure 2.5), rather than viscous stresses due to hydrodynamic interactions, which are dissipative and act over an interflagellar distance of $\sim$ 10 μm in the fluid.

To test this hypothesis, we first investigate flagellar beating in a cell with an impaired distal fiber. Secondly, additional understanding on the role of coupling is possible by studying synchronization properties of 'mechanically' isolated flagella. In order to characterize mechanically isolated flagella, we study the mutant *vfl3*, in which the distal fiber is impaired (details in section 2.3.1). By comparing the results of these experiments with those performed on wt in Chapter 4, we gain insights into the role of the distal fiber in flagellar synchronization.

5.4.1   RESULTS IN ABSENCE OF FLOW

We observed the motility of 20 *vfl3* cells at the tip of the micropipette. Each individual flagellum of *vfl3* beats actively with normal waveforms and frequencies. In *vfl3*, the number of flagella varies from 0 to 3, and we considered only cells with 2 flagella. We do not refer to the flagella as *cis-* and *trans-* since the morphology of the mutant often does not allow a clear identification of the eyespot. Furthermore, some cells grow two flagella of the same type, either *cis-* or *trans-*. From our experiments with biflagellated *vfl3* cells in absence of any forcing, we report the following observations: first, the two flagella are always observed to beat in asynchronous fashion for the entire duration of the recordings, with no frequency locking recorded in flagellar beating. Also, for most cells, the two flagella beat in the same direction, in contrast with wt cells, whose flagella beat in opposite directions when performing a breaststroke; see also [81]. For all 20 cells considered, we found the slower flagellum to beat at 48.6 $\pm$ 8.8 Hz and the faster one at 63.1 $\pm$ 6.9 Hz. These observations are consistent with a synchronization mechanism relying on the distal striated fiber, since for the mutant *vfl3* with an impaired mechanical connection between the flagella, the *cis-* and the *trans-* flagellum beat at their own intrinsic frequency. The beating frequency of each *vfl3* flagellum presents significant fluctuations from one cell to another. Also for the same cell, the intrinsic beating frequency of each flagellum can vary up to 10 Hz over the course of a recording.

5.4.2   RESULTS WITH BACKGROUND FLOW

To investigate how an external forcing can affect the beating frequency in this mutant and whether it can force the flagella to synchronize with each other, we performed the Experiment type 1 described in section 4.1. We imposed axial flow on *vfl3* at velocities $U_F = 100 - 1308$ μm.s^{-1} and $f_F = 42 - 77$Hz on 7 cells. We collected 155 experiments and we characterized the experimental Arnold tongue similarly to wt in section 4.3.2.
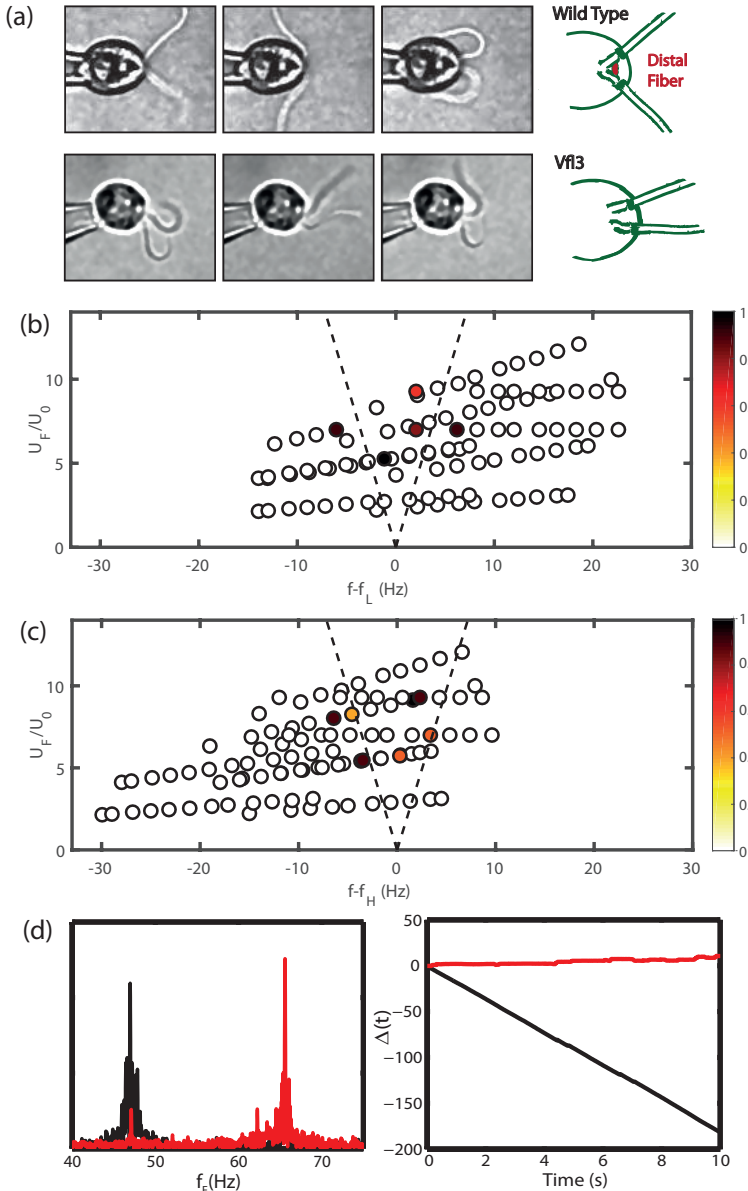
Figure 5.11: (a) Snapshots representing the stroke patterns in *C. reinhardtii* wt (*top*) and in *vfl3* mutant (*bottom*). The mutant has impaired distal fiber, resulting in absence of interflagellar synchronization. **(b, c)** Synchronization region in (f_F, U_F)-domain in presence of axial flow **(a)**. Separate representations for the slower flagellum **(b)** and for the faster flagellum **(c)**. The x-axis represents $\nu = f - f_L$ in **(b)** and $\nu = f - f_H$ in **(c)**. Each marker represents a separate recording with colormap based on the time fraction when flagella are synchronized with the external forcing. This time is 1 (black) in case of full synchrony and is 0 (white) in case of no synchrony. **(d)** Experiment where the faster flagellum phase locks with the background flow. (*Left*) Fast Fourier Transform showing $f_L = 47.7$ Hz (black line) and $f_H = 65.5$ Hz (red line). (*Right*) The black line shows the phase difference $\Delta(t) = \phi_L(t)/2\pi - \phi_F(t)/2\pi$ between forcing and flagellum beating at lower frequency. The red line shows the phase difference $\Delta(t) = \phi_H(t)/2\pi - \phi_F(t)/2\pi$ between forcing and flagellum beating at higher frequency.

CHAPTER 5

In figure 5.11(b) we represented the results for the slow flagellum in each cell in the separate recordings in the (ν, U_F)-domain. The frequency detuning is $\nu = f - f_L$, with f_L in the range $f_L = 51.2 \pm 5.7$ Hz. The forcing velocity has been normalized with respect to the free swimming velocity of wt. For comparison, the plot shows the limits of the Arnold tongue based on fitting parameters extracted for wt during axial flow. Regarding the slower flagellum (figure 5.11(b)), we observe periods of synchronization in only 5 experiments. These events always occur within 5 Hz from the intrinsic frequency f_L. In the other experiments, no phase locking with the flow is detected, even when the forcing frequency f is very close to f_L.

The results for the fast flagellum are shown in figure 5.11(c). For the fast flagellum, phase locking was detected in 7 experiments, in the range of 5 Hz from the intrinsic frequency f_H, with f_H in the range $f_H = 61.6 \pm 4.4$ Hz. When the forcing is activated, the difference in intrinsic frequency between the two flagella is not reduced, and we never observed phase locking between the two flagella, even at high flow velocities $(U_F = 1308 \ \mu\text{m.s}^{-1})$, and even in experiments where the intrinsic beating frequency between the two flagella only differed by ≈ 5 Hz. Furthermore, in 12% of the experiments, one of the two flagella has some periods of synchrony with the background flow, as in the example in figure 5.11(d). In this experiment, the fast flagellum (red line), whose intrinsic frequency is $f_F = 64.1$ Hz, is phase locked with the forcing for most of the recording at $f = 65.5$ Hz. The forcing velocity is $U_F = 984 \ \mu\text{m.s}^{-1}$. The slower flagellum intrinsic frequency $f_L = 50.2$ Hz, remains unaffected by the external forcing. From the results on *vfl3*, we conclude that the two flagella are never synchronized with each other, regardless of whether or not an external hydrodynamic forcing is applied. In wt, with axial flow above $800 \ \mu\text{m.s}^{-1}$, we observed consistent phase locking between the cell and the forcing in all the experiments with forcing frequency f_F within 5 Hz from the intrinsic frequency f_0 (results for wt in section 4.3.2). Instead in *vfl3* at similar velocity, phase locking between one flagellum and the forcing is observed only in 8% of the experiments and never for the entire recording time.

5.4.3   DISCUSSION

In *vfl3*, the two flagella behave as two independent self-sustaining oscillators. Each flagellum beats at its own intrinsic frequency. Frequency locking happens indifferently for the slow (figure 5.11 (b)) or for the fast flagellum (figure 5.11 (c)) as long as the frequency detuning is within 5 Hz. In fact, phase locking could happen only if the detuning parameter ν was smaller than the coupling strength ϵ, deduced from our experiments with wt *C. reinhardtii* (see section 4.3.2). In most of the experiments, however, neither of the flagella synchronizes with the background flow, even when the forcing frequency was close to the intrinsic frequency ($\nu \approx 0$). Additionally, in our experiments, the interflagellar frequency mismatch is never reduced by imposing the external forcing, and it is not possible to induce the two flagella of *vfl3* to beat in synchrony by hydrodynamic forcing.

Our results for *vfl3* in presence of axial flow are in agreement with the hypothesis that impaired mechanical connection between the two flagella in *C. reinhardtii* prevents robust frequency locking. Recently, similar conclusions were drawn by Wan et al. [134].

Previous studies have suggested the dominance of the *cis-* over the *trans-* flagellum [70–73]. We find no evidence supporting the view that one flagellum is more prone to synchronization than the other one. In our experiments, both flagella responded to external forcing in a similar way, despite a significant discrepancy in intrinsic frequency. Any difference in synchronization affinity in the two flagella is likely mediated by the mechanical connection between them.

Even though, in the present study, we focused on the organism *C. reinhardtii*, our results on the importance of elastic stresses in the cell cortex for flagellar synchronization have wide implications for other ciliated microorganisms. As a matter of fact, contractile fibers connecting flagella and cilia are found across a variety of organisms [135]. In particular, for multiciliated cells, the network of elastic actin fibers connecting dozens of cilia was reported to play a role in coordination of ciliary beating [136, 137]. Perturbing the bridges between the actin fibers resulted in loss of metachronal synchrony of cilia beating [136]. Further investigation in other ciliated organisms is needed to assess the prevalence of such intracellular coupling.

5.5 ASYMMETRIC LOADING OF THE CIS- AND TRANS- FLAGELLA OF WT C. REINHARDTII

We confirmed the importance of intracellular coupling in mediating flagellar synchronization. The strength of this coupling is unknown. We discussed in section 2.3, that *cis-* and *trans-* are intrinsically different; the *trans-* flagellum intrinsically beats at a frequency 30% higher than the *cis-*, and in the breaststroke pattern observed in *C. reinhardtii* the *cis-* flagellum is dominant [70–73]. In our experiments (section 4.3.2), the flagella could be synchronized with a flow at a frequency close to that of the *cis-*flagellum, but not to the *trans-* flagellum. This suggests that the coupling between the two flagella is not symmetrical. However, further evidence is needed.

Here, we investigate the effect of an external load applied selectively to the *cis-* or *trans-* flagellum. This characterization allows us to compare the different coupling strength of *cis-* and *trans-* flagella with the flow and the interflagellar coupling strength.

5.5.1 ASYMMETRIC LOADING

Given the short distance between the two flagella, it is difficult to hydrodynamically isolate one flagellum from the other. Instead, with the same experimental setup discussed in section 3.2, we performed experiments with flows oriented at an angle $\theta = \pi/4$ and $\theta = -\pi/4$ with respect to the pipette axis. These flows are named respectively '*cis*-flow' and '*trans*-flow'. The cell is oriented as in figure 5.12(a), where the upper flagellum is the *cis*-flagellum.
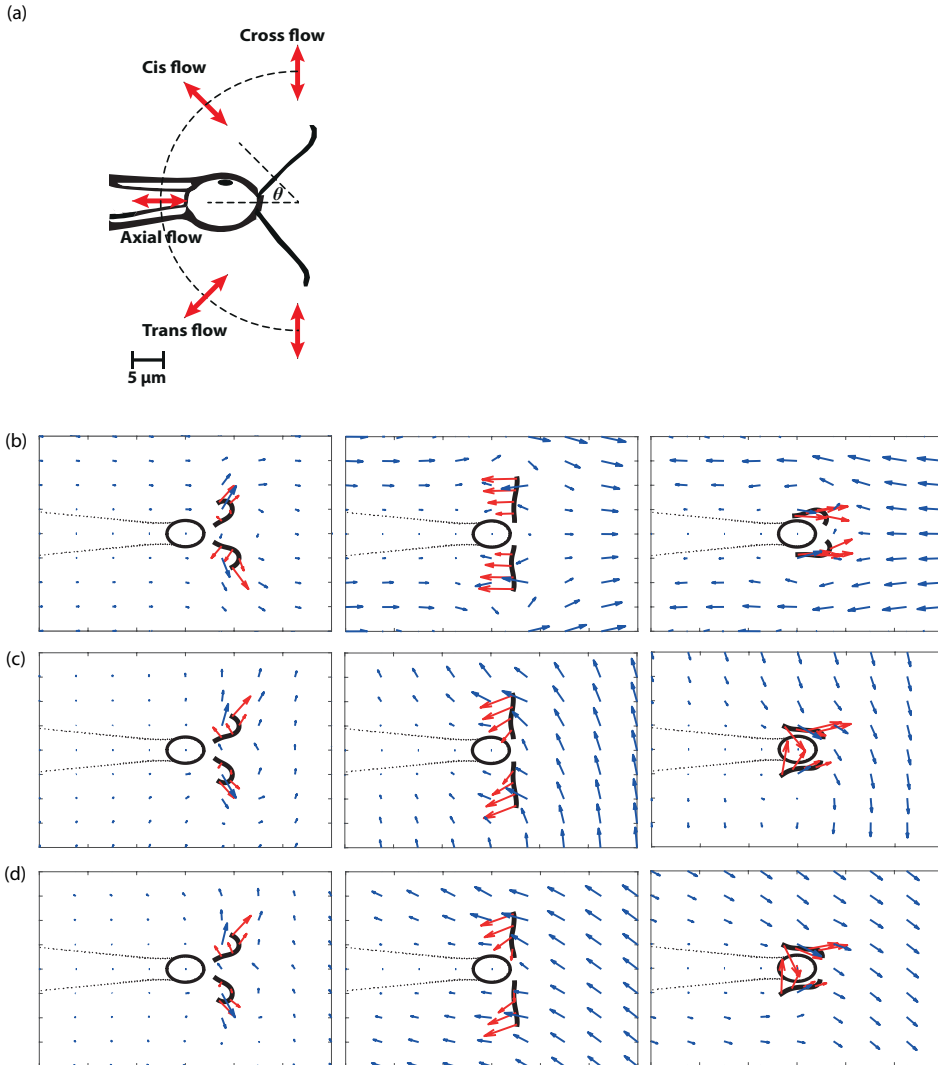
Figure 5.12: (a) Sketch representing directions of the periodic background flow. *Cis*-flow and *trans*-flow form, respectively, an angle $\theta = \pi/4$ and $\theta = -\pi/4$ with the pipette axis, assuming the upper flagellum is the *cis*-flagellum. Axial flow is parallel to the pipette axis while cross flow is perpendicular to the pipette axis. **(b-d)** Snapshots of flow field at $U_F = 47.6 \ \mu\text{m.s}^{-1}$ and frequency $f_F = 47.6$ Hz during respectively: axial flow **(b)**, cross flow **(c)** and *cis*-flow **(d)**. The red arrows represent the force distribution exerted by the flagella on the flow.

Cis-flow and *trans*-flow were imposed on the cell at a constant velocity $U_F = 478.5 \pm 36.4 \ \mu\text{m.s}^{-1}$. While axial and cross flow impose the same forcing on the two flagella, the *cis*-flow and *trans*-flow do not generate the same force on the *cis*- and *trans*- flagella. The tested frequencies were within the range $f_F = 47 - 60$ Hz, with a forcing amplitude $A_F = 4.5 \pm 0.2 \ \mu$m. For each cell, both *cis*-flow and *trans*-flow were imposed successively at each f_F and recorded for 12 s. We also tested forcing frequencies close to the *trans*-flagellum intrinsic beating frequency.
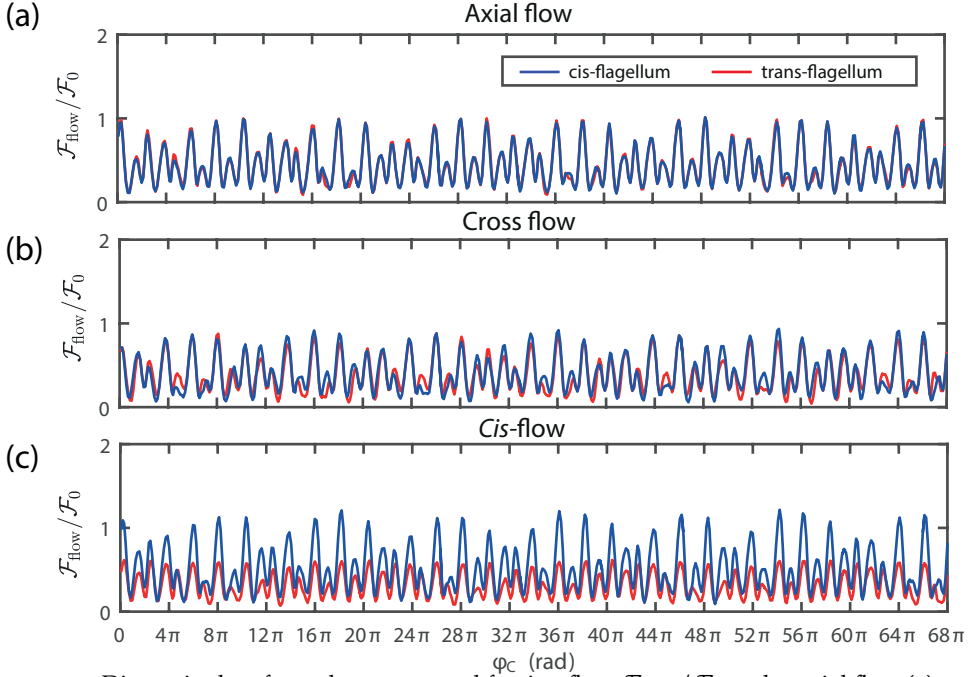
Figure 5.13: Dimensionless force due to external forcing flow $\mathcal{F}_{\text{flow}}/\mathcal{F}_0$ under axial flow **(a)**, cross flow **(b)** and *cis*-flow **(c)**. *Cis*-flow imposes a larger load on the *cis*-flagellum (blue line) rather than on the *trans*-flagellum (red line).

To quantify the difference in hydrodynamic force imposed by a *cis*-flow and a *trans*-flow on the two flagella, we computed $\mathcal{F}_{\text{flow}}/\mathcal{F}_0$ as described previously in section 5.2. We considered *cis*-flow and *trans*-flow at frequency $f_F = 47.6$ Hz. Under the flow conditions considered, flagellar motion is not synchronized with the external forcing in any of the flow directions. To show how the load imposed by *cis*-flow or *trans*-flow compares with axial flow and cross flow, we resolved the velocity field in these 4 flow directions for the same velocity and frequency ($U_F = 476 \ \mu\text{m.s}^{-1}$ and $f_F = 47.6$ Hz). Snapshots of the flow field are shown in figure 5.12(b-d), while the non-dimensional drag force imposed by the flow $\mathcal{F}_{\text{flow}}/\mathcal{F}_0$ is shown in figure 5.13. The force and flow field for *trans*-flow is not represented, since it is symmetrical with respect to the *cis*-flow. If we consider the drag forces imposed by *cis*-flow on both *cis*- and *trans*-flagellum, shown in figure 5.13(c), we find that the force amplitude varies with Δ, i.e. the phase difference between flagella and flow, as discussed in section 5.2.3. $\mathcal{F}_{\text{flow}}/\mathcal{F}_0$ is the highest when the flagella are in antiphase with the flow ($\Delta \approx 0.5$). If we consider the force imposed by *cis*-flow (figure 5.13(c)), there is a clear difference in the magnitude of $\mathcal{F}_{\text{flow}}$ on the *cis*- (blue line) and on the *trans*-flagellum (red line). In detail, the maximum force imposed by *cis*-flow on the *cis*-flagellum is 9.5 pN, while on the *trans*-flagellum it is 4.9 pN. The force imposed by *cis*-flow on the *cis*-flagellum is $\approx$ 2 times larger than the force imposed by the same flow on the *trans*-flagellum. Likewise, when considering instead the *trans*-flow, the viscous forces due to the external flow are almost 2 times larger on *trans*-flagellum. For comparison, we also showed the forces imposed by axial flow and cross flow for the same flow velocity and

frequency. We observe that the maximum force imposed on *cis*-flagellum by cross flow is 7.5 pN, while the maximum force imposed on *cis*-flagellum by axial flow is 9.2 pN. These calculations show that the *cis*-flow and *trans*-flow impose asymmetric forcing on the flagella. The *cis*-flow imposes a significantly larger force on the *cis*-flagellum than on the *trans*-flagellum. Conversely, the *trans*-flow imposes on the *trans*-flagellum a significantly larger force than on the *cis*-flagellum.
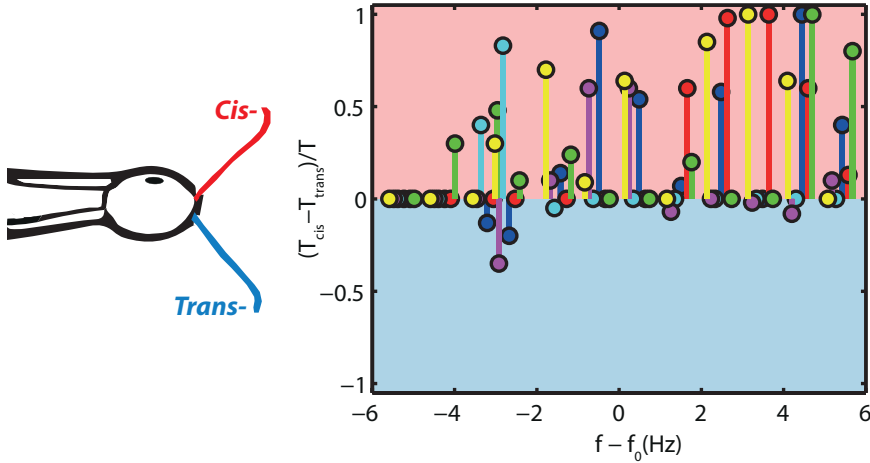
Figure 5.14: Difference between T_{cis} (time fraction when flagellar beating is phase-locked with the *cis*-flow) and T_{trans} (time fraction when flagellar beating is phase-locked with the *trans*-flow). Results are normalized by the total experiment time $T = 12$ s and are shown as a function of the frequency detuning $\nu = f_F - f_0$, with $f_0 = 53.1 \pm 2.1$ Hz. The dots are coloured to distinguish the results for different cells.

5.5.2   EXPERIMENTAL RESULTS

For each frequency imposed, we measured the time fraction when flagellar beating is synchronized with the flow (see section 4.3.2). We report T_{cis}/T as the non dimensional duration of synchronization measured under *cis*-flow conditions and T_{trans}/T as the one measured under *trans*-flow conditions. Figure 5.14 shows the normalized difference between T_{cis} and T_{trans} as a function of the frequency detuning $f - f_0$ for each separate experiment. Results were collected on 6 cells, represented by different colors of the dots. The average intrinsic frequency is $f_0 = 53.1 \pm 2.1$ Hz. For each cell and each forcing frequency, we report $T_{cis} - T_{trans}$, i.e. the difference between the time that flagella spent synchronized with *cis*-flow and the time they were synchronized with the symmetric *trans*-flow. Hence, a positive value for $T_{cis} - T_{trans}$ represents a tendency of the flagella to synchronize with a *cis*-flow more than with a *trans*-flow. Since the *cis*-flow and *trans*-flow are equivalent in amplitude and frequency and differ only in the direction, we would expect the distribution of our experimental results to be centered at zero. Indeed, when for a given f_F, the flagella synchronize for the entire duration of the experiment, then $T_{cis} - T_{trans} \cong 0$. Likewise, when the flagella synchronize neither with *cis*-flow nor with *trans*-flow, then $T_{cis} - T_{trans} \cong 0$ as well. We observe that, even though *cis*-flow and *trans*-flow have the exact same velocity and frequency and differ only for the direction along

which they are imposed ($\pi/4$ and $-\pi/4$ with respect to the pipette axis), they induce very different responses from the cell. Indeed, we find that $T_{cis} - T_{trans}$ is almost always positive (see figure 5.14). In fact, in 47% of the experiments, the *cis*-flow is triggering phase locking, while the *trans*-flow does not. In addition, in almost all experiments were the flagella were only synchronized with the flow for a fraction of the experiment, they synchronized longer under *cis*-flow than under *trans*-flow. This trend is observed consistently for each cell and in each separate experiment. It must be mentioned that, in all the experiments, the two flagella are always coupled with each other and phase slips between the two are within the slip occurrence observed in unperturbed cells, discussed in Appendix B. Hence, even though the flow is imposing a higher load on one of the two flagella the occurrence of slips between the two does not increase. Furthermore, we investigated whether inducing synchronization with the *trans*-flagellum would allow to control the *cis*-flagellum. For this purpose, we applied *cis*-flow and *trans*-flow at frequency close to the *trans*-flagellum ($f_F = 64 - 76$ Hz). We imposed a very high flow velocity in the range $U_F = 1000 - 1500 \ \mu m.s^{-1}$.
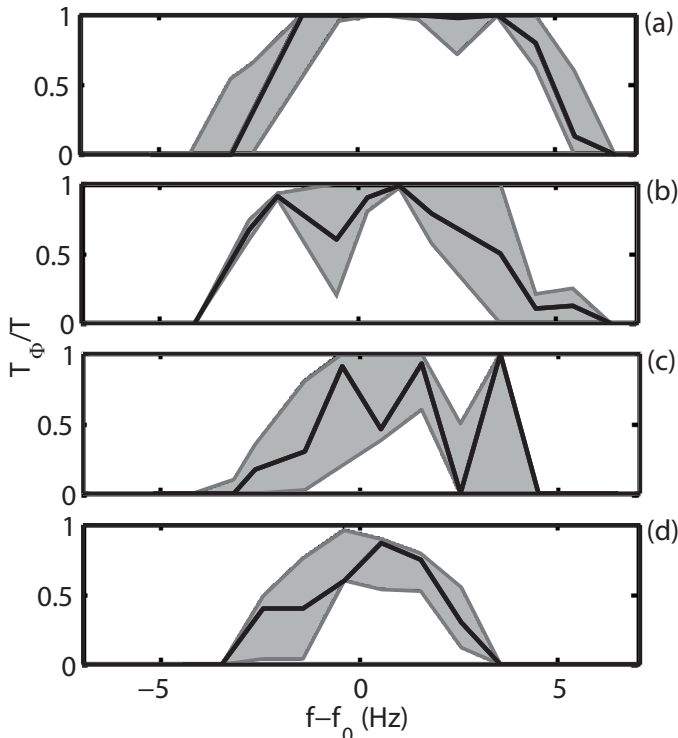
Figure 5.15: Time fraction when flagellar beating is phase locked with the flow as a function of $\nu = f_F - f_0$. Results for *cis*-flow **(a)**, axial flow **(b)**, *trans*-flow **(c)** and cross flow **(d)**. The black line is the median value computed in different cells while the shaded area indicates the 20th and 80th percentiles.

In the experiments with *cis*-flow and *trans*-flow at $f_F = 64 - 76$ Hz, we do not observe phase locking of flagella with the background flow. Only in one experiment at $U_F = 1$ mm.s^{-1} and $f_F = 68.7$ Hz, the cell went through a few periods of slips, and the *trans*-flagellum synchronized with the external forcing during slip. From these results we

conclude that it is not possible to synchronize the flagella with a flow at high frequency. Even when in one instance we synchronized the *trans*-flagellum with the flow, the *cis*-flagellum did not follow.

We computed the coupling strength ϵ between flagella and forcing by fitting equation 4.14, presented in section 4.3.1, to the experimental results for *cis*-flow and *trans*-flow. The average amplitude of the coupling strength is $\epsilon = 1.9 \pm 0.9$ Hz for the *trans*-flow and $\epsilon = 3.4 \pm 0.7$ Hz for the *cis*-flow. In order to compare the cell behaviour for the four flow directions discussed in this study, we show in figure 5.15 the time fraction T_Φ/T where flagella are phase locked with the flow as a function of the frequency detuning $\nu = f_F - f_0$. We considered approximately the same flow velocity in all directions. Results for axial flow and cross flow at several velocities were discussed in sections 4.3.2 and 4.3.3, and here we represent $U_F = 541.4 \pm 47$ μm.s^{-1} for the axial flow and $U_F = 498.2 \pm 1.9$ μm.s^{-1} for the cross flow (see figure 5.15(a,b)). We find the largest ϵ for the *cis*-flow, followed by axial flow having the coupling strength $\epsilon = 2.5 \pm 0.1$. The smallest synchronization region is obtained with the cross flow, measuring $\epsilon = 1.8 \pm 0.1$. The amplitude of the synchronization region is linear with the hydrodynamic load imposed by the flow on the flagella. In fact, as discussed in section 5.5.1, the highest load on *cis*-flagellum is imposed by *cis*-flow.

5.5.3   DISCUSSION

By imposing an asymmetric load on the two flagella, we observed that a load imposed on the *cis*-flagellum has a higher coupling strength than a load imposed on the *trans*-flagellum. This disparity in coupling strength indicates that the intrinsic frequency f_0 is more likely to be perturbed by a forcing acting on the *cis*-flagellum. This outcome is consistent with the hypothesis that the *cis*-flagellum has a dominant role in regulating the beating frequency of the cell [71, 83]. Results for the forcing at high frequency ($f_F \geq 60$ Hz) show that, even with a very strong forcing (up to 1500 μm.s^{-1}), it is not possible to shift the intrinsic beating frequency of the cell by forcing the *trans*-flagellum.

Our experimental results indicate that the flagellar beating frequency can be externally modulated and controlled by imposing a forcing on the *cis*-flagellum. The *trans*-flagellum, on the other hand, is less sensitive to external mechanical forcing. Our observations suggest that the phase dynamics of the *trans*-flagellum is not influenced directly by the external forcing, but instead follows that of the *cis*-flagellum. This strong coupling of the *trans*-flagellum with the *cis*-flagellum is possibly due to the mechanical connection between the two flagella.

6

CONCLUSIONS AND FUTURE PERSPECTIVES

This chapter summarizes the conclusions presented in chapters 4 and 5 and presents future research perspectives on the topic. In chapter 5, we presented several different experiments that are self-contained studies, therefore only the main conclusions of this work are listed here.

6.1 CONCLUSIONS

The objectives of this study were presented in section 2.5. We wanted to investigate the dominant synchronization mechanism in cilia. Since it has been suggested that flagella and cilia do respond to hydrodynamic perturbations [12, 44, 91], we developed an experimental method that allowed us to actively interact with the living organism by imposing an external hydrodynamic forcing. The main conclusions of this work are twofold. On the one hand, we compare the behaviour of *C. reinhardtii* with an ideal self-sustained oscillator and highlight the close analogy found (chapter 4). On the other hand, we present arguments that highlight the limits of hydrodynamic interactions in flagellar synchronization, and we provide evidence to support the importance of intracellular coupling (chapter 5).

LIMITS OF HYDRODYNAMICS

Our results indicate that eukaryotic flagella respond to hydrodynamic forces and can be synchronized with an external flow. However, in *C. reinhardtii*, synchronization between the two flagella, having an intrinsic frequency mismatch of 30%, requires a coupling strength of $\approx 15 - 20$ Hz [114]. In our experiments we observe that, even if we impose hydrodynamic forces an order of magnitude larger than the forces experienced by free-swimming cells, the flagella synchronize with the external forcing only in a range of 5 Hz; hence, only with a coupling strength of 5 Hz. We confirm this result by computing numerically the flow field around the cell in a typical experiment. We find that the hydrodynamic force imposed by the external flow is an order of magnitude larger than the hydrodynamic interaction between flagella, yet the two flagella are coupled together but are not coupled with the external flow. Therefore, while flagella can synchronize with an external hydrodynamic forcing, in *C. reinhardtii* the coupled beating of the two flagella, which intrinsically beat at different frequency, appears not to be a consequence of hydrodynamic interactions.

In our experiments, we imposed on a single cell a periodic background flow mimicking the hydrodynamic forces imposed on the flagella of a freely swimming cell. The cell couples with this external flow by shifting its intrinsic beating frequency to lock with the frequency of the flow. With these experiments, we investigated the similarity between wt and an ideal self sustained oscillator. Similar to an ideal self sustained oscillator, *C. reinhardtii* can synchronize with an external hydrodynamic forcing within a certain frequency range delimited by an Arnold tongue. This Arnold tongue is consistent among several wt cells and delineates a very reproducible behaviour. We also measured the transition time from the intrinsic frequency to the forcing frequency, and we found that, although it varies significantly among experiments, it is inversely proportional to the forcing strength. Similar to an ideal self-sustained oscillator, once the forcing stops, the intrinsic beating frequency is immediately restored. Furthermore, we observed that even a forcing imposed for long time (up to 10 minutes) does not produce permanent modifications in the intrinsic beating frequency of the cell.

IMPORTANCE OF INTRACELLULAR COUPLING

The limited role of hydrodynamic forces in flagellar synchronization in *C. reinhardtii* suggests that another synchronization mechanism has to be involved. We investigate as synchronization mechanism the intracellular coupling between flagella. In wt flagella are mechanically coupled internally to the cell via the distal striated fiber [65]. We performed experiments on the *vfl3* mutant of *C. reinhardtii* in which this connection is impaired. We observed that the flagella in *vfl3* are never synchronized. This result confirms the hypothesis that the mechanical connection between the two flagella through the distal fiber is responsible for the flagellar synchronization observed in wt. Recently, similar conclusions have been drawn by Wan *et al.* [134].

6.2 FUTURE PERSPECTIVES

As discussed above, synchronization between flagella in *C. reinhardtii* is due to a cell internal mechanical coupling between the flagella. An open question is whether this mechanism is a more general synchronization mechanism in ciliated organisms. This possibility is discussed in this section together with suggestions on future investigations on flagellar synchronization.

IS INTRACELLULAR COUPLING A GENERAL SYNCHRONIZATION MECHANISM IN CILIA?

We pointed out that intracellular coupling between flagella is likely at the origin of the synchronous beating observed in *C. reinhardtii*. Given that contractile fibers connecting flagella and cilia are present in a variety of organisms [135], is intracellular coupling a general synchronization mechanism in cilia? A recent study by Wan and Goldstein

discussed the role of intracellular coupling in algae with 4, 8, and 16 flagella [134]. Their results suggest that synchronization among multiple flagella is the consequence of combined hydrodynamic interactions and intracellular coupling. Other studies on multi-ciliated cells reported that damaging of the intracellular coupling in the ciliary network resulted in loss of metachronal synchrony [136, 137], suggesting that contractile fibers connecting cilia inside the cell cortex are essential for achieving cilia coordination.

SUGGESTIONS FOR FUTURE EXPERIMENTS WITH BACKGROUND FLOW

Suggestions on experimental characterizations involving hydrodynamic interactions are discussed below.

Flagella 'stalling point'
The combination of experimental data with numerical flow computation have allowed us to quantify several properties of *C. reinhardtii*, such as the work produced during its typical limit cycle and the force and rate of work imposed on flagella by the background flow. A completion of this quantitative analysis on flagellar kinematics would be achieved by altering the flow viscosity and measuring the flagella 'stalling point'. It has been reported that an increase in fluid viscosity up to a certain value (2 cP) caused *C. rehinartdii* cells to increase the propulsive force [133]. Another study on free swimming *C. reinhardtii* cells in viscous and viscoelastic fluids points out that altered viscosity causes modifications in flagellar waveform, frequency, and swimming speed [138]. With the experimental method described in this thesis, a single cell can be observed in conditions of altered flow viscosity and in presence of external hydrodynamic forcing. This experiment would allow to characterize the stalling load of flagella and the maximum rate of work produced in such condition. Comparison with the rate of work produced in normal flow viscosity would indicate whether or not *C. reinhardtii* is normally swimming at its maximum efficiency. Furthermore, the effects of altered viscosity on interflagellar coupling could be directly quantified.

An alternative method to reach the stalling point for *C. reinhardtii* could be imposing a strong unidirectional flow. In a recent study on *C. reinhardtii*, a unidirectional flow parallel to the pipette axis was applied. The stalling velocity was 0.5 mm.s^{-1} [117]. In our experiments with oscillatory flow, we never observed stalling, even at a flow velocity up to 3 mm.s^{-1}. A comparison of flagellar 'stalling load' in experiments with increased flow viscosity and oscillatory flow and in experiments with unidirectional flow in normal fluid viscosity would provide insights on the different response of flagella to static and dynamic loads.

Further investigation of the role of the distal fibers
The experiments that we performed on the *vfl3* mutant of *C. reinhardtii* highlighted the crucial role of the distal fiber in mediating flagellar synchronization. However, it must be pointed out that the behaviour of mutant cells, in this case *vfl3*, is not as consistent among different organisms as wt [60]. Indeed, as mentioned in section 5.4, some *vfl3* cells grow three flagella, and in cells with two flagella, the beating frequency shows large fluctuations in time. Therefore, it would be indeed better to study the

CHAPTER 6

role of the distal fiber on wt by impairing this structure in normal wt cells, but it does not seem possible nowadays. It is possible to mechanically remove one flagellum without damaging the cell [92, 134]. However, since the distal fiber is internal to the cell, damaging mechanically its structure would cause damage to the cell membrane, and this would alter the cell motility and lead eventually to its death.

To conclude, the possibility to impair the connection of the distal fiber in healthy living *C. reinhardtii* cells would constitute an absolute proof of the role played by distal fibers in flagella synchronization. More generally, as intracellular coupling could be a mechanism regulating synchronization in other multi-ciliated organisms, the experimental approach presented in this manuscript could be applied to other multi-flagellated cells to study the impact of both hydrodynamic forcing and intracellular coupling in flagellar synchronization.

A

PIEZOELECTRIC STAGE CHARACTERIZATION

The majority of the experiments performed in this study addresses the behaviour of *C. reinhardtii* under external periodic hydrodynamic forcing. As discussed in section 3.2, we generate this forcing by a piezoelectric stage controlled via a LabView user interface. We send to Labview a sequence of points as the one shown in figure A.1. This sequence is then either looped infinitely, or for a limited number of periods. Each point represents the stage position in time in X direction. The time interval between two consecutive points is 0.266 ms, corresponding to the highest sampling frequency possible in our piezoelectric stage. Calibration tests are performed by recording, at 900 fps, a glass bead sticking at the bottom of the flow chamber, which thereby directly follows the motion of the stage. In figure A.1 is shown the imposed sequence of points with amplitude $A_i = 47.2$ μm. The points sequence imposed approximates a triangular waveform (black points). We chose this pattern in order to have a constant velocity during the unidirectional displacement. However, given the high speed imposed to the stage, the actual stage motion reconstructed from images is sinusoidal (red points). The actual stage displacement has the same frequency of the imposed sequence of points ($f_F = 59$ Hz), but with a lower amplitude $A_F = 10$ μm. We found that the piezoelectric stage frequency of motion is always identical to the one imposed, but the amplitude is different. The stage motion is highly non-linear in the frequency range considered ($40 - 80$ Hz), therefore we performed calibration experiments for each single forcing frequency f_F that we intended to impose on *C. reinhardtii* and for each flow direction. An example of calibration curves for axial flow is shown in figure A.2. For each frequency, we plot the measured stage motion A_F as a function of the imposed motion A_i. On each curve, we fitted a polynomial trend $A_F = c1 \cdot A_i^2 + c2 \cdot A_i + c3$, with $c1, c2, c3$ polynomial coefficients.
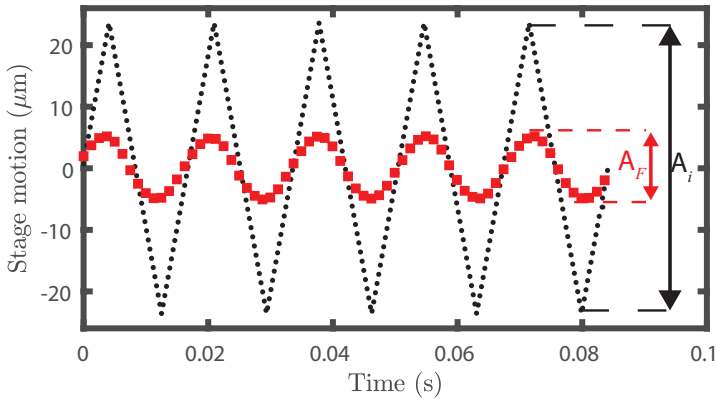
Figure A.1: Stage motion as a function of time. The sequence of points imposed by Labview interface resembles a triangular waveform with amplitude $A_i = 47.2$ μm and frequency $f_F = 59$ Hz (*black dots*). The effective stage displacement measured by tracking a bead has instead amplitude $A_F = 10$ μm and same frequency (*red dots*).
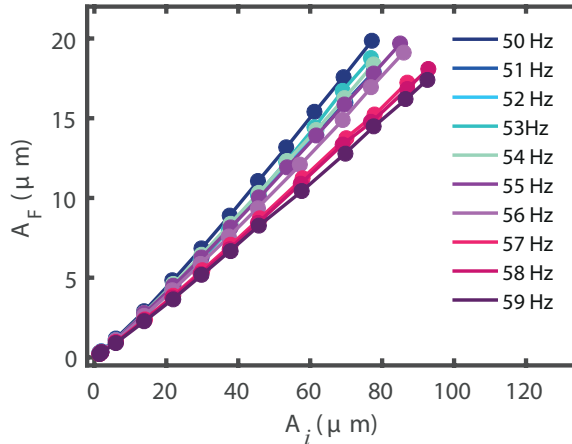
Figure A.2: Calibration curves of the piezoelectric stage for *Axial flow*. For each frequency f_F, a separate calibration curve is obtained. The x-axis represents the amplitude imposed to the stage A_i, while the y-axis shows the measured amplitude of displacement in the stage, corresponding to the effective amplitude of forcing A_F.

B

INTERFLAGELLA SLIPS CHARACTERIZATION

We monitored the occurrence of slips by recording cells held at the tip of a micropipette in absence of external flow perturbations. We observed 23 cells and performed 41 recordings in absence of flow for up to 80 seconds consecutively. We measured the time between consecutive slip events and computed its occurrence. Results are shown in figure B.1(a). In several experiments, no slips were observed (white bars). Among the cells that experienced slips, the time between slip events is well described by an exponential decay with time constant $\tau_{\text{slip}} = 3.4 \, s$.
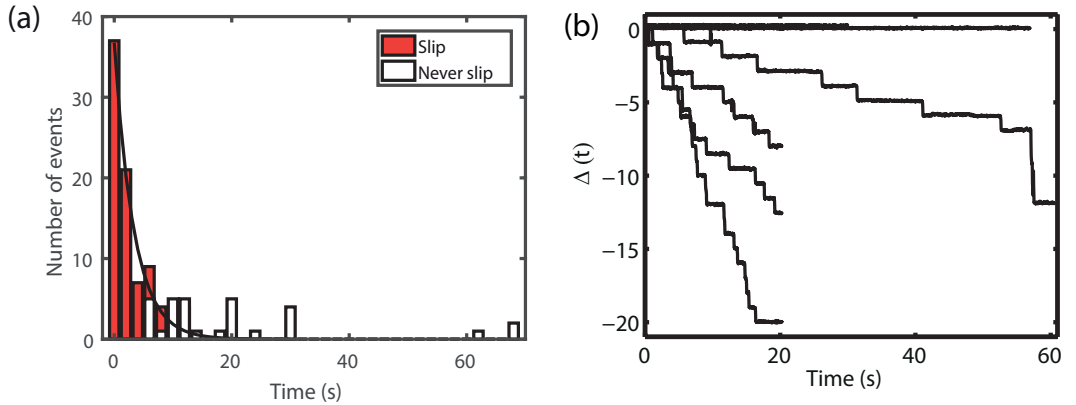
Figure B.1: (a) Histograms of the time between slips in 31 experiments without flow. White bars represent the experiments in which the cell never slips, while red bars are the cells that slip. On the latter, an exponential decay has been fitted with time constant $\tau_{\text{slip}} = 3.4$ s. **(b)** Phase difference $\Delta_f(t)$ between *cis-* and *trans*-flagellum in 7 cells shows the occurrence of slip events.

A more accurate description of the behaviour of flagella as self-sustained oscillators relies on the phase dynamics.

The interflagellar phase difference is obtained as $\Delta_f(t) = \phi_{\text{cis}}(t) - \phi_{\text{trans}}(t)/2\pi$. Details about extraction of $\phi_{\text{cis}}(t)$ and $\phi_{\text{trans}}(t)$ are in section 4.1.2. In figure B.1(b), the phase difference between the two flagella $\Delta_f(t) = \theta_{\text{cis}}(t) - \theta_{\text{trans}}(t)$ is shown for 7 cells. There are cells that never show slip events for up a to 1 minute recording. Furthermore, slips are always negative, meaning that *cis*-flagellum is lagging behind one beating cycle per slip event. Given that the phase dynamics of the two flagella are nearly identical, with few interflagellar slips recorded, in the experiments with external forcing, we consider $\phi(t)$ to represent the phase of both beating flagella and

deduce the time-dependent phase difference $\Delta(t)$ between the flagella and the external forcing flow $\Delta(t) = (\phi(t) - \phi_\mathrm{F}(t))/2\pi$, where $\phi_\mathrm{F}(t) = 2\pi f_\mathrm{F} t$.

REFERENCES

[1] E. Klarreich, "Discovery of coupled oscillation put 17th-century scientist ahead of his time," *SIAM News*, vol. 35, no. 8, p. 20, 2002.

[2] M. Rosenblum and A. Pikovsky, "Synchronization: From pendulum clocks to chaotic lasers and chemical oscillators," *Contemporary Physics*, vol. 44, no. 5, pp. 401–416, 2003.

[3] I. Harary and B. Farley, "In vitro studies on single beating rat heart cells: Ii. intercellular communication," *Experimental cell research*, vol. 29, no. 3, pp. 466–474, 1963.

[4] R. M. Smeal, G. B. Ermentrout, and J. A. White, "Phase-response curves and synchronized neural networks," *Philosophical Transactions of the Royal Society B: Biological Sciences*, vol. 365, no. 1551, pp. 2407–2422, 2010.

[5] S. H. Strogatz, I. Stewart, *et al.*, "Coupled oscillators and biological synchronization," *Scientific American*, vol. 269, no. 6, pp. 102–109, 1993.

[6] R. E. Mirollo and S. H. Strogatz, "Synchronization of pulse-coupled biological oscillators," *SIAM Journal on Applied Mathematics*, vol. 50, no. 6, pp. 1645–1662, 1990.

[7] C. Brennen and H. Winet, "Fluid mechanics of propulsion by cilia and flagella," *Annual Review of Fluid Mechanics*, vol. 9, no. 1, pp. 339–398, 1977.

[8] J. Elgeti, R. G. Winkler, and G. Gompper, "Physics of microswimmers – single particle motion and collective behaviour: A review," *Reports on progress in physics*, vol. 78, no. 5, p. 056 601, 2015.

[9] G. Taylor, "Analysis of the Swimming of Microscopic Organisms," *Proc. Math. Phys. Eng. Sci.*, vol. 209, no. 1099, pp. 447–461, 1951.

[10] E. M. Purcell, "Life at low reynolds number," *Am. J. Phys*, vol. 45, no. 1, pp. 3–11, 1977.

[11] E. W. Knight-Jones, "Relations between Metachronism and the Direction of Ciliary Beat in Metazoa," vol. 95, pp. 503–521, 1954.

[12] D. R. Brumley, K. Y. Wan, M. Polin, and R. E. Goldstein, "Flagellar synchronization through direct hydrodynamic interactions," *Elife*, vol. 3, e02750, 2014.

[13] J. Hussong, N. Schorr, J. Belardi, O. Prucker, J. Rühe, and J. Westerweel, "Experimental investigation of the flow induced by artificial cilia.," *Lab on a chip*, vol. 11, no. 12, pp. 2017–22, 2011.

[14] G. M. Whitesides, "The origins and the future of microfluidics.," *Nature*, vol. 442, no. 7101, pp. 368–73, 2006.

[15] M. Fliegauf, T. Benzing, and H. Omran, "When cilia go bad - cilia defects and ciliopathies," *Nature Reviews: Molecular Cell Biology*, vol. 8, 1, 2007.

[16]   D. W. Pelle, C. J. Brokaw, K. A. Lesich, and C. B. Lindemann, "Mechanical properties of the passive sea urchin sperm flagellum," *Cell Motility and the Cytoskeleton*, vol. 66, 7, 2009.

[17]   B. J. Nelson, I. K. Kaliakatsos, and J. J. Abbott, "Microrobots for minimally invasive medicine," *Annual Review of Biomedical Engineering*, 2010.

[18]   E. W. Jager, O. Inganäs, and I. Lundström, "Microrobots for micrometer-size objects in aqueous media: Potential tools for single-cell manipulation," *Science*, vol. 288, 2000.

[19]   H. Hess, G. D. Bachand, and V. Vogel, "Powering nanodevices with biomolecular motors," *Chemistry - A European Journal*, vol. 52, 2004.

[20]   N. Lane, "The unseen world: Reflections on Leeuwenhoek (1677) 'concerning little animals'," *Phil. Trans. R. Soc. B*, vol. 370, no. 1666, p. 20 140 344, 2015.

[21]   B. Alberts, A. Johnson, J. Lewis, M. Raff, K. Roberts, and P. Walter, *Molecular Biology of the Cell, Fourth Edition*, 4th ed. Garland Science, 2002.

[22]   Y. Sowa and R. M. Berry, "Bacterial flagellar motor," *Quarterly reviews of biophysics*, vol. 41, no. 02, pp. 103–132, 2008.

[23]   I. Gibbons, "Transient flagellar waveforms during intermittent swimming in sea urchin sperm. ii. analysis of tubule sliding," *Journal of Muscle Research & Cell Motility*, vol. 2, no. 1, pp. 83–130, 1981.

[24]   B. Afzelius, R. Dallai, S. Lanzavecchia, and P. Bellon, "Flagellar structure in normal human spermatozoa and in spermatozoa that lack dynein arms," *Tissue and Cell*, vol. 27, no. 3, pp. 241–247, 1995.

[25]   H. Lodish, A. Berk, S. Zipursky, P. Matsudaira, D. Baltimore, and J. Darnell, "Cilia and flagella: Structure and movement," *Molecular Cell Biology, 4th ed.; WH Freeman & Co. Ltd.: San Francisco, CA, USA*, 2000.

[26]   C. Silflow and K. Iyadurai, "The chlamydomonas vfl3 gene product is required for correct positioning of nascent basal bodies," in *Molecular Biology of the Cell*, American Society of Cell Biology, vol. 13, 2002, 326A–326A.

[27]   I. Gibbons, "Sliding and bending in sea urchin sperm flagella.," in *Symposia of the Society for Experimental Biology*, vol. 35, 1982, p. 225.

[28]   C. B. Lindemann and K. A. Lesich, "Detergent-extracted models for the study of cilia or flagella," *Cytoskeleton Methods and Protocols*, pp. 337–353, 2010.

[29]   D. M. Woolley, R. F. Crockett, W. D. Groom, and S. G. Revell, "A study of synchronisation between the flagella of bull spermatozoa, with related observations," *Journal of Experimental Biology*, vol. 212, no. 14, pp. 2215–2223, 2009.

[30]   P. Rompolas, R. S. Patel-King, and S. M. King, "An outer arm dynein conformational switch is required for metachronal synchrony of motile cilia in planaria," *Molecular biology of the cell*, vol. 21, no. 21, pp. 3669–3679, 2010.

[31]   (). Eukaryotic flagellum, Wikipedia, [Online]. Available: https://commons.wikimedia.org/wiki/File:Eukaryotic_flagellum.svg.

[32] O. S. Pak and E. Lauga, "Theoretical models of low-reynolds-number locomotion," in *Fluid-Structure Interactions in Low-Reynolds-Number Flows*, Royal Society of Chemistry, 2015, pp. 100–167.

[33] G. Hancock, "The self-propulsion of microscopic organisms through liquids," in *Proceedings of the Royal Society of London A: Mathematical, Physical and Engineering Sciences*, The Royal Society, vol. 217, 1953, pp. 96–121.

[34] E. Lauga and T. R. Powers, "The hydrodynamics of swimming microorganisms," *Reports on Progress in Physics*, vol. 72, no. 9, p. 096 601, 2009.

[35] G. Batchelor, "The stress system in a suspension of force-free particles," *Journal of fluid mechanics*, vol. 41, no. 03, pp. 545–570, 1970.

[36] N. Bruot and P. Cicuta, "Realizing the physics of motile cilia synchronization with driven colloids," *Annual Review of Condensed Matter Physics*, vol. 7, pp. 323–348, 2016.

[37] J. Gray, "The Mechanism of Ciliary Movement.–VI. Photographic and Stroboscopic Analysis of Ciliary Movement," *Proceedings of the Royal Society of London. Series B, Containing Papers of a Biological Character*, vol. 107, no. 751, pp. 313–332, 1930.

[38] M. Sanderson and M. Sleigh, "Ciliary activity of cultured rabbit tracheal epithelium: Beat pattern and metachrony," *Journal of Cell Science*, vol. 47, no. 1, pp. 331–347, 1981.

[39] S. Gueron and K. Levit-Gurevich, "Energetic considerations of ciliary beating and the advantage of metachronal coordination," *Proceedings of the National Academy of Sciences*, vol. 96, no. 22, pp. 12 240–12 245, 1999.

[40] M. Cosentino Lagomarsino, B. Bassetti, and P. Jona, "Rowers coupled hydrodynamically. modeling possible mechanisms for the cooperation of cilia," *The European Physical Journal B-Condensed Matter and Complex Systems*, vol. 26, no. 1, pp. 81–88, 2002.

[41] A. Pikovsky, O. Popovych, and Y. Maistrenko, "Resolving clusters in chaotic ensembles of globally coupled identical oscillators," *Physical Review Letters*, vol. 87, no. 4, p. 044 102, 2001.

[42] G. M. Cicuta, E. Onofri, M. C. Lagomarsino, and P. Cicuta, "Patterns of synchronization in the hydrodynamic coupling of active colloids," *Physical Review E*, vol. 85, no. 1, p. 016 203, 2012.

[43] P. Lenz, J.-F. Joanny, F. Jülicher, and J. Prost, "Membranes with rotating motors," *Physical Review Letters*, vol. 91, no. 10, p. 108 104, 2003.

[44] T. Niedermayer, B. Eckhardt, and P. Lenz, "Synchronization, phase locking, and metachronal wave formation in ciliary chains," *Chaos*, vol. 18, no. 3, p. 037 128, 2008.

[45] A. Vilfan and F. Jülicher, "Hydrodynamic flow patterns and synchronization of beating cilia," *Phys. Rev. Lett.*, vol. 96, no. 5, p. 058 102, 2006.

[46] N. Uchida and R. Golestanian, "Synchronization in a carpet of hydrodynamically coupled rotors with random intrinsic frequency," *EPL (Europhysics Letters)*, vol. 89, no. 5, p. 50 011, 2010.

[47] N. Uchida and R. Golestanian, "Generic conditions for hydrodynamic synchronization," *Physical Review Letters*, vol. 106, no. 5, p. 058 104, 2011.

[48] B. M. Friedrich and F. Jülicher, "Flagellar Synchronization Independent of Hydrodynamic Interactions," *Phys. Rev. Lett.*, vol. 109, no. 13, p. 138 102, 2012.

[49] L. Rothschild and M. Swann, "The fertilization reaction in the sea-urchin egg," *Journal of Experimental Biology*, vol. 26, no. 2, pp. 164–176, 1949.

[50] I. H. Riedel, K. Kruse, and J. Howard, "A self-organized vortex array of hydrodynamically entrained sperm cells," *Science*, vol. 309, no. 5732, pp. 300–303, 2005.

[51] L. D. Zarzar, P. Kim, and J. Aizenberg, "Bio-inspired design of submerged hydrogel-actuated polymer microstructures operating in response to ph," *Advanced materials*, vol. 23, no. 12, pp. 1442–1446, 2011.

[52] M. Vilfan, G. Kokot, A. Vilfan, N. Osterman, B. Kavčič, I. Poberaj, and D. Babič, "Analysis of fluid flow around a beating artificial cilium," *Beilstein journal of nanotechnology*, vol. 3, no. 1, pp. 163–171, 2012.

[53] S. Sareh, J. Rossiter, A. Conn, K. Drescher, and R. E. Goldstein, "Swimming like algae: Biomimetic soft artificial cilia," *Journal of the Royal Society Interface*, rsif20120666, 2012.

[54] R. Dreyfus, J. Baudry, M. L. Roper, M. Fermigier, H. A. Stone, and J. Bibette, "Microscopic artificial swimmers," *Nature*, vol. 437, no. 7060, pp. 862–865, 2005.

[55] C. L. Van Oosten, C. W. Bastiaansen, and D. J. Broer, "Printed artificial cilia from liquid-crystal network actuators modularly driven by light," *Nature materials*, vol. 8, no. 8, p. 677, 2009.

[56] J. M. den Toonder and P. R. Onck, "Microfluidic manipulation with artificial/bioinspired cilia," *Trends in biotechnology*, vol. 31, no. 2, pp. 85–91, 2013.

[57] J. Kotar, M. Leoni, B. Bassetti, M. C. Lagomarsino, and P. Cicuta, "Hydrodynamic synchronization of colloidal oscillators.," *Proc. Natl. Acad. Sci. U.S.A.*, vol. 107, no. 17, pp. 7669–73, 2010.

[58] R. Di Leonardo, A. Búzás, L. Kelemen, G. Vizsnyiczai, L. Oroszi, and P. Ormos, "Hydrodynamic synchronization of light driven microrotors," *Physical Review Letters*, vol. 109, no. 3, p. 034 104, 2012.

[59] N. Coq, A. Bricard, F.-D. Delapierre, L. Malaquin, O. Du Roure, M. Fermigier, and D. Bartolo, "Collective beating of artificial microcilia," *Physical Review Letters*, vol. 107, no. 1, p. 014 501, 2011.

[60] E. Harris, *The chlamydomonas sourcebook*, Vols. 1 and 3. Elsevier Science, 2009.

[61] U. Rüffer and W. Nultsch, "High-speed cinematographic analysis of the movement of chlamydomonas," *Cell Motil.*, vol. 5, no. 3, pp. 251–263, 1985.

[62] C. L. Dieckmann, "Eyespot placement and assembly in the green alga chlamydomonas," *Bioessays*, vol. 25, no. 4, pp. 410–416, 2003.

[63]   T. M. Mittelmeier, J. S. Boyd, M. R. Lamb, and C. L. Dieckmann, "Asymmetric properties of the chlamydomonas reinhardtii cytoskeleton direct rhodopsin photoreceptor localization," *The Journal of cell biology*, vol. 193, no. 4, pp. 741–753, 2011.

[64]   F. R. Cross and J. G. Umen, "The chlamydomonas cell cycle," *The Plant Journal*, vol. 82, no. 3, pp. 370–392, 2015.

[65]   C. D. Silflow and P. A. Lefebvre, "Assembly and motility of eukaryotic cilia and flagella. lessons from chlamydomonas reinhardtii," *Plant Physiol.*, vol. 127, no. 4, pp. 1500–1507, 2001.

[66]   K. A. Johnson and J. L. Rosenbaum, "Basal bodies and dna," *Trends in Cell Biology*, vol. 1, no. 6, pp. 145–149, 1991.

[67]   G. B. Witman, "Chlamydomonas phototaxis," *Trends in cell biology*, vol. 3, no. 11, pp. 403–408, 1993.

[68]   Y. Arakaki, H. Kawai-Toyooka, Y. Hamamura, T. Higashiyama, A. Noga, M. Hirono, B. J. Olson, and H. Nozaki, "The simplest integrated multicellular organism unveiled," *PLoS One*, vol. 8, no. 12, e81641, 2013.

[69]   D. L. Ringo, "Flagellar motion and fine structure of the flagellar apparatus in chlamydomonas," *The Journal of cell biology*, vol. 33, no. 3, pp. 543–571, 1967.

[70]   R. Kamiya and G. B. Witman, "Submicromolar levels of calcium control the balance of beating between the two flagella in demembranated models of chlamydomonas.," *The Journal of Cell Biology*, vol. 98, no. 1, pp. 97–107, 1984.

[71]   R. Kamiya and E. Hasegawa, "Intrinsic difference in beat frequency between the two flagella of chlamydomonas reinhardtii," *Experimental cell research*, vol. 173, no. 1, pp. 299–304, 1987.

[72]   U. Rüffer and W. Nultsch, "Flagellar photoresponses of chlamydomonas cells held on micropipettes: I. change in flagellar beat frequency," *Cytoskeleton*, vol. 15, no. 3, pp. 162–167, 1990.

[73]   ——, "Flagellar photoresponses of chlamydomonas cells held on micropipettes: Ii. change in flagellar beat pattern," *Cell motil. Cytoskeleton*, vol. 18, no. 4, pp. 269–278, 1991.

[74]   M. Polin, I. Tuval, K. Drescher, J. P. Gollub, and R. E. Goldstein, "Chlamydomonas swims with two "gears" in a eukaryotic version of run-and-tumble locomotion," *Science*, vol. 325, no. 5939, pp. 487–490, 2009.

[75]   K. Y. Wan and R. E. Goldstein, "Rhythmicity, recurrence, and recovery of flagellar beating," *Phys. Rev. Lett.*, vol. 113, p. 238 103, 23 2014.

[76]   V. F. Geyer, F. Jülicher, J. Howard, and B. M. Friedrich, "Cell-body rocking is a dominant mechanism for flagellar synchronization in a swimming alga.," *Proc. Natl. Acad. Sci. U.S.A.*, vol. 110, no. 45, pp. 18 058–63, 2013.

[77]   C. J. Horst and G. B. Witman, "Ptx1, a nonphototactic mutant of chlamydomonas, lacks control of flagellar dominance.," *The Journal of cell biology*, vol. 120, no. 3, pp. 733–741, 1993.

[78] J. A. Schmidt and R. Eckert, "Calcium couples flagellar reversal to photostimulation in chlamydomonas reinhardtii," *Nature*, vol. 262, no. 5570, pp. 713–715, 1976.

[79] U. Rüffer and W. Nultsch, "Flagellar photoresponses of chlamydomonas cells held on micropipettes: Iii. shock response," *Plant Biology*, vol. 108, no. 3, pp. 255–265, 1995.

[80] R. E. Goldstein, "Green algae as model organisms for biological fluid dynamics," *Annual review of fluid mechanics*, vol. 47, pp. 343–375, 2015.

[81] H. J. Hoops, R. L. Wright, J. W. Jarvik, and G. B. Witman, "Flagellar waveform and rotational orientation in a chlamydomonas mutant lacking normal striated fibers.," *J. Cell Biol.*, vol. 98, no. 3, pp. 818–824, 1984.

[82] R. L. Wright, B. Chojnacki, and J. W. Jarvik, "Abnormal basal-body number, location, and orientation in a striated fiber-defective mutant of chlamydomonas reinhardtii," *J. Cell Biol.*, vol. 96, pp. 1697–1707, 1983.

[83] K. C. Leptos, K. Y. Wan, M. Polin, I. Tuval, A. I. Pesci, and R. E. Goldstein, "Antiphase synchronization in a flagellar-dominance mutant of chlamydomonas.," *Phys. Rev. Lett.*, vol. 111, no. 15, p. 158 101, 2013.

[84] R. E. Goldstein, "Batchelor prize lecture fluid dynamics at the scale of the cell," *Journal of Fluid Mechanics*, vol. 807, pp. 1–39, 2016.

[85] J. Elgeti, U. B. Kaupp, and G. Gompper, "Hydrodynamics of sperm cells near surfaces," *Biophysical journal*, vol. 99, no. 4, pp. 1018–1026, 2010.

[86] K. Drescher, R. E. Goldstein, N. Michel, M. Polin, and I. Tuval, "Direct measurement of the flow field around swimming microorganisms," *Phys. Rev. Lett.*, vol. 105, no. 16, p. 168 101, 2010.

[87] J. S. Guasto, K. a. Johnson, and J. P. Gollub, "Oscillatory Flows Induced by Microorganisms Swimming in Two Dimensions," *Phys. Rev. Lett.*, vol. 105, no. 16, p. 168 102, 2010.

[88] D. L. Kirk, *Volvox: Molecular-genetic origins of multicellularity and cellular differentiation*. Cambridge: Cambridge University Press, 1998.

[89] B. Guirao and J.-F. Joanny, "Spontaneous creation of macroscopic flow and metachronal waves in an array of cilia.," *Biophys. J.*, vol. 92, no. 6, pp. 1900–17, 2007.

[90] R. R. Bennett and R. Golestanian, "Emergent run-and-tumble behavior in a simple model of chlamydomonas with intrinsic noise," *Phys. Rev. Lett.*, vol. 110, no. 14, p. 148 102, 2013.

[91] R. E. Goldstein, M. Polin, and I. Tuval, "Noise and Synchronization in Pairs of Beating Eukaryotic Flagella," *Phys. Rev. Lett.*, vol. 103, no. 16, p. 168 103, 2009.

[92] ——, "Emergence of synchronized beating during the regrowth of eukaryotic flagella," *Phys. Rev. Lett.*, vol. 107, no. 14, p. 148 103, 2011.

[93] J. S. Hyams and G. G. Borisy, "Flagellar coordination in chlamydomonas reinhardtii: Isolation and reactivation of the flagellar apparatus," *Science*, vol. 189, no. 4206, pp. 891–893, 1975.

[94]   B. M. Friedrich, "Hydrodynamic synchronization of flagellar oscillators," *ArXiv preprint arXiv:1509.07849*, 2015.

[95]   M. Okuno and Y. Hiramoto, "Mechanical stimulation of starfish sperm flagella," *Journal of Experimental Biology*, vol. 65, no. 2, pp. 401–413, 1976.

[96]   I. Gibbons, C. Shingyoji, A. Murakami, and K. Takahashi, "Spontaneous recovery after experimental manipulation of the plane of beat in sperm flagella," *Nature*, vol. 325, no. 6102, pp. 351–352, 1987.

[97]   C. Shingyoji, I. R. Gibbons, and A. Murakami, "Effect of imposed head vibrations on the stability and waveform of flagellar beating in sea urchin spermatozoa," *J. Exp. Biol.*, vol. 156, pp. 63–80, 1991.

[98]   L. Fredrickson-Hemsing, S. Ji, R. Bruinsma, and D. Bozovic, "Mode-locking dynamics of hair cells of the inner ear," *Phys. Rev. E*, vol. 86, no. 2, p. 021 915, 2012.

[99]   R. Jeanneret, M. Contino, and M. Polin, "A brief introduction to the model microswimmer chlamydomonas reinhardtii," *ArXiv preprint arXiv:1606.01936*, 2016.

[100]   L. Incoll, S. Long, and M. Ashmore, "Si units in publications in plant science," *Commentaries in Plant Sci*, vol. 2, pp. 83–96, 1981.

[101]   *The Chlamydomonas Resource Center at the University of Minnesota*.

[102]   E. Dinc, L. Tian, L. M. Roy, R. Roth, U. Goodenough, and R. Croce, "Lhcsr1 induces a fast and reversible ph-dependent fluorescence quenching in lhcii in chlamydomonas reinhardtii cells," *Proceedings of the National Academy of Sciences*, vol. 113, no. 27, pp. 7673–7678, 2016.

[103]   G. Quaranta, M.-E. Aubin-Tam, and D. Tam, "Hydrodynamics versus intracellular coupling in the synchronization of eukaryotic flagella," *Physical Review Letters*, vol. 115, no. 23, p. 238 101, 2015.

[104]   A. Pikovsky, M. Rosenblum, and J. Kurths, *Synchronization: A universal concept in nonlinear sciences*. Cambridge university press, 2003, vol. 12.

[105]   R. Adler, "A study of locking phenomena in oscillators," *Proceedings of the IRE*, vol. 34, no. 6, pp. 351–357, 1946.

[106]   P. Welch, "The use of fast fourier transform for the estimation of power spectra: A method based on time averaging over short, modified periodograms," *IEEE Transactions on audio and electroacoustics*, vol. 15, no. 2, pp. 70–73, 1967.

[107]   L. Cohen, *Time-frequency analysis*. Prentice Hall PTR Englewood Cliffs, NJ: 1995, vol. 778.

[108]   K. Y. Wan, K. C. Leptos, and R. E. Goldstein, "Lag, lock, sync, slip: The many 'phases' of coupled flagella," *Journal of the Royal Society Interface*, vol. 11, no. 94, p. 20 131 160, 2014.

[109]   S. L. Hahn, *Hilbert transforms in signal processing*. Artech House Boston, 1996, vol. 2.

[110]   S. H. Strogatz, "Exploring complex networks," *Nature*, vol. 410, no. 6825, pp. 268–276, 2001.

[111] S. H. Strogatz, "From Kuramoto to Crawford: exploring the onset of synchronization in populations of coupled oscillators," *Phys. D*, vol. 143, no. 1-4, pp. 1–20, 2000.

[112] R. Ma, G. S. Klindt, I. H. Riedel-Kruse, F. Jülicher, and B. M. Friedrich, "Active phase and amplitude fluctuations of flagellar beating," *Phys. Rev. Lett.*, vol. 113, no. 4, p. 048 101, 2014.

[113] T. Rossing and N. H. Fletcher, *Principles of vibration and sound*. Springer Science & Business Media, 2012.

[114] U. Rüffer and W. Nultsch, "Comparison of the beating of cis-and trans-flagella of chlamydomonas cells held on micropipettes," *Cell Motil.*, vol. 7, no. 1, pp. 87–93, 1987.

[115] C. Jongsma, "Kinematics and kinetics of *Chlamydomonas rehinardtii* under imposed flow," TU Delft, 2016.

[116] J. S. Hyams and G. G. Borisy, "Flagellar coordination in chlamydomonas reinhardtii: Isolation and reactivation of the flagellar apparatus," *Science*, vol. 189, no. 4206, pp. 891–893, 1975.

[117] G. S. Klindt, C. Ruloff, C. Wagner, and B. M. Friedrich, "Load response of the flagellar beat," *Physical Review Letters*, vol. 117, no. 25, p. 258 101, 2016.

[118] P. Sartori, V. F. Geyer, A. Scholich, F. Jülicher, and J. Howard, "Dynamic curvature regulation accounts for the symmetric and asymmetric beats of chlamydomonas flagella," *Elife*, vol. 5, e13258, 2016.

[119] R. G. Brown and P. Y. Hwang, "Introduction to random signals and applied kalman filtering: With matlab exercises and solutions," *Wiley*, 1997.

[120] M. Piccardi, "Background subtraction techniques: A review," in *Systems, man and cybernetics, 2004 IEEE international conference on*, IEEE, vol. 4, 2004, pp. 3099–3104.

[121] P.-O. Persson and G. Strang, "A simple mesh generator in matlab," *SIAM Review*, vol. 46, no. 2, pp. 329–345, 2004.

[122] D. Koller, J. Weber, T. Huang, J. Malik, G. Ogasawara, B. Rao, and S. Russell, "Towards robust automatic traffic scene analysis in real-time," in *Pattern Recognition, 1994. Vol. 1-Conference A: Computer Vision & Image Processing., Proceedings of the 12th IAPR International Conference on*, IEEE, vol. 1, 1994, pp. 126–131.

[123] H. Power and G. Miranda, "Second kind integral equation formulation of stokes flows past a particle of arbitrary shape," *SIAM J. Appl. Math.*, vol. 47, no. 4, pp. 689–698, 1987.

[124] E. E. Keaveny and M. J. Shelley, "Applying a second-kind boundary integral equation for surface tractions in stokes flow," *Journal of Computational Physics*, no. 230, 2011.

[125] J. Gray and G. Hancock, "The propulsion of sea-urchin spermatozoa," *Journal of Experimental Biology*, no. 32, 20, 1955.

[126] J. B. Keller and S. I. Rubinow, "Slender-body theory for slow viscous flow," *Journal of Fluid Mechanics*, no. 75, 1976.

[127] D. S.-W. Tam, "Motion at low reynolds number," Massachusetts Institute of Technology, 2008.

[128] A. Savitzky and M. J. Golay, "Smoothing and differentiation of data by simplified least squares procedures," *Analytical Chemistry*, vol. 36, no. 8, 1964.

[129] P. Holoborodko. (). Low-noise lanczos differentiators, [Online]. Available: http://www.holoborodko.com/pavel/numerical-methods/numerical-derivative/smooth-low-noise-differentiators/.

[130] M. Okuno, "Inhibition and relaxation of sea urhin sperm flagella by vanadate," *Journal of Cell Biology*, vol. 85, 1, 1980.

[131] K. Machin, "Wave propagation along flagella," *Journal of Experimental Biology*, no. 35, 1958.

[132] S. E. Spagnolie and E. Lauga, "The optimal elastic flagellum," *Physics of Fluids*, vol. 22, no. 031901, 2010.

[133] T. Yagi, I. Minoura, A. Fujiwara, R. Saito, T. Yasunaga, M. Hirono, and R. Kamiya, "An axonemal dynein particularly important for flagellar movement at high viscosity implications from a new chlamydomonas mutant deficient in the dynein heavy chain gene dhc9," *Journal of Biological Chemistry*, vol. 280, no. 50, pp. 41 412–41 420, 2005.

[134] K. Y. Wan and R. E. Goldstein, "Coordinated beating of algal flagella is mediated by basal coupling," *Proceedings of the National Academy of Sciences*, vol. 113, no. 20, E2784–E2793, 2016.

[135] M. Sleigh, "Contractility of the roots of flagella and cilia," *Nature*, vol. 277, pp. 263–264, 1979.

[136] M. E. Werner, P. Hwang, F. Huisman, P. Taborek, C. Y. Clare, and B. J. Mitchell, "Actin and microtubules drive differential aspects of planar cell polarity in multiciliated cells," *J. Cell Biol.*, vol. 195, no. 1, pp. 19–26, 2011.

[137] E. R. Brooks and J. B. Wallingford, "Multiciliated cells," *Curr. Biol.*, vol. 24, no. 19, R973–R982, 2014.

[138] B. Qin, A. Gopinath, J. Yang, J. P. Gollub, and P. E. Arratia, "Flagellar kinematics and swimming of algal cells in viscoelastic fluids," *Scientific reports*, vol. 5, 2015.

ACKNOWLEDGEMENTS

Like small hesitant streams
the same lake we entered
Earth and gravity conspired to meet you
We laughed, we swam, we mixed with each other
- we learned the substance of us

Stronger now i leave - as a big river
carrying your pieces with me and flowing into the unknown
Until the next crossroad my fellows
Until the next sea

A. Kostakou

CURRICULUM

Greta Quaranta was born on July 12, 1988, in Turin, Italy. She graduated in Biomedical Engineering in 2012 at Polytechnic University of Turin, Italy with a thesis on Mechanical characterization of actin crosslinking proteins. She developed the M.Sc. thesis during a research internship at Massachusetts Institute of Technology, Boston, USA. During the time spent in M.I.T. at Mechanobiology Laboratory held by Prof. Roger Kamm, Greta developed a great interest in cells microfluidics and, once graduated, she wanted to pursue a PhD on this topic. In May 2013, Greta started her 4 years PhD project 'Hydrodynamics of Miniml biolocomotion' at Delft University of Technology in the Lab for Aero- and Hydrodynamics, under the supervision of Dr. Daniel Tam and Prof. dr. ir. Jerry Westerweel. This project addressed, both experimentally and numerically, flagellar synchronization in the algae *C.reinhardtii*. The results of this study are discussed in the present manuscript. Greta can be contacted by email at greta.quaranta@gmail.com.

LIST OF PUBLICATIONS

JOURNAL PUBLICATIONS

[1] G. Quaranta, M.-E. Aubin-Tam, and D. Tam, "Hydrodynamics vs. Intracellular Coupling in the Synchronization of Eukaryotic Flagella" *Phys. Rev. Lett*, vol. 115:238101, 2015.

SELECTED CONFERENCE CONTRIBUTIONS

[1] G. Quaranta, V. Badloe, D. Wei, M.-E. Aubin-Tam, and D. Tam, "Synchronization of Chlamydomonas with a Periodic Bbackground Flow: the Importance of Intracellular Coupling.", *11th European Fluid Mechanics Conference*, 12-16 September 2016, Seville, Spain.

[2] G.Quaranta, M.E. Aubin-Tam, and D. Tam, "Synchronization of Eukaryotic Flagella with an Imposed Periodic Flow.", *Burgers Symposium*, 16-17 June 2016, Lunteren, The Netherlands.

[3] G.Quaranta, M.E. Aubin-Tam, and D. Tam, "Synchronization of Eukaryotic Flagella with an Imposed Periodic Flow.", *68th American Physical Society Division of Fluid Dynamics Conference*, 22-24 November 2015, Boston, USA.

[4] G.Quaranta, M.E. Aubin-Tam, and D. Tam, "Flagellar synchronization with a periodic background flow", *10th European Fluid Mechanics Conference*, 14-18 September 2014, Copenhagen, Denmark.